Kingdom of Saudi Arabia
Ministry of Education
Jazan University

JAZAN UNIVERSITY

JOURNAL OF
JAZAN UNIVERSITY
For
Applied Sciences

A Refereed Scientific Periodical

ISSN:1658-6913

Vol. 10 No 2 November 2022(Rabi` al-Thani 1443 H)

Publication Rules

The University of Jazan provides an opportunity for scholars to publish their scholarly work on research. The editorial board will consider manuscripts from all fields of knowledge. Manuscripts submitted in either Arabic or English, and if the due accepted for publication, may not be published elsewhere, without permission of the Editor-in-Chief. The journal issues one volume per year. The types of manuscript classification used by the Editorial Board run as follows:

1. **Article:**
   An author's original work contributing new knowledge to the field in which research was conducted.
2. **Review Article:**
   A critical synthesis of the current literature in a particular filed, or a synthesis of the literature in a particular field during an explicit period of time.
3. **Brief Article:**
   A short article (note) with the characteristics of an article.
4. Book Reviews
5. **Forum:**
   Letters to the editor, comments, responses, preliminary results or findings, and miscellany

General Instructions

1. Submission of manuscripts:

Original manuscripts should be typewritten (one side only), using an A4 size paper, double spaced along with 3 copies. All pages are to be numbered consecutively, including tables and graphs. Tables, other illustrations, and references should be presented on separate sheets with their proper text position indicated.

2. Abstracts:

Manuscripts for articles, review articles, and brief articles require both Arabic and English abstracts, using no more than 200 words, in single column (13cm wide), for each version.

3. Tables and other illustrations:

Tables, charts, figures, and plates should fit the journal's page size (12.5 com x 18cm). All inner drawings must be presented on high quality. Tracing paper is necessary, using black Indian ink as well. Photographs may be submitted, but on glossy print paper in either black or color.

4. Abbreviations and Units:

A4 sizes and quantities should be expressed according to international standards. Standardized abbreviation should only be used. The names of periodicals should be abbreviated in accordance with the words of scientific periodicals.

5. Title Page:

Should contain the title, name of the authors, name and address of the institution, where the work was carried out. The title should be brief and use strong keywords. Scientific names of organism should be clearly stated and should be typed italic.

6. Text:

The organization of the manuscript should be as follows: Introduction, materials, results, discussion, and references. Results and discussions can be combined in one section. Acknowledgement (if needed) should be brief and added before the reference sections.

1. References:

Citation of the references (within the text) should be indicated by author. Date, style, and references should be listed in an alphabetical order and conform to the following examples: Periodical citations in the text are to be enclosed in one line brackets, e.g.(6).

Periodical references are to be presented in the following

form:

References number in line brackets ( ), author's name followed by a given name and/or initials, the title of an article or periodical (italicized), volume number, year of publication (in parentheses) and pages e.g.

Basahy, A.Y. (1992). Protein and Amino Acid contents in seeds of some soybean cultivate (Glycin Max 1) Arab Gulf J. Sci. Res. 11(2), 221-228.

Book Citation:

Book references should include the following:

Reference number ( ), author's surname followed by a given name and/or title of the book (italicized), place of publication, publisher, and year of publication.

Example:

Lehman. H.C. (1953). Age and Achievement. Princeton: Princeton University Press.

2. Content Notes:

Content notes are to be presented on separate sheets. They will be printed below a solid line separating the content notes from the text.

9. The manuscripts and forum items submitted to the journal for publication contain the author's conclusions and opinions, and if published they do no bear a conclusion or opinion of the Editorial Board.

10. Authors will be provided with 20 reprints free of charge, along with two issues of the journal. Additional copies could be purchased, if ordered when the proofs are returned. Price will be shown on the order form.

11. It is the responsibility of the researcher to make sure that the manuscript is free of linguistic, grammatical and typo errors.

12. The editors' board has the right to set priorities of publishing the research.

13. The journal is not obligated to repeat the research it reaches, whether it was approved for publication or not.

14. All the received research is subject to primary examination by the editorial board in order to determine their eligibility for arbitration. The editorial board is entitled to excusing itself from accepting the research without giving reasons.

15. The journal is published twice a year.

Kingdom of Saudi Arabia
Ministry of Education
Jazan University

JOURNAL OF
JAZAN UNIVERSITY

For

Applied Sciences

A Refereed Scientific Periodical

(Vol.10 No2 November 2022) Rabi` al-Thani 1444 H

ISSN:1658-6913

Journal Jazan University for applied sciences

Vol.10 No2 November 2022 (Rabi` al-Thani1444 H)

Correspondence

All correspondence should be directed to:
Editor-in-chief of Jazan University Journal of Applied Sciences, Jazan - University City
Administrative Tower - PO Box 114 - Zip Code 4514, Kingdom of Saudi Arabia
jas@jazanu.edu.sa

فهرس المحتويات

الموضوع | صفحة

Delivering Awareness Lecture of Common Patients'-Known Terms of Over-The-Counter Drugs amongFinal-Year Pharmacy Students is associatedwith Smooth and Efficient Community Pharmacy Practice

Rayan A. Ahmed[1]*, Mohamed E. Ahmed[2], Reem O. Elagi1[1], Hatim A. Masmali1[1], Amal Y. Jandali1[1], and Ali A. Aloqayli1[1]

[1]Jazan University, College of Pharmacy, Department of Pharmacology and Toxicology, Jizan 45142, P.O. Box 114, Kingdom of Saudi Arabia
[2]King Saud bin Abdulaziz University for Health Sciences, Kingdom of Saudi Arabia

ABSTRACT

Saudi Arabian freshly-graduated pharmacists start shifting to work in community pharmacies. Being less confident, spending long dispensing time, making errors during dispensing are some challenges encountered by newly-graduated pharmacists. This study determined how lack in knowledge among final-year pharmacy students at Jazan University negatively impact on dispensing process; however, the same coin has been flipped the side after intervention. The knowledge of names, characters, and marks of over the counter drugs known by patients in Jazan region and its impact on dispensing process (time/errors) and overall students' performance (satisfaction level) have been assessed. However, a recorded lecture containing around a hundred of names, characters, and marks of the drugs known by the patients in Jazan has been delivered. Exploring the role of intervention in resolving these issues, the same previous parameters have been re-assessed. The study was conducted utilizing patient, pharmacist and pharmacy-stimulated scenario

(online setting). Participants' responses were registered as time required to prepare prescriptions, true and wrong dispensing attempts made and the level of satisfaction (pre-intervention and post-intervention). This study showed that there were significant reduction in dispensing time, dispensing errors number and increase the satisfaction level after intervention as compared to pre-intervention. Being familiar with those marks, characters, and names of over the counter marketed drugs known by the patients in Jazan might help final-year pharmacy students in drugs dispensing process and increase their overall performance while working in the community pharmacies.

Keywords: Awareness, Community Pharmacy, Pharmacy Practice, OTC drugs

1. INTRODUCTION

In Saudi Arabia, the changes in the health care system has been significantly noted. (Alhamoudi and Alnattah 2018). There are two major sectors in the scheme: governmental and non-governmental (Alhamoudi and Alnattah 2018). Regarding pharmaceutical profession; there are several authorities, including the Ministry of Health, the Saudi Commission for Health Specialties, the Saudi Food and Drug Administration and the Saudi Pharmaceutical Society. Moreover, one of the issues related to pharmacy profession in the Kingdom of Saudi Arabia was the scarcity of nationally-born pharmacists (Almaghaslah et al. 2019). In 2012, it was stated that Saudi Arabia had low percentage of pharmacists (3-5%) (Almaghaslah et al. 2019). Therefore, The Ministry of Civil Services and Ministry of Health recruited foreign pharmacists to fill this gap (Almaghaslah et al. 2019). Saudi Arabia had only one pharmacy college, which is in Riyadh at King Saud University (1959 up to 2001) (Alhamoudi and Alnattah 2018). Recently, the government has shown greater interest in reducing the shortage in pharmaceutical services by launching pharmacy colleges all over the kingdom trying to meet the increasing in demand for national pharmaceutical services (Almaghaslah et al. 2019). Currently, there are 27 pharmacy colleges offering a bachelor of pharmacy (B-Pharm) and/or doctor of pharmacy (Pharm D) programs, according to the 2016 Statistical Yearbook of Saudi Arabia (Alhamoudi and Alnattah 2018). This rapid increase in pharmacy colleges has led to rise in students intake, with the number of students enrolled in pharmacy colleges hitting over 14,000 (2018) (Alhamoudi and Alnattah 2018).

Furthermore, the number of community pharmacies in Saudi Arabia is around 8000 and the availability of qualified and well-trained pharmacists is one of the targets for localization of pharmaceutical services (Aljameeli 2018).

Community pharmacies play a critical role in providing pharmaceutical and health care services which directly affect the patient health outcomes. Pharmacist counselling role in particular actively enhances patients knowledge about diseases and drugs which leads to less misuse of drugs and improves the overall health outcomes (Alaqeel and Abanmy 2015). In more details, the community pharmacist is expected to provide support for patients and physicians improving medication adherence and rationalizing prescriptions (Lenjisa 2015). Freshly-graduated pharmacists are expected to play an essential and expanded role inside the health institutions (community pharmacy) by providing a high-quality of pharmaceutical and health care services (Sahir et al. 2014). Getting sufficient and efficient training, the pharmacist directly enhances the services provided by the pharmacy. Nowadays, in Saudi Arabia, most pharmacy students trained in the community pharmacy as a part of their internship program. During the internship, the students are enrolled in around 60 days community pharmacy training which not only impact on their knowledge but also improve their communication skills. However, numerous challenges are still being faced by internship students. Some of these challenges are dispensing issues and misunderstanding of patients' needs which is due to lack of experience. These issues, consequently, lead to lower their overall performance. However, solving these issues will not only lead to improve the population health but also achieve the

satisfaction of the patients about community pharmacy services provided. Though, few studies have been undertaken to discuss and to solve this issue particularly in Saudi Arabia.

It has been known for a long period of time that the pharmacist's role is primarily dispensing medication. Recently, his role has been expanded to include consultation to other healthcare providers about drugs and therapeutic protocols. Besides that the pharmacist involved in counseling patients about drug related issues examples of which are drug side effects, drug interactions and drug monitoring etc. (Lenjisa 2015). Being in the front line, the pharmacist in the community pharmacy is facing a wide range of challenges; however, they should be overcome to ensure that these roles and services continue (Hayden and Parkin 2020). Preventing infection, managing supply chains, preventing stock piling, and providing evidence-based medical information are some of the other expanded roles of the pharmacist that can be offered in the community pharmacy nowadays (Hayden and Parkin 2020).

One of the major issues that pharmacist faces while providing the service is dispensing errors which is described as: "a discrepancy between a prescription and the medicine delivered to the patient by the pharmacy based on this prescription, including the delivery of medication of lower pharmaceutical or due to lower information quality" (Gogazeh 2020). Another definition for medication errors is "any preventable events that may cause or lead to inappropriate medication use or patient harm" (Aljameeli 2018). These errors are expected to occur due to several factors such as errors during practice procedures (prescribing, transcription, distributing, and selling prescriptions) and errors

related the products (packing) (Lenjisa 2015, Sahir et al. 2014, Naybour, Remenyte-Prescott, and Boyd 2019). Moreover, the main causes of dispensing errors were misreading and complex prescriptions, confusing similar names or similar packaging "look-alike sound-alike", and lack of knowledge (Gogazeh 2020). In addition, long waiting time during dispensing process in the community pharmacy is another major concern. Not having sufficient knowledge of patients' terms used while ordering medications may be involved in increasing waiting time in the pharmacy. To encourage clients repeated use of the same pharmacy with high satisfaction, high-quality services and fulfill customers' requirements such as reducing waiting time must be taken in consideration (Afolabi and Erhun 2005, Dansky and Miles 1997). Previous studies have shown that pharmacy design, interruptions, and other environmental factors in the pharmacy play an important role in increasing the incidence of errors in dispensing (Gogazeh 2020). Having some background information about medication in the drug stores is one of the major elements of efficiently practice pharmacy as a career in the community drug stores; however, making mistakes during dispensing process is one of the reasons that could be threaten the pharmacy profession (Abdel-Qader et al. 2020).

The purpose of this study was to assess if final-year pharmacy students possible lack of knowledge of the names, characters, and marks of over-the-counter drugs commonly used by patients in the Jazan region could have a negative impact on the dispensing process (dispensing time, dispensing errors, and overall students' performance and satisfaction). Final-year pharmacy students, on the

other hand, were exposed to a recorded lecture including around a hundred of these names, characters, and marks. The same previous parameters were then re-assessed to see what effect the intervention played in resolving these issues.

2. MATERIALS AND METHODS

2.1. The simulated pharmacist

The simulated pharmacist approach was used to assess the way of pharmacists deal with clients' orders during a routine community pharmacy visit. The simulated pharmacist was randomly selected from a population of final-year pharmacy students or graduated students who is willing to join the community pharmacy as an intern student. The student at this level has already taken all pharmacology courses at Jazan University College of Pharmacy. The sample size of the study including both males and females was (N=40).

2.2. The simulated patient

The simulated patient approach that let a person pretend, during a regular visit to the pharmacy, a patient or a client asking for wanted medications. The simulated patient was any Arabic speaker who was trained to visit a simulated pharmacy and ask for medications (males and females) (N=4). Using students as simulated patients or clients has been utilized in numerous research previously (Alaqeel and Abanmy 2015, Bin Abdulhak et al. 2011, Alte, Weitschies, and Ritter 2007**,** Weiss et al. 2010, Gokcekus et al. 2012). Assuring the scenario was carried out consistently, the authors have trained the simulated patients several times on the number of questions that should be asked, recording dispensing time using a stop watch,

counting error number in dispensing, correcting the quiz, and filling excel sheet.

2.3. The simulated pharmacy

The study was planned to be performed at a community pharmacy (onsite) or (online simulated pharmacy) in Jazan, Saudi Arabia. Simulated Pharmacy has been created in several pharmacy schools with several purpose (education-training-research) (Soto et al. 2016**,** Sansom and Cox 2013, T. and M. 2015). However, we were able to conduct this study in a simulated pharmacy using a virtual classroom (online) which was loaded with cards displaying the drugs in the pharmacy. The cards include all drug-related information such as patient-known names, marks, and characters, generic names, trade names, indications, and medications photographs.

2.4. Intervention: Video generation

A half an hour video was recorded using the materials collected from (N=15 pharmacies) in Jazan region (North, South, East, and West). This video was used as an intervention in this study to evaluate multiple parameters in community pharmacy practice. The material produced contains around 100 OTC drugs which contains marks, names, or characters familiar to the patients living in Jazan, Saudi Arabia.

2.5. The study scenario

Data was collected from 15 randomly chosen neighborhood pharmacies (North, South, East, and West) Jazan City with clear intention of gathering information from different areas of the city. Information was gathered from one facility to the next until it was noticed that every drug store visited

provided repeated information. A PDF file was generated (published as a booklet in Takween publisher, Jeddah, Saudi Arabia), which has drugs information such as generic names, trade names, indications, drugs photos, and most importantly names, marks, and characters familiar among patients in Jazan area. This material was recorded as a 30-min video which later used as an intervention.

Moreover, the study consisted of two parts (pre-and post-intervention) and all were conducted in Arabic. A pilot study was carried out on six participants (3 males and 3 females) to ensure the content and delivery of the scenario. To ensure the scenario was performed in a consistent manner, the authors trained simulated patient several times before conducting the experiment. Confirming accuracy of collected data, the results of the pilot study were checked by all authors. All participants voluntary involved in the study.

In the simulated pharmacy sessions, the randomly chosen simulated pharmacist was verbally asked to dispense three ordered medications (one by one) by the simulated patient using names, marks, and characters (not hidden) known by the patients in Jazan area. The simulated pharmacist was given cards representing the desired drugs that have names, marks, and characters of the drugs (hidden) known by patient in Jazan. The only information shown to the simulated pharmacist in the card was the drug photo from which the wanted drug can be predicted. The dispensing time was calculated in triplicate. The number of true and wrong tries was counted. After that, 15 randomly selected multiple-choice questions (MCQ), related to names, marks, and characters of drugs familiar to patients in Jazan city, were

taken by the simulated pharmacist and the correct answers were counted. In response to their participation in the study, the simulated pharmacists were then asked about their satisfaction level participating in the dispensing procedure using five-points Likert scale as (fully satisfied-satisfied-neutral-not satisfied-fully not satisfied). Collectively, the form used to fill participants' responses has an initial segment for gathering demographic details, 15 MCQ, and a five-point Likert scale. After that, all participants were asked to watch a 30-min video featuring a list of drugs with generic names, trade names, indications, images of drugs, and most significantly names, marks, and characters of OTC drugs known by patients in the Jazan area. Then the same previous procedure was repeated overnight to assess the same parameters (post-intervention).

2.6. Data collection

The data was collected by appointed and trained data collectors as explained previously in the simulated patient section.

2.7. Ethical consideration

Ethical approval for this study was obtained from the Scientific Research Ethics- Jazan University (HAPO-10-Z-001) reference number (REC42/1/125), 5 May 2021. Written informed consent was obtained from study participants. Confidentiality of the data and the privacy of the participants were maintained.

2.8. Statistical analysis

Pre-and post-intervention data obtained from the simulated pharmacist dispensing process (time of dispensing and number of errors), quiz marks, and satisfaction level (Likert scale) were entered and checked by the authors

involved in the study. Then the statistical analysis of the data was done via (SPSS v.24) statistical software. Descriptive analysis was conducted, mean and SD calculated for continuous variables, frequency and percentage distribution used for categorical variables. Boxplot graphs were drawn to compare the distribution and outliers in continuous variables between pre-and post-intervention groups. To examine significant differences in the study variables between pre-and post-intervention groups, t test for dependent variables and McNemar tests were carried out. The *P* values less than 0.05 were considered statistically significant.

3. RESULTS

3.1. Panadol Extra as an OTC drug referred to as "The Red Panadol" by patients in the Jazan area

The photo in (Figure 1A) shows the package of the Panadol Extra designed by GlaxoSmithKline (GSK) drug company. Other information such as generic name, indication, and most importantly the common mark known by patients in Jazan region which is the red color, as seen the package, were shown. However, the same information was revealed in Arabic (Figure 1B). Information used in Figure 1 was taken from the collected materials to generate the booklet.

***Figure* 1A: Panadol Extra as an OTC drug referred to as "The Red Panadol" by patients in the Jazan area.** The picture on the left side shows the English version of Panadol Extra package as an example of the booklet content generated which has common names, marks, and characteristics of OTC drugs known by patients in Jazan area besides the generic and trade names, drug photo and the indication. **Figure 1B:** on the right side shows the Arabic version of same drug packaging.

3.2.

3.3. Participants' distribution by gender

Out of 40 students who responded, 24 (60%) were males and 16 (40%) were females.

3.4. Changes in OTC drugs dispensing time among final-year pharmacy students

Changes in dispensing time between pre-and post-intervention groups were studied. Mean and SD were calculated and analyzed using t test. Significant differences (*P* value < 0.05) were

identified in three times and average time as well among the two groups. The mean of the average time in pre-intervention was 48.6 sec with 22.2 SD compared to the mean 26.2 sec and 13.8 SD (post-intervention) (Table 1). In Figure 2, the boxplot shows the distribution of pre-and post-intervention time of dispensing data as follow: minimum score, lower quartile, median, upper quartile, maximum score and outliers. The median of dispensing time was 46 sec before intervention compared with 22 sec after intervention. Also, it is illustrated that 4 responses were identified to be mild upper outliers' values in the post-intervention group. Some extreme outliers in the pre-intervention group were excluded before analysis (data not shown).

Time	**Pre**		**Post**		
	Mean	**SD**	**Mean**	**SD**	**P value**
Time 1	39.3	24.0	26.2	20.0	0.003*
Time 2	56.7	38.2	24.7	14.0	0.001*
Time 3	49.6	35.0	25.4	16.8	0.001*
Average Time	48.6	22.2	26.2	13.8	0.001*

**Significant at 1%*

Table 1. The influence of intervention in changing dispensing time of OTC drugs among final-year pharmacy students from Jazan University College of Pharmacy. All participants (N=40) were asked to dispense three randomly chosen medications wanted by patients (pre-and post-intervention). The time of dispensing were calculated in sec for each participant. Then the mean and SD were calculated for all times (1, 2, and 3) in the pre-and post-intervention groups. **P<* (0.001-0.03) considered statistically significant as compared to pre-intervention group.

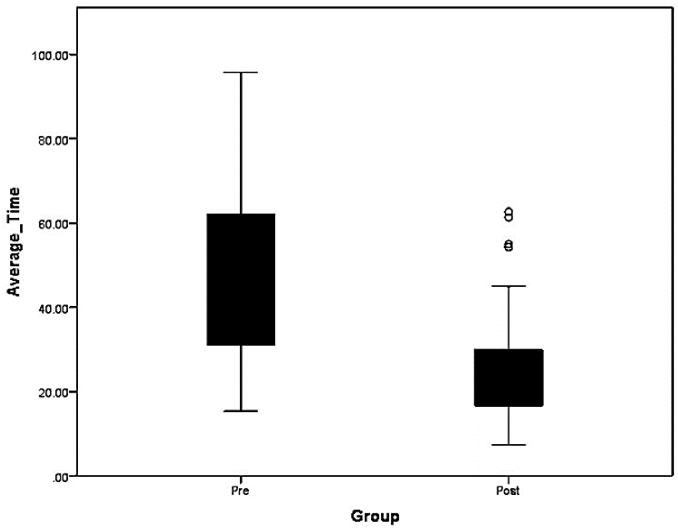

***Figure* 2: Changes in OTC drugs dispensing time among final-year pharmacy students (College of Pharmacy, Jazan University) (pre-intervention vs. post-intervention).** The average values of dispensing time in sec were plotted against (pre-and post-intervention) groups. Vertical bars indicate the minimum score, lower quartile, median, upper quartile, and maximum score. Significant changes were found between the groups. The outliers are indicated in the boxplot as (o).

3.5. Changes in number of OTC dispensing errors among final-year pharmacy students

Errors frequencies during OTC dispensing process in pre-and post-intervention groups were observed (Table 2). The true and wrong frequencies were calculated and tested by McNemar test. Significant differences (P value < 0.05) were identified in three statements and the total as well. Number of correct attempts in pre-intervention was 46 compared to 100 for post-intervention; however, the corresponding wrong responses were 74 and 20, respectively. The boxplot (Figure 3) showed the distribution of the error in dispensing data pre-and post-intervention as follow: minimum score, lower quartile,

median, upper quartile, and maximum score. The median of dispensing error was 46 before intervention compared with zero error after intervention. Also, the figure showed that 75% of respondents had at least one error before the intervention.

To confirm the previous results; respondents were subjected a quiz consisting of 15 multiple choices questions (MCQ). The quiz was then corrected. Table 3 showed that the mean of quiz scores in pre-intervention was 9.2 with 2.3 SD; however, the mean and SD of post-intervention quiz scores was 12.5 and 2.1 SD respectively. The results were analyzed by t test for dependent samples indicated significant difference with *P* value < 0.05 in the quiz scores of the post-intervention group as compared to pre-intervention one. In Figure 4, the boxplot showed the pre-and post-intervention distribution of the participants quiz as follow: minimum score, lower quartile, median, upper quartile, and maximum score. The median of quiz score was 10 before intervention compared with 13 after intervention. Also, it is illustrated that two responses were identified to be mild lower outliers' values in the post-intervention group.

Attempt	**Pre**		**Post**		
	True	False	True	False	P value
Attempt 1	9	31	30	10	0.001*
Attempt 2	18	22	36	4	0.001*
Attempt 3	19	21	34	6	0.001*
Total Attempts	46	74	100	20	0.001*

**Significant at 1%*

Table 2. The influence of the intervention in changing errors number in dispensing of OTC drugs among final-year pharmacy students from Jazan University College of Pharmacy. All participants (N=40) were asked to dispense three randomly chosen medications wanted by patients (pre-and post-intervention). The number of correctly and incorrectly prepared OTC drugs was calculated for each participant in three attempts. The total counts of true and false attempts in each group were also calculated (pre-and post-intervention). The statistical analysis indicates that there is a significant difference between pre-and post-intervention number of errors in dispensing with *$P<$ (0.001).

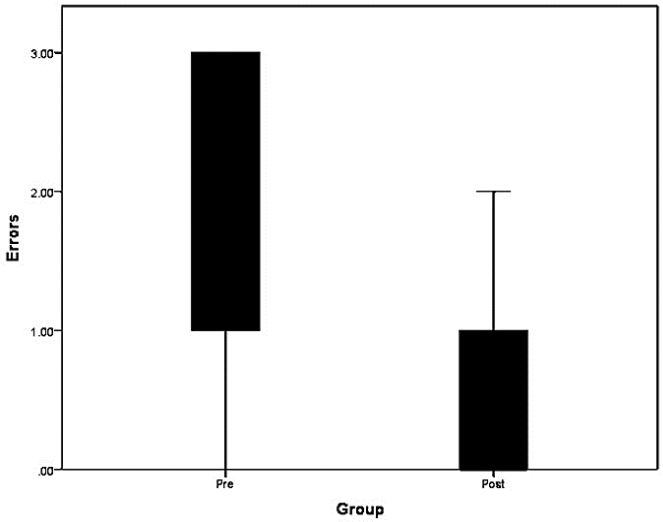

***Figure* 3: Changes in dispensing number of errors of OTC drugs among final-year pharmacy students (College of Pharmacy, Jazan University) (pre-intervention vs. post-intervention).** The total errors of dispensing for each participant were illustrated in the boxplot (pre-and post-intervention) groups. Vertical bars indicate the minimum score, lower quartile, median, upper quartile, and maximum score). Significant changes were found between the groups.

Time	Pre		Post		
	Mean	SD	Mean	SD	P value
Quiz	9.2	2.3	12.6	2.1	0.001*

**Significant at 1%*

Table 3. The influence of intervention in changing quiz score among final-year pharmacy students from Jazan University College of Pharmacy. All participants were given a quiz (15 MCQ /15 min). The mean and SD of quiz scores were calculated for post-intervention group as compared with their respective pre-intervention group. The statistical analysis indicates that there is a significant difference between pre-and post-intervention in number of dispensing errors with **P<* (0.001)

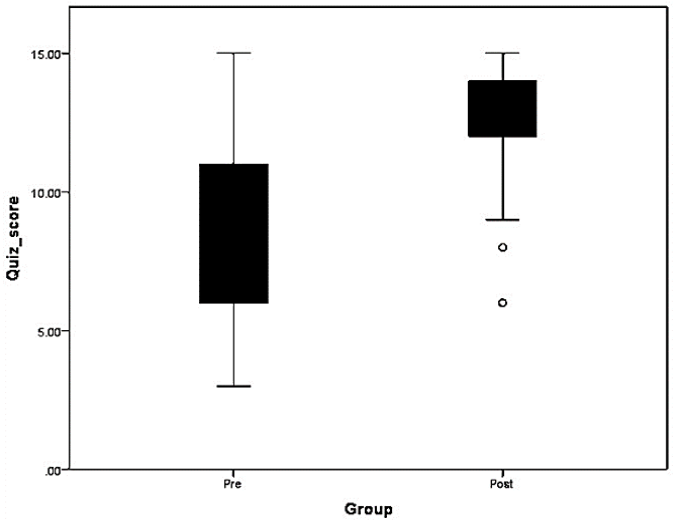

***Figure* 4: Changes in quiz score among final-year pharmacy students (College of Pharmacy, Jazan University) (pre-intervention vs. post-intervention).** The quiz scores for all participants (pre-and post-intervention) groups were distributed on boxplot. Vertical bars indicate the minimum score, lower quartile, median, upper quartile, and maximum score. Significant changes were found between the groups. The outliers are indicated in the figure as (o).

3.6. Pre and post intervention changes in dispensing time and errors impact on confident level of the final-year pharmacy students

Due to the impact of intervention in the reduction of dispensing times and errors, we assumed that this effect may have an impact on the satisfaction level of the participants after completing the drug dispensing process. Therefore, confidents levels of the participants were assessed using five-points Likert scale as shown in Table 4. Then the percentages were calculated. In the pre-intervention group, 35% of the participants were not satisfied and 37.5% were neutral; however, a dramatic change has been seen after implementing the intervention. There were 87.5% satisfied participants. However, only one participant representing (2.5%) was not satisfied after the intervention.

Scale	Pre		Post	
	Out of 40	%	Out of 40	%
Fully satisfied	5	12.5	20	50.0
Satisfied	6	15.0	15	37.5
Neutral	15	37.5	4	10.0
Not satisfied	11	27.5	1	2.5
Fully not satisfied	3	7.5	0	0

Table 4. Changing in dispensing time and errors impacts on the confident level of final-year pharmacy students (College of Pharmacy, Jazan University) (pre-intervention vs. post-intervention). All participants' confident level (pre-and post-

intervention) were evaluated using a five-point Likert scale. The responses were distributed under each point on the scale and the percentages were calculated.

4. DISCUSSION

Collectively, results in the present study demonstrate that there is lack in knowledge of numerous names, marks, and characteristics of commonly patients-known OTC drugs among final-year pharmacy students in Jazan University. The lack of knowledge can be clearly seen as an increase in time and number of errors during dispensing of OTC drugs. These results were confirmed by quiz taken by all study participants. The average score of the quiz was relatively low. Moreover, the percentage of satisfaction levels of participants involving this study were also low. However, after exposing the participants to a 30-min lecture which contains around 100 names, characters, and marks of commonly patients-identified OTC drugs by the patients in Jazan area, there were significant changes in the same previously measured parameters which can be seen as a significant drop-in dispensing time, decrease in the number of dispensing errors. These results were in parallel with the average quiz score which is significantly increased. Moreover, the percentage levels of the participants confidence were significantly increased as compared to pre-intervention group.

Patient management is a diverse series of tasks that includes a team of healthcare professionals with a wide spectrum of expertise and abilities. The central role of the pharmacist is drug dispensing. In England and Wales, community and hospital pharmacies together dispense approximately 900 million medicines annually and 134-341 estimated errors in dispensing have been

reported only in the community pharmacies (James et al. 2009). Community pharmacists play a vital role in delivering other services which have significant effects on patient health care outcome (Almaghaslah et al. 2019). Pharmacy students nowadays, as a part of their internship program, involve in providing pharmaceutical and health care services in the community pharmacies (Lenjisa 2015). Obtaining adequate and effective training improves the quality of the services provided as not only impacts on the students' knowledge but also improve their communication skills. Nonetheless, various obstacles are still being faced by the internship students, example of which is dispensing difficulties such as misunderstanding of patient needs which is due to lack of knowledge and experience. Such problem, subsequently, contributes to lower overall performance of final-year students and subsequently workers' and patients' satisfaction. In a review study, over 20 contributing factors attributed to medication errors have been mentioned. These factors include staff in-experience, poor communication, lack of training and knowledge, which all have sort of association with the hypothesis of this study (James et al. 2009). On the other hand, solving this problem would not only contribute to improve workers performance (decrease dispensing time and errors) and confident level, but also ensuring patients' satisfaction about services provided by community pharmacies.

Lacking of knowledge and experience and being unaware of the patients' terminologies that they use to request their over the counter medications are examples of the problems that pharmacists may encounter during their daily work in the pharmacy (Hayden and

Parkin 2020). These issues may lead to negative consequences such as medication dispensing errors which eventually may harm patients somehow (Ferner and Aronson 2006**,** Dilsha et al. 2020). However, the issue of medication errors can be prevented if their nature is identified and characterized (Dilsha et al. 2020). Numerous studies have been undertaken to examine factors that are associated with dispensing errors and their results have been used to enhance drug safety (James et al. 2008, Beso, Franklin, and Barber 2005, Samaranayake et al. 2013). These factors, which differ from one setting to another, include high workload, insufficient and in-experienced workers, cryptic handwriting, workplaces physical disturbances, and alike drug names (look-alike/sound-alike medicine names) (Gogazeh 2020, James et al. 2009, Dilsha et al. 2020, Anacleto et al. 2007, Peterson, Wu, and Bergin 1999,Withanachchi, Karandagoda, and Handa 2004). However, due to the lack of expertise of community pharmacy employees, particularly those who have recently-joined, few studies have delineated the issue of medication errors. Results from this study showed that enormous number of final-year pharmacy students at Jazan University were not familiar of these terms which consequently led to increase in time of dispensing (long waiting in the pharmacy) and incorrectly dispense medications. The findings also demonstrated that the times have been taken by final-year pharmacy students to dispense drugs were relatively long and the total errors in dispensing were high before the intervention. However, few participants were able to figure out these terms and correctly dispensed medications in relatively a short time, got excellent score in the quiz and were highly-satisfied about their

performance. These results may be attributed to the intelligence of some students, which help them to predict what they have been requested to dispense or have been previously exposed to such information.

To encourage customers visiting the same pharmacy and getting their medications re-filled repeatedly; the provided services should be in a high-quality and comply with market requirements such as reducing waiting time in the pharmacy, decreasing errors in dispensing (Naybour et al. 2019, Afolabi and Erhun 2005). Post-intervention results showed that the dispensing time and number of errors were significantly reduced. However, the average score of the quiz taken by the participants after intervention was increased. Moreover, the level of confidence during practice was significantly increased. These results indicate that the lecture given has a strong impact in reversing the previously measured parameters which may be associated with smooth and efficient practice in the community pharmacy. Nonetheless, few participants showed notable results in the dispensing time (outliers), dispensing errors, relatively low grade in the quiz (outliers) and they were neutral on their satisfaction level after the intervention. These results may be attributed to that those participants did not pay full attention to the information in the lecture or did not take the study seriously. Moreover, having a look on the dispensing time (sec) within and between groups, we found a huge variation in pre-intervention group (153.3) and (19) or post-intervention (95) and (10) sec which may be attributed to that the randomly chosen drugs to be dispensed are sometime easier to figure out and find them in the pharmacy than others.

Some of the major limitations that we have confronted in this study are the small sample size due to the low number of graduated students (approximately 80 students), 40 out of which participated in the study. Some of participants quit in the middle of the study with no reasons. The number of participants were not equal in gender (males more than females). Additionally, we were willing to conduct the part of the study in real pharmacy settings but we were unable due to precautions taken to reduce coronavirus outbreak.

The present study highlights the current deficiencies of knowledge and experience in dispensing practices, and overall future pharmacist performance at community pharmacies. However, pharmacy schools should have an important role to fill the knowledge gap and prepare the students to efficiently and smoothly work in the community pharmacies particularly during their internship period of time.

Based on the results from this study, we are highly recommended that pharmacy academic institutions take initiative of their students' development by building a good foundation to them before starting community pharmacy rotation as a part of the internship year. Moreover, in a collaboration with other colleges of pharmacy all over the kingdom, we recommend generating a book that has the most patients'-common terms, marks, and characteristics of OTC drugs and implementing it in the curriculum of pharmacy colleges (annually updated). Annual workshop is an alternative choice to increase student's awareness of these important names, marks, and characteristics of OTC drugs and improve students' performance while practicing at the community pharmacy. In addition, all final-year pharmacy students should be

enforced to pick the community pharmacy rotation as a part of their internship program (not optional rotation) since this career path will be the future of Saudi pharmacists (Saudization). Finally, training also is better to be a little bit earlier (second or third year in the curriculum of pharmacy colleges all over the kingdom) trying to get the students involved in the pharmacy daily work and exposed to the some of major challenges of pharmacy practice. earlier (second or third year in the curriculum of pharmacy colleges all over the kingdom) trying to get the students involved in the pharmacy daily work and exposed to the some of major challenges of pharmacy practice.

FUNDING

This research did not receive any specific grant from funding agencies in the public,

commercial, or not-for-profit sectors.

DECLARATION OF INTEREST

None.

AUTHORS CONTRIBUTION

Rayan A. Ahmed: Conceptualization, study design, original draft writing, proof reading and data collection and interpterion.
Mohamed E. Ahmed: Statistical analysis, interpterion and original draft writing.
Reem O. Elagi: Original draft writing, data collection and interpterion.
Hatim A. Masmali: Original draft writing and data collection.
Amal Y. Jandali: Conceptualization, original draft writing and data collection.
Ali A. Aloqayli: Original draft writing and data collection.
* All authors have critically reviewed and approved the final draft and are responsible for the content and similarity index of the manuscript.

REFERENCES

Abdel-Qader, Derar H., Ahmad Z. Al Meslamani, Penny J. Lewis, and Salim Hamadi. 2020. "Incidence, Nature, Severity, and Causes of Dispensing Errors in Community Pharmacies in Jordan." *International Journal of Clinical Pharmacy*. doi: 10.1007/s11096-020-01126-w.

Bin Abdulhak, Aref A., Mohamad A. Altannir, Mohammed A. Almansor, Mohammed S. Almohaya, Atallah S. Onazi, Mohammed A. Marei, Oweida F. Aldossary, Sadek A. Obeidat, Mustafa A. Obeidat, Muhammad S. Riaz, and Imad M. Tleyjeh. 2011. "Non Prescribed Sale of Antibiotics in Riyadh, Saudi Arabia: A Cross Sectional Study." *BMC Public Health*.

Afolabi, Margaret O., and Wilson O. Erhun. 2005. "Patients\' Response to Waiting Time in an out-Patient Pharmacy in Nigeria." *Tropical Journal of Pharmaceutical Research.* doi: 10.4314/tjpr.v2i2.14601.

Alaqeel, Sinaa, and Norah O. Abanmy. 2015. "Counselling Practices in Community Pharmacies in Riyadh, Saudi Arabia: A Cross-Sectional Study." *BMC Health Services Research* 15(1):1–9. doi: 10.1186/s12913-015-1220-6.

Alhamoudi, Abdulhakem, and Ashraf Alnattah. 2018. "Pharmacy Education in Saudi Arabia: The Past, the Present, and the Future." *Currents in Pharmacy Teaching and Learning* 10(1):54–60. doi: 10.1016/j.cptl.2017.09.014.

Aljameeli, Abdulaah. 2018. "Occupied Pharmacies!" *Al Madina Newspaper*.

Almaghaslah, Dalia, Abdulrhman Alsayari, Rayah Asiri, and Najla Albugami. 2019. "Pharmacy Workforce in Saudi Arabia: Challenges and Opportunities: A Cross-Sectional Study." *International Journal of Health Planning and Management* 34(1):e583–93. doi: 10.1002/hpm.2674.

Alte, Dietrich, Werner Weitschies, and Christoph A. Ritter. 2007. "Evaluation of Consultation in Community Pharmacies with Mystery Shoppers." *Annals of Pharmacotherapy*. doi: 10.1345/aph.1H565.

Anacleto, Tânia Azevedo, Edson Perini, Mário Borges Rosa, and Cibele Comini César. 2007. "Drug-Dispensing Errors in the Hospital Pharmacy." *Clinics*. doi: 10.1590/S1807-59322007000300007.

Beso, Adnan, Bryony Dean Franklin, and Nick Barber. 2005. "The Frequency and Potential Causes of Dispensing Errors in a Hospital Pharmacy." *Pharmacy World and Science*. doi: 10.1007/s11096-004-2270-8.

Dansky, K. H., and J. Miles. 1997. "Patient Satisfaction with Ambulatory Healthcare Services: Waiting Time and Filling Time." *Hospital and Health Services Administration*.

Dilsha, R. A. N., H. M. I. P. Kularathne, M. T. M. Mujammil, S. M. M. Irshad, and N. R. Samaranayake. 2020. "Nature of Dispensing Errors in Selected Hospitals Providing Free Healthcare: A Multi-Center Study in Sri Lanka." *BMC Health Services Research*. doi: 10.1186/s12913-020-05968-y.

Ferner, Robin E., and Jeffrey K. Aronson. 2006. "Clarification of Terminology in Medication Errors: Definitions and Classification." *Drug Safety*.

Gogazeh, Esraa. 2020. "Dispensing Errors and Self-Medication Practice Observed by Community Pharmacists in Jordan." *Saudi Pharmaceutical Journal*. doi: 10.1016/j.jsps.2020.01.001.

Gokcekus, Laika, Hale Zerrin Toklu, Rumeysa Demirdamar, and Bulent Gumusel. 2012. "Dispensing Practice in the Community Pharmacies in the Turkish Republic of Northern Cyprus." *International Journal of Clinical Pharmacy*. doi: 10.1007/s11096-011-9605-z.

Hayden, John C., and Rebecca Parkin. 2020. "The Challenges of COVID-19 for Community Pharmacists and Opportunities for the Future." *Irish Journal of Psychological Medicine*.

James, K. Lynette, Dave Barlow, Robin Burfield, Sarah Hiom, Dave Roberts, and Cate Whittlesea. 2008. "A Study of Unprevented Dispensing Incidents in Welsh NHS Hospitals." *International Journal of Pharmacy Practice*. doi: 10.1211/ijpp.16.3.0008.

James, K. Lynette, Dave Barlow, Rowena McArtney, Sarah Hiom, Dave Roberts, and Cate Whittlesea. 2009. "Incidence, Type and Causes of Dispensing Errors: A Review of the Literature." *International Journal of Pharmacy Practice*. doi: 10.1211/ijpp/17.1.0004.

Lenjisa, Jimma Likisa. 2015. "Analysis of Dispensing Practices at Community Pharmacy Settings in Ambo Town, West Shewa, Ethiopia." *Journal of Community Medicine & Health Education*. doi: 10.4172/2376-0214.1000329.

Naybour, Matthew, Rasa Remenyte-Prescott, and Matthew J. Boyd. 2019. "Reliability and Efficiency Evaluation of a Community Pharmacy Dispensing Process Using a Coloured Petri-Net Approach." *Reliability Engineering and System Safety* 182(October 2018):258–68. doi: 10.1016/j.ress.2018.09.022.

Peterson, G. M., M. S. H. Wu, and J. K. Bergin. 1999. "Pharmacists' Attitudes towards Dispensing Errors: Their Causes and Prevention." *Journal of Clinical Pharmacy and Therapeutics*. doi: 10.1046/j.1365-2710.1999.00199.x.

Sahir, Arooj, Jamila Sahir, MairaFaizullah Shah, and Nisar-ur-Rehman. 2014. "Archives of Pharmacy Practice on Pharmacy Education." *Archives of Pharmacy Practice* 5(2):95. doi: 10.4103/2045-080x.132668.

Samaranayake, N. R., S. T. D. Cheung, W. C. M. Chui, and B. M. Y. Cheung. 2013. "The Pattern of the Discovery of Medication Errors in a Tertiary Hospital in Hong Kong."

International Journal of Clinical Pharmacy. doi: 10.1007/s11096-013-9757-0.

Sansom, Victoria E., and Emily A. Cox. 2013. "Student Pharmacists' Perspective on Actual vs. Simulated Pharmacy Practice Experiences." *Currents in Pharmacy Teaching and Learning*. doi: 10.1016/j.cptl.2012.09.012.

Soto, Cory, Jamie Stiner, Daniel O. Noji, Jeffrey M. Rusheen, and Yue Ming Huang. 2016. "Creating a Simulated Pharmacy." *Simulation in Healthcare*. doi: 10.1097/SIH.0000000000000163.

T., Joshi, and Boyd M. 2015. "An Evaluation of the Impact of New Undergraduate Pharmacy Business Simulation Module on Students' Perceived Preparedness for Practice." *International Journal of Pharmacy Practice*.

Weiss, Marjorie C., Anneka Booth, Bethan Jones, Sarah Ramjeet, and Eva Wong. 2010. "Use of Simulated Patients to Assess the Clinical and Communication Skills of Community Pharmacists." *Pharmacy World and Science*. doi: 10.1007/s11096-010-9375-z.

Withanachchi, Nimnath, Wimal Karandagoda, and Yujiro Handa. 2004. "A Performance Improvement Programme at a Public Hospital in Sri Lanka: An Introduction." *Journal of Health Organization and Management*. doi: 10.1108/14777260410560820.

إلقاء محاضرة توعوية بالمصطلحات الرائجة بين المرضى للأدوية اللاوصفية على طلاب وطلابات السنة الأخيرة في كلية الصيدلة وارتباطه بسلاسة وكفائة التدريب في صيدليات المجتمع

ريان عبدالباسط أحمد[1]*، محمد الدقيري أحمد[٢]، ريم عثمان علاقي[1]، حاتم أحمد مسملي[1]، أمل يحيى جندلي[1]، علي أحمد العقيلي[1]

قسم الأدوية والسموم ، كلية الصيدلة، جامعة جازان،المملكة العربية السعودية

الملخص

لوحظ في الآونة الأخيرة توجه خريجي كليات الصيدلة السعوديون للعمل في صيدليات المجتمع. كون الخريج أقل ثقة عند بدء العمل، ويقضي وقتاً طويلاً في تحضير الأدوية للمرضى، ويرتكب أخطاء أثناء عملية التحضير مقارنة بالممارس للمهنة منذ زمن فهذه من أهم التحديات التي تواجه الصيدلي حديث التخرج عند بدء العمل في صيدليات المجتمع. في هذه الدراسة تم تحديد مدى تأثيرالنقص المعرفي، لطلاب وطالبات السنة الأخيرة في تخصص الصيدلة ، جامعة جازان، بأهم المصطلحات المتعارف عليها بين المرضى عند رغبتهم في الحصول على دواء معين من الصيدلية ومدى تأثيره العكسي على عملية تحضير الأدوية إضافة إلى إمكانية عكس هذه المعادلة بعد التدخل الملائم. تم تقييم وقياس مستوى المعرفة بأسماء وعلامات الأدوية التي لا تستلزم وصفة طبية لصرفها والمتعارف عليها بين المرضى في منطقة جازان ومدى تأثيرها على عملية تحضيرالأدوية (وقت التحضير/عددالأخطاء المرتكبة عند التحضير) إضافة إلى رضا طالب السنة الأخيرة عن نفسه في عملية التحضير. بعد ذلك، تم دراسة دور المؤثر الخارجي وذلك بتقديم محاضرة مسجلة تحتوي على حوالي مائة اسم وعلامة للأدوية التي لا تستلزم وصفة طبية لصرفها والمتعارف عليها بين المرضى في منطقة جازان. لدراسة دور المؤثر الخارجي والذي استخدم في حل هذه الإشكالية، تم إعادة تقييم نفس المعاييرالمذكورة سابقا. أجريت هذه الدراسة باستخدام سيناريو يعبر عن شخص مريض والصيدلي والصيدلية (افتراضياً). حيث تم تسجيل ردود المشاركين في الدراسة حسب الوقت الذي يتطلبه إعداد الوصفات الطبية وعدد المحاولات الصحيحة والخاطئة لتحضير الأدوية ومستوى رضا الطلاب والطالبات في السنة الأخيرة بكلية الصيدلة جامعة جازان عن أدائهم عند المشاركة في عملية تحضير الأدوية للمرضى (قبل التدخل بالمؤثر الخارجي مقارنةً بما بعده). أوضحت هذه الدراسة أن هناك تغيرات واضحة من خلال تقليل وقت التحضيرللأدوية وعدد الأخطاء المرتكبة أثناء عملية التحضير إضافة إلى زيادة مستوى الرضا عن الأداء بعد التدخل بالمؤثر الخارجي مقارنةً بما قبله. معرفة طلاب وطالبات السنة الأخيرة بكلية الصيدلة بهذه العلامات وأسماء الأدوية التي يتم صرفها بدون وصفة طبية

والمتعارف عليها بين المرضى في المنطقة قد يسهم في تحسين عملية صرف الأدوية وزيادة كفاءة الأداء العام لهم أثناء التدريب والعمل في صيدليات المجتمع.

الكلمات المفتاحية: التوعية، الصيدلية المجتمعية، التدريب الصيدلاني، الأدوية التي لا تستلزم وصفة طبية لصرفها

A Study on Mathematical Models for Treatment of Wastewater

Ahmed Hussein Msmali[1*], Zico Mutum[1], Waleed Ali Rajhi[1], Sami Mohammed Hazazi[1]

[1]Department of Mathematics, Faculty of Science, Jazan University, Saudi Arabia;

Abstract

One of the most challenging factors throughout the world is inadequate access to clean water. Over the years, wastewater plants have chosen many alternative processes in producing clean water. However, wastewater plants are likely to experience problems due to the involving of organic matter or pollutants. Mathematical modelling for wastewater treatment process along with the study of removing different types of pollutants will facilitate the wastewater plants. In this paper, we study some mathematical models describing that varying influent flow rate has a significant impact on the behaviour of the concentration throughout the system. In addition, the modelling with different Monod equations can provide useful information of substrate microorganism growth in wastewater treatment plants.

Keywords: Wastewater Treatment; Mathematical Model; Monod, Residence Time;

1. Introduction

Mathematical modeling of wastewater treatment plants play an important role in the process design and in determination of optimal operating condition. Some research has been undertaken in the development of mathematical models, their calibration and application to large wastewater treatment plants. The mathematical model is widely used for full - scale wastewater treatment plants in the Activated Sludge Model No.1, that would describe the biological removal of organics and nitrogen. In the later version of ASM model, the extension of the model for biological phosphorus removal and more mechanical descriptions of biological processes are provided. Some small wastewater treatment plants generally do not provide much opportunities for control of influent conditions, nor for control of operating parameters based on on-line measurement. Therefore, modeling of the small wastewater treatment process focusing on attaining improvements in the area of process design would be more effective. Figure 1, provides the modeling procedure for the optimal function of wastewater treatment plants

.

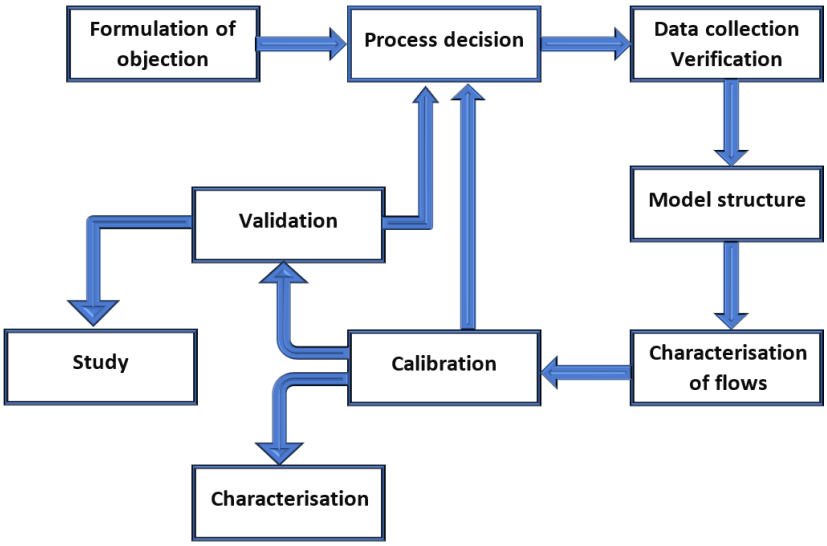

Figure 1: Structure of ASM models for wastewater treatment process.

Saudi Arabia has witnessed one of the fastest socio-economic development over the last decades, and urbanization increases gradually. As a result, water demand for all purpose has tremendously increased, in a country with hot climate with limited natural water resources. According to *Qatrah* [4], Saudi Arabia is the world's third largest per capita consumer of water after the United States of America. The gap of the demand of water supply was filled through ground water resources, water desalination, and minimal use of treated wastewater. So, the existence of wastewater treatment plants is important to bridge the gap of water demand and supply. The treated wastewater is considered as an integral part of water resources in Saudi Arabia used it as a major supply for nonportable water demands such as agricultural, industrial and commercial uses [5]. The Ministry of Water and Electricity aims to provide entire sewage collection and treated wastewater services to every city with a population above five thousand by 2025 [6].

There are thirty-four major wastewater treatment plants with a capacity of 748 million cubic meters per year, and 15 more are under construction. The reuse of water in Saudi Arabia is growing both at the level of buildings and at the level of cities. At city level, treated wastewater is being reused for landscaping, irrigation and in industries such as refining. In the capital city of Saudi Arabia, 50 million cubic meters per year is pumped over 40km and 60m elevation to irrigate 15,000 hectares of wheat, fodder, orchards and palm trees [7]. The major wastewater treatment plants in Saudi Arabia serving various cities are given in Table 1.

Sl.	City	Plant Name	Design (m^3/day)	Treatment Scheme	Actual (m^3/day)	Disposal
1	Buraidah	Buraidah	11000	FP+MP	13000	To sand dunes
2	Unaizah	Unaizah	7080	AL	9900	To Wadi
3	Al-Kharj	Al-Kharj	21000	AL+SF	21600	To Wadi
4	Qatif	Sanabis	8340	2 stage FP	22195	Gulf
5	Qatif	Gesh	8990	2 stage FP	15930	Gulf
6	Qatif	Awamia	9260	2 stage FP	13430	Gulf
7	Qatif	Qatif	210000	OD	35000	Gulf + L.I.
8	Al-Hasaa	Oyoon	6310	2 stage FP	17100	To Lagoon
9	Al-Hasaa	Emran	13320	2 stage FP	22100	To Lagoon
10	Al-Hasaa	Hufuf-Mubarraz	29500	2 stage FP	136780	To Lagoon
11	Khafji	Khafji	25000	2 stage FP	5190	Gulf
12	Jeddah	Al-Khomra	36000	TF (stone)	66000	Red Sea
13	Jeddah	Plant C	40000	PCS	63000	L.I. + Lagoon
14	Jeddah	Plant A	32000	PCS	55000	L.I. + Red Sea
15	Jeddah	Bani Malik	8000	PCS	6500	L.I. mostly
16	Jeddah	Al-Jamia	8000	PCS	7000	Red Sea + L.I.
17	Jeddah	Tertiary (Al-Khomra)	30000	TF+O+C+SF+RO	20000	Red Sea L.I.
18	Jeddah	Al-Iskan	3000	AS	3,500	
18	Makkah	Old plant	24000	TF (stone)	65000	Wadi +A.I.
19	Makkah	New	50,000	PF+AC+NDN		
20	Riyadh	Al-Hayer old (South)	200,000	TF + PL+ASD	200,000	Wadi + A.I.+Ref.
21	Riyadh	Al-Hayer new (North)	200000	AS + NDN+F	200000	Wadi + A.I.+Ref.
22	Riyadh	Refinery	20000	C+F+RO+IE	13500	
23	KSU	KSU Plant	8000	Settling, TF	8000	L.S. + power plant
24	Riyadh	Diplomatic Quarter	9300	Screening, AS	9500	L.I.
25	Dammam	Dammam	208000	OD	140000	Gulf + L.I.
26	Al-Khobar	Al-Khobar	133000	OD	100000	Gulf
27	Madinah	New	120000	AS	100000	Wadi + L.I. + A.I.
28	Safwa	Safwa	7570	CM	8600	Gulf
29	Khamis-Mushait	Al-Dhoba	7500	OD	10,000	Wadi + L.I. + A.I.
30	Abha	Abha	9000	Aeration	11500	Wadi
31	Taif	Taif	67000	AS+NDN+F+ACF	34000	L.I. + A.I.
32	Jubail	Jubail Industrial city	12500	Tertiary	38630	A.I.
33	Saihat	Saihat		Secondary	15717	
34	Aramco 9 plants	Saudi Aramco	66000	Variable	66000	A.I. + Sea

Table 1: Major wastewater treatment plants in Saudi Arabia; L.I indicates Landscape irrigation; A.I. is Agricultural irrigation; Ref Refinery; FP is Facultative ponds; MP is Maturation ponds; AS is Activated sludge; TF is Trickling filters; SF is Sand filters; RO indicates Reverse Osmosis; IE is Ion exchange; OD indicates Oxidation ditch; PCS is Package contact stabilization; AL is Aerated lagoons; O indicates Ozonation; C is Clarification; NDN is Nitrification-Denitrification; PL indicates Polishing lagoons; ASD is Anaerobic sludge digestion; F is the Filtration; CM is the Completely mixed; ACF is the Activated carbon filters and PF is the Plug flow (source: King Abdullah University of Science and Technology).

The most popularly used secondary treatment mechanism for wastewater in Saudi Arabia is conventional activated sludge systems. Some of the common treatment techniques are filtrations and chlorination and a few of the wastewater plants used reverse osmosis. The treated wastewater is suitable for various applications in industry and agricultural irrigation, as long as the plants are operated according to the international standards. In [8], the authors apply mathematical modeling approaches for pump station in a sewer system to reduce energy and economical cost. They focused on the quantity and quality model of the sewer network by studying the sequence of rainfall events effecting the flow condition in pump stations. The cumulative frequency analysis of water volume and pollutants is done to assess the pump rule efficiently. Optimization concept is applied to perform the iteration of the inflow and the volume of water. In [9], the authors studied the effect of coagulation process as a pretreatment method on real tannery

wastewater prior to anaerobic digestion (AD) facilitating the removal of heavy metals and minimizing the effect on the biological process.

Mathematical modeling of wastewater treatment process plays an important role in the process of designing and optimizing the performance of existing plants. Many researchers have developed mathematical models to calibrate and apply in large wastewater treatment plants. The widely used mathematical model for full scale wastewater treatment plant is the activated sludge model No.1 (ASM1) [1]. This model describes the biological removal of organic and nitrogen, and validates its optimal performance by statistical models. The more advanced mechanical description of biological processes is provided in the updated version of the ASM model. The activated sludge model is one of the most important treatment processes for various wastewaters, and about 90% of the municipal wastewater treatment plants used it in their treatment process [2,3].

In this paper, Section 2 provides some popular types of membrane used in wastewater plants Section 3 study some of the mathematical models for the dynamic behaviors of wastewater treatment process. In section 4 provides the analysis of the mathematical models about the bioreactor for wastewater plants. And finally, Section 5 states the conclusion of our study.

2. Membrane for Wastewater Treatment Process

In wastewater treatment process, membrane technology is defined as a number of different processes using synthetic membranes to separate chemical substances, which has been recognized as the key technology for the separation of contaminants from polluted sources thus purifying original waters [15]. Membranes are selective barriers that separate two different phases, allowing the passage of certain components and the retention of others. The driving force for transport in membrane processes can be a gradient of pressure, chemical potential, electrical potential or temperature across the membrane. Membrane processes rely on a physical separation, usually with no addition of chemicals in the feed stream and no phase change, thus standing out as alternatives to conventional processes. In this section, we highlight some of the most popular membranes for wastewater treatment plants.

2.1 Ultrafiltration

Ultrafiltration is often used as a pre-treatment step prior to RO treatment, its efficacy in the removal of viruses is more widely reported in the scientific literature than for other membrane-based technologies. It can separate particles between 10 $\boldsymbol{\mu m}$ (micrometer) which is between microfiltration and reverse osmosis [12]. It is very prominent water filter with low energy consumption in the removal of pathogenic microorganism, macromolecules and suspended matters. There is some limitation for ultrafiltration membrane such as the inability to remove any dissolved inorganic substances from water and regular cleaning to maintain high pressure water flow. The induced amination of ultrafiltration with high flux membrane was found to be resistant to organic fouling (collection of carbon-based material), and can be applicable to the wastewater treatment plants.

Kwang et al. [19] used a combination of coagulation and ultrafiltration (UF) on a pilot scale for wastewater reclamation. They improved the removal of MS2 bacteriophage by optimizing the pH of the secondary effluent to a range of 5–6 depending on the effluent. Once improved, the virus removal factor was in the 6.8–7.5 log10 range. Additionally, to obtain a more stable transmembrane pressure, an additional sedimentation step was required. The ideal combination was a hybrid coagulation-sedimentation-UF system.

2.2 Microfiltration

It is a pressure driven process where the separated compounds are 0.1- 0.2 μm (micrometer) such as nanoparticles [12]. It is considered as the first treatment of RO membrane process. It can remove little or no organic matter, however, when pre-treatment is applied increases removal of organic material can occur. It can be used as a pre-treatment to RO to reduce the fouling potential. The main disadvantage of this membrane is that it cannot filter contaminants (dissolved solids) that are less than 1mm in size [25]. The microfiltration is not suitable for virus removal.

2.3 Sand filtration

Some of the commonly used wastewater treatment is sand filtration and usually have less than one-unit log 10 virus removal. The advance wastewater treatment plants, north of Dhahran, in Saudi Arabia uses twenty-four DynaSand filters, for irrigation purposes [20]. In the paper [21], the authors reported on the molecular mechanism for unprecedented high virus removal from a practical sand filter. They have developed functionalized sand filters using a water extract of *Moringa Oleifera* seeds. Then they tested the efficiency of the obtained sand using MS2 bacteriophage virus, obtaining an impressive 7 log10 reduction in virus content. The mechanism implies that MS2 has affinity for some components from the seeds and binds to it. It also implies that the functionalized sand will progressively get saturated and will eventually have to be replaced or regenerated in some way.

2.4 Reverse osmosis

In [22], recently reviewed the treatment of waterborne pathogens by reverse osmosis. They provide complete description of the type of pathogens that are waterborne which are divided in three different groups: protozoans (5–100 μm), bacteria (0.5 –1.0 μm) and viruses (0.01 – 0.1 μm); as well as requirements for Reverse Osmosis membrane materials. They indicated that Reverse Osmosis is seldom used to remove pathogens from water even if it is one of the techniques reported by the EPA with indicative log removals above 6. This is because reverse osmosis is typically coupled with a pre-treatment system, often ultrafiltration, to reduce foulants which may interfere with the reverse osmosis process. However, RO can be used in combination with such a suitable pretreatment, to remove particulate matter, and post treatment, to complete the removal of any remaining contaminants.

2.5 Nanofiltration

Nanofiltration (NF) is used to remove ions that contribute mainly to the osmotic pressure hence allows operation pressure that are lower than those of RO. For this filtration, the effective pre-treatment is needed for some heavily polluted water. These membranes are sensitive to free chlorine and difficult to separate soluble element from water. Some studies had reported that nanofiltration membranes were used for water treatment and its composite membrane had greater hydrophilic surface which gave rise to high pure water flux compared to the pure polymer [23].

3. Mathematical Modeling for Wastewater treatment

Over the years, the knowledge, understating of biological, and chemical wastewater treatment have advanced approaches over the conventional techniques. These new approaches include the application of mathematics, statistics, physics, chemistry and bioprocess engineering. In this section, we highlight mathematical modeling approaches for better treatment of raw wastewater in wastewater treatment plants. The models for a wastewater treatment plant describes the biochemical and physical process involved in the technical purification of wastewater. The figure 2 shows the mechanism of the wastewater treatment process. In this section, we study some mathematical models used to

facilitate or optimize the treatment of raw wastewater from wastewater treatment plants.

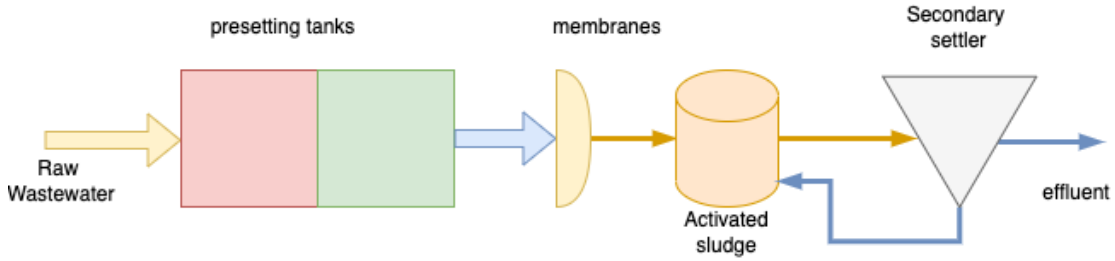

Figure 2: Approaches for wastewater treatment process.

In [8], the authors apply mathematical modeling approaches for pump station in sewer system to reduce energy and economical cost. They focused on the quantity and quality model of the sewer network by studying the sequence of rainfall events effecting the flow condition in pump stations. The cumulative frequency analysis of water volume and pollutants is performed to assess the pump rule efficiently. Optimization concept is applied to perform the iteration of the inflow and the volume of water. In [9], the authors studied the effect of coagulation process as a pretreatment method on real tannery wastewater prior to anaerobic digestion (AD) facilitating the removal of heavy metals and minimizing the effect on the biological process.

3.1 Kinetic Models

The first order kinetic model is a nonlinear model that has been used to predict pollutant removal in wastewater treatment system [10]. The model equation is given as follows;

$$\frac{dS}{dt} = -kS, \quad \text{where} \quad S_{out} = S_{in}e^{-k(HRT)}. \tag{1}$$

The S_{out} is the concentration of the pollutant at the system outlet (mg/liter), S_{in} is the concentration of the pollutant at the system inlet (mg/liter), and HRT is the duration of hydraulic retention of the system expressed in days. The monitoring data are adjusted to generate the above equation (1) and the similar process for this treatment is mentioned in [11].

The first order kinetic model equation provides the parameter k representing the rate of removal of pollutant from the water.

The rate of change in substrate concentration in the system with assuming the first order model for substrate removal from wastewater treatment plant is given as follow

$$\frac{-dS}{dt} = \frac{QS_{out}}{V} = \frac{QS}{V} = -kS. \tag{2}$$

Under steady state conditions, the rate of change in substrate concentration due to accumulation $\frac{-dS}{dt}$ is negligible and the equation given in (1) can be written as

$$\frac{S_{out} - S}{HRT} = kS. \tag{3}$$

The second-order kinetic model to predict substrate removal from the wastewater treatment system is given as,

$$\frac{dS}{dt} = -k\,X\left(\frac{S_{out}}{S_{in}}\right)^2. \tag{4}$$

After linearization, we have

$$\frac{S_{out}HRT}{S_{in} - S_{out}} = HRT + \frac{S_{in}}{kX}, \tag{5}$$

where $\frac{S_{in}}{kX}$ is considered as the model constant.
We can also write the above equation (4) as

$$\frac{S_{out}HRT}{S_{in}-S_{out}} = a + bHRT, \tag{6}$$

where the constants a and b will be drawn as y-intercept and the slope of the line respectively. In the above-mentioned equations, HRT is expressed as per day, and the pollutant removal speed constant or k is calculated by $a = \frac{S_{out}}{(k*X)}$, where X is the average biomass inside the reactor. If $\frac{S_{out}}{S_{in}-S_{out}}$ expressed the removal efficiency and is denoted by E, we can write $\frac{HRT}{E} = a + bHRT$.

3.2 Modified Stover-Kincannon Model

This model is used to determine the change rate of substrate concentration at steady state. The Stover-Kincannon considers the substrate removal rate as a function of organic loading rate at steady state [13]. The equation of this model is given as follows;

$$\frac{dS}{dt} = \frac{Q}{V}.(S_{in}-S_{out}) = \frac{U_{\max\left(\frac{QS_{in}}{A}\right)}}{K_B + \left(\frac{QS_{in}}{A}\right)}, \tag{7}$$

after linearization we have,

$$\frac{V}{Q(S_{in}-S_{out})} = \frac{K_B}{U_{max}} * \frac{V}{Q.S_{in}} + \frac{1}{U_{\max}}. \tag{8}$$

The intercept and the slope of the equation (6), will be $\frac{1}{U_{\mathrm{m}}}$ and $\frac{K_B}{U_{\mathrm{m}}}$ respectively. The effluent substrate concentration is calculated by using the following equation (5), provided organic loading rate and influent substrate concentration are given. The S_{in} and S_{out} are the influent and effluent substrate concentrations respectively, U_{max} the maximum rate of substrate utilization (g/liter.day), K_B is the saturation constant (g/liter.day), and Q is the flow rate (1/day).
The substrate balance equation for the reactor can be written as follows:

$$QS_{in} = QS_{out} + V\left(\frac{dS}{dt}\right). \tag{9}$$

Using equation (3), we have the following:

$$QS_{in} = QS_{e=out} + V\left(\frac{U_{\max\left(\frac{QS_{in}}{A}\right)}}{K_B + \left(\frac{QS_{in}}{A}\right)}\right). \tag{10}$$

Solving equation (8), we obtained the following equations representing the effluent substrate concentration by equation (9) and the volume of the anaerobic filter represented by equation (10).

$$S_{out} = S_{in} - \frac{U_{\max} S_{in}}{K_B + \left(\frac{QS_{in}}{V}\right)}. \tag{11}$$

$$V = \frac{QS_{in}}{\left(\frac{U_{\max} S_{in}}{S_{out}-S_{in}}\right) - K_B}. \tag{12}$$

3.3 Monod Model

Monod equation is a mathematical model used to study the behavior of the growth of microorganism in an aqueous environment with the limited nutrients. It is used for a small wastewater treatment plant to describe relationship between the rate of nitrates removal and available substrates [14]. It determines the specific rate of substrate utilization; the equation is given as follows:

$$r_{su} = \frac{KS_e}{K_s + S_e} X, \tag{13}$$

where r_{su} is the rate of substrate utilization (g/l.day), S_e and X are the effluent substrate concentration (g/l) and active biomass concentration (g/l), respectively. The equation for substrate utilization can be written as follow:

$$U = \frac{-r_{su}}{X} = \frac{KS_e}{K_s + S_e}. \tag{14}$$

The equation that determines the rate of microorganism's fluctuations in the wastewater treatment plant can be written as,

$$\frac{ds}{dt} = \frac{QS_0}{V} - \frac{QS_e}{V} - \frac{\mu X}{V}, \tag{15}$$

where μ is the specific biomass growth rate (per day) and V is the reactor volume. The equation for the specific biomass growth rate can be written as follows:

$$\mu = \frac{U_{\max S_e}}{K_s + S_e} = \frac{1}{SRT} + K_d, \tag{16}$$

$$SRT = \frac{XV}{QX_e}, \tag{17}$$

where SRT is the solid retention time, and K_d is the constant death rate of the biomass.

3.4 Residence time model

The settling tank as shown in Figure 1, is the model with 2 tanks in series. All other compartments were best modelled as 1 tank. No bypass flows were identified. We assume that the setting tank has a dead volume of about 70-80%, the membranes was completely mixed, the activated sludge compartment had a volume of 10- 15% and the secondary settler also had about 40% volume. We expect that there was no back flow except for the recirculation from the settler to the activated sludge tank. The mathematical model governing the above Figure 1, is given by the following system of equations adopted from [24].

$$\frac{dX_1}{dt} = \frac{Fin}{0.3V_1}[X_{in} - X_1] \tag{18}$$

$$\frac{dX_2}{dt} = \frac{Fin}{0.3V_1}[X_1 - X_2] \tag{19}$$

$$\frac{dX_3}{dt} = \frac{Fin}{V_3}[X_2 - X_3] \tag{20}$$

$$\frac{dX_4}{dt} = \frac{Fin}{0.9V_4}[X_3 - 2.6\,X_4 + 1.6X_5] \quad (22)$$

$$\frac{dX_5}{dt} = \frac{Fin}{V_5}2.6[X_4 - X_5] \quad (22)$$

Where $X_i, i = 1,2,3,4,5$ represents the residence time (time it takes to entirely exchange the volume of the reactor) for each compartment and it is expressed in days.

Parameter	Liter/days
Fin	750
V_1	850
V_2	3540
V_3	1250
V_4	2690
V_5	3690

Table 2: Parameter values for the flow rate and volume.

The above system of equations (18)- (22) are simulated using MAPLE software with the assumed parameters from Table 2.

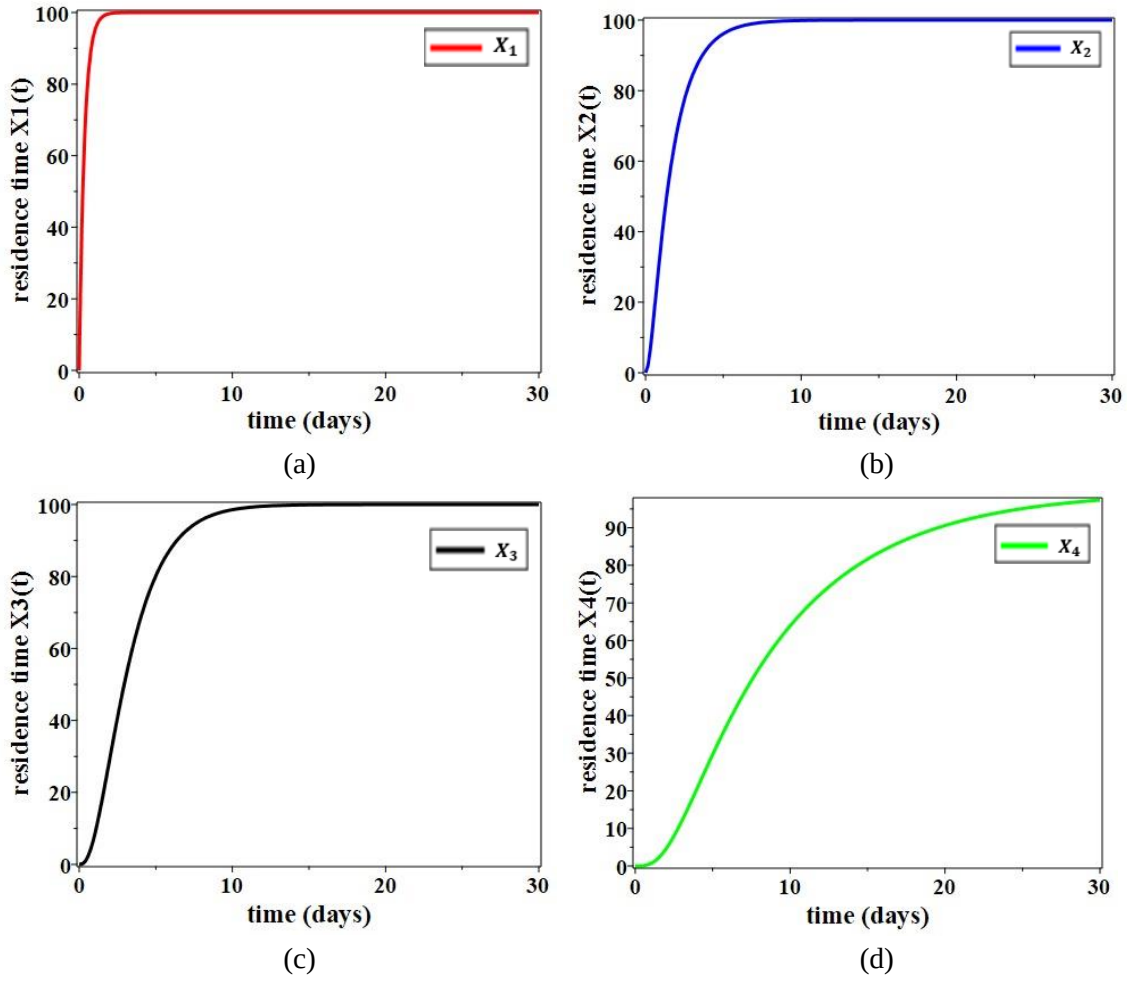

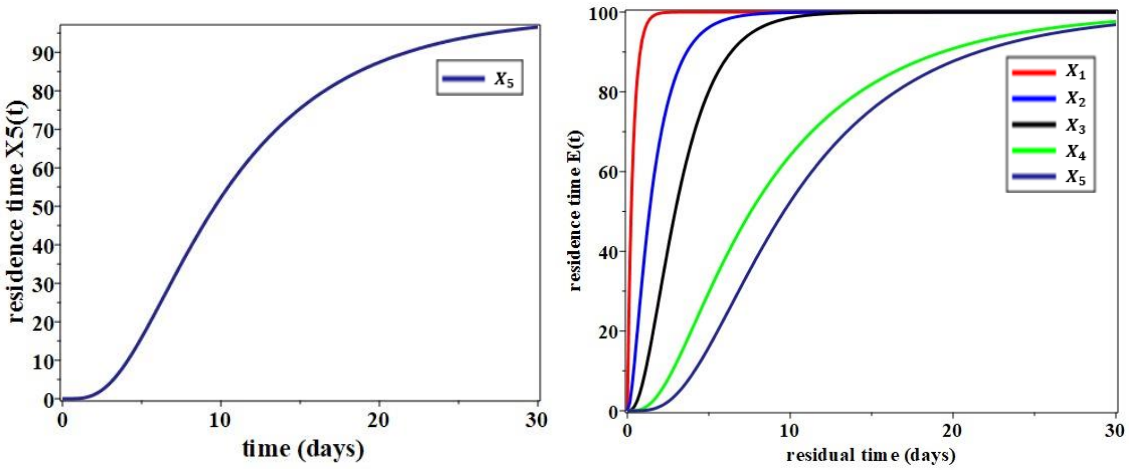

(e) (f)

Figure 3: Residence time distribution curve from validation trace experiment for (a) Equation (7), (b) Equation (8), (c) Equation (9), (d) Equation (10), (e) Equation (11), and (f) system of all the equations (7)-(11).

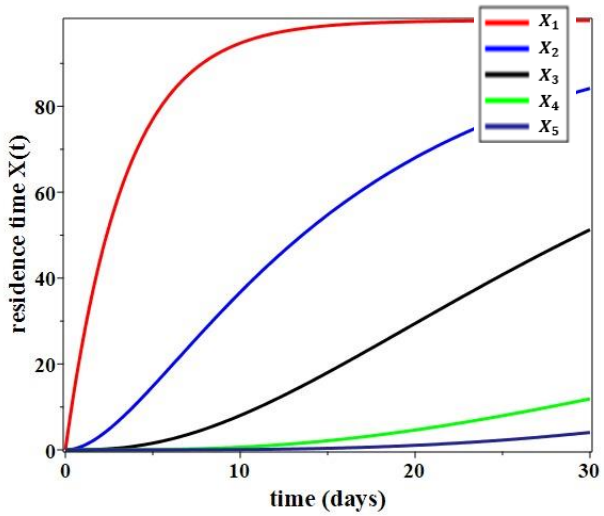

Figure 4: Residence time distribution curve from validation trace experiment with the flowrate of 75 liter/meter.

The figure 4 shows the behavior of the residence time depends on the flowrate in the reactor. We observed from the above figures that with lower flowrate corresponds to lower the residence time of the wastewater treatment reactor and vice versa.

3.4.1 Stability Analysis

In this section, we study the local stability of the steady state x_s by examining the above system of equations. The steady state is asymptotically stable if the real parts of all eigenvalues are negative. If one eigenvalue has a positive real part then the steady state is unstable. While the stability of the steady state x_s depends on the sign of the real parts of the eigenvalues, the nature of the solution around the steady state depends essentially on the nature of the eigenvalues. The Jacobian Matrix for the system of equations (18)-(22) is given as follows;

$$Ja = F_{in}\begin{bmatrix} -\frac{3.33}{V_1} & 0 & 0 & 0 & 0 \\ \frac{3.33}{V_2} & -\frac{3.33}{V_2} & 0 & 0 & 0 \\ 0 & \frac{1}{V_3} & -\frac{1}{V_3} & 0 & 0 \\ 0 & 0 & \frac{1.11}{V_4} & -\frac{2.88}{V_4} & \frac{1.78}{V_4} \\ 0 & 0 & 0 & \frac{2.6}{V_5} & -\frac{2.6}{V_5} \end{bmatrix} \quad (23)$$

The Eigenvalues of the above Matrix (23) is

$$F_{in}\begin{bmatrix} -\frac{3.33}{V_1} \\ -\frac{3.33}{V_2} \\ -\frac{1}{V_3} \\ -\frac{5\times10^{-5}\left(26\times10^{3}V_4 + 28889V_5 - 10^{4}\sqrt{A}\right)}{V_4V_5} \\ -\frac{5\times10^{-5}\left(26\times10^{3}V_4 + 28889V_5 + 10^{4}\sqrt{A}\right)}{V_4V_5} \end{bmatrix}, \quad (24)$$

where $A = 6.76\,V_4^2 + 3.4671\,V_4\,V_5 + 8.3457\,V_5^2$. In this study we found that all the eigenvalues were negative, hence the steady state was a stable node and the trajectory approach the neighbourhood of the node.

4. Bioreactor model

The performance of many biological processes that are carried out in well-stirred reactors may be improved by replacing a single bioreactor with a cascade of two or more bioreactors [17]. The standard reactor cascade (SRC) and the step-feed reactor cascade (SFRC) are commonly used in wastewater treatment plants. In SRC, the feed stream flows into the first reactor of the cascade. The SFRC is similar to the standard configuration in that the product steam from the first reactor flows into the second reactor. They differ in how the feed stream is treated.

A continuous flow bioreactor is also used to improve the performance of the reactor in wastewater treatment plants. It contains a microorganism through which a substrate flows at a continuous rate. The microorganism grows in the vessel through consumption of the substrate to produce more microorganism, and the product flow out the reactor. To get the optimal performance, a single continuous flow bioreactor is often replaced by a sequence of bioreactors. In a standard reactor cascade, the feed stream flows into the first reactor of the cascade [18].

We model a bioreactor as well-mixed vessel containing microorganism (X), through which a substrate (S) flows at a continuous rate (F). The microorganism grows in the vessel to produce more cells and products (P), while the substrate is consumed leading to a decrease in S. The unused substrate, microorganisms and products flow out of the reactor. This model arises in a multitude of applications, one of which is in the modeling of biological wastewater treatment process. Before the contaminated wastewater can be released into

rivers, the level of pollution in the water must be reduced to an acceptable level.

4.1 Modeling of microorganism growth

In membrane bioreactors, a permeable membrane is used which physically retains microorganisms
inside the reactor whilst allowing the substrate and products to leave. Entrapping the microorganisms in this manner increases their concentration and results in a greater conversion of the substrate [16]. A general way to model a specific growth rate of microorganism μ growing on a limiting substrate is to use the Monod model. This can be written as follows,

$$\boldsymbol{Monod_1} = \frac{\boldsymbol{\mu_m S}}{\boldsymbol{K_s + S}} \tag{25}$$

$$\boldsymbol{Monod_2} = \boldsymbol{\mu_m}\left(\frac{\boldsymbol{S}}{\boldsymbol{K_s X + S}}\right). \tag{26}$$

Where $\boldsymbol{\mu_m}$ is the maximum specific growth rate, $\boldsymbol{K_s}$ is the Monod constant, and $\boldsymbol{S}$ is the concentration of the substrate in the reactor.

We can model the growth of microorganism in bioreactors by using the above two equations (25) and (26).There involves free parameters while modelling with biological and physical systems. The number of parameters should be reduced by non-dimensionalising the problem. By introducing dimensionless variables for the substrate and microorganism concentration, the system of the non-dimensional model is given by the following equations;

$$\frac{dS^*}{dt^*} = \frac{(S_0^* - S^*)}{\tau^*} - Monod_i \tag{27}$$

$$\frac{dX^*}{dt^*} = \frac{(X_0^* - X^*)}{\tau^*} + R^*X^* + Monod_i - k_d^*X^* . \tag{28}$$

Where $\boldsymbol{i = 1, 2}$. $\boldsymbol{S_0^*}$ is the dimensionless substrate concentration in the feed, $\boldsymbol{X_0^*}$ is the dimensionless microorganism concentration in the feed, $\boldsymbol{k_d^*}$ is the death rate of the microorganism, and $\boldsymbol{\tau^*}$ denotes the dimensionless residence time.

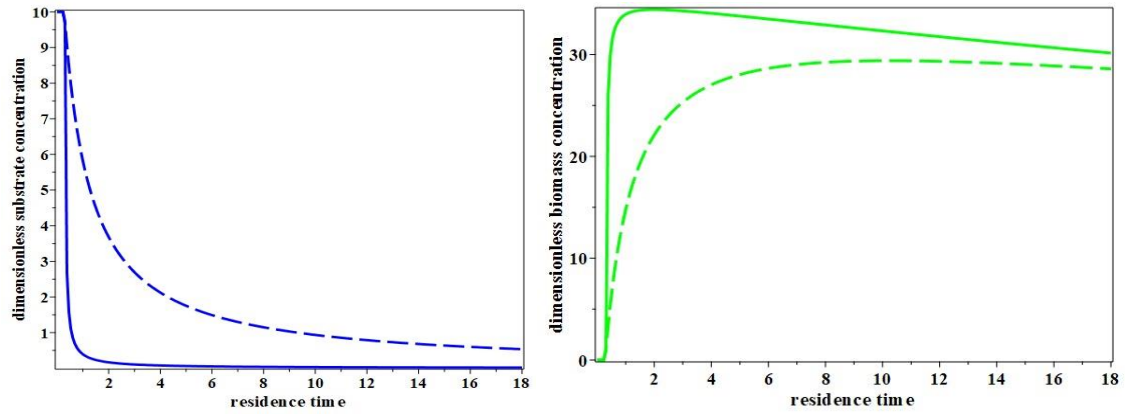

(a) (b)

Figure 5. The substrate (a) and biomass (b) concentration with Monod1 (solid line) and Monod2 (dash line) with respect to residence time.

The above Figure 5 (a) shows that the subtract concentration decreases with the increase in the residence time. There is peak decrease at the subtract concentration with the Monod 1 equation, which is shown by the solid blue color curve. It converges to zero as the residence time increases overtime. However, with Monod 2 (blue dash curve) equation there is gradually decreasing of subtract concentration with respect to residence time. The green curves in Figure 5 (b) shows a rapid increase of the biomass concentration with respect to the increase of residence time and gradually decreases over a period of time. The solid green curve represents the biomass concentration equation with Monod 1, and the dash green curve represents the Monod 2. The Monod 1 and 2 equations play an important role to understand the dynamic behavior growth rate of subtract and biomass in the wastewater treatment system.

5. Conclusions

Mathematical modelling of wastewater treatment plants for the optimal performance is a challenging and not easy task. The study of the behavior of inflows in the wastewater reactor needs frequently sampling and analysis, which are costly. Applying suitable mathematical models can provide cost effective and more manageable of the wastewater treatment process. Different process requires different types of membrane in wastewater treatment. We highlighted the models used to determine the rate of change of substrate concentration at steady state. In Kinetic models, the substrate removal rate is considered as a function of the organic loading rate at steady state. We adopt the residence time model for the five compartments in a wastewater treatment plant and simulated. The simulation process shows high subtract concentration influenced by the inflow rate in the compartments. The model predicts the residence time at the secondary setter compartment is at a minimum as compared with the other compartments. Moreover, we study the model for biomass and substrate concentration with two different Monod equations. The Monod equations provide useful information to understand the biological wastewater treatment process. Our future research directions would focus on the extension of the fractional-order models in predicting the biochemical oxygen demand based on different Monod equations.

Acknowledgments: The authors would like to thank Scientific Research Ethics Committee, Jazan University, Ministry of Higher Education, Saudi Arabia, for financial support of this research with grand number FS10-085.

References

1. M. Henze, C.P.L Grady, et al., “Activated Sludge Model No. 1”, *IWA Scientific and Technical Reports* No. 1, IAWPRC London, UK, 1987.
2. O. Alagha, A. Allazem, et al., “Suitability of SBR for wastewater treatment and reuse: Pilot-Scale reactor operated in different anoxic conditions”, *Int. J. Environ. Res. Public Health*, 17 (5), 1617, 2020.
3. N. Mu’azu, N. Jarrah, M. Zubair, and O. Alagha, “Removal of phenolic compounds from water using sewage sludge-based activated carbon adsorption: A review”, *Int. J. Environ. Res. Public Health* Vol.14, 1094, 2017.
4. National Water Company, Launches Qatrah – National Conservation Program For Reducing Individual Water https://www.nwc.com.sa/English/OurCompany/MediaCenter/NewsandEvents/News/Pages/National-Water-launches-qatrah-the-national-.aspx, access on Jan. 2021.
5. Ministry of Water and Electricity, https://www.mewa.gov.sa/en/Pages/default.aspx access on February 2021, access on Jan. 2021.
6. J.E. Drewes, C. Patricio Roa Garduno, and G.L. Amy (2012), “Water reuse in the kingdom of Saudi Arabia- status, prospects and research needs”, *Water Science & Technology-Water Supply*, *12*, pp.926–936, 2012.
7. Water supply and sanitation in Saudi Arabia, https://en.wikipedia.org/wiki/Water_supply_and_sanitation_in_Saudi_Arabia, access on Jan. 2021.
8. D. Ganora, S. Isacco, and P. Claps, 2017. “Framework for enhanced stormwater management by optimization of sewer pumping stations”, *J. Environ. Eng.*, 143 (8): 04017025, 2017.

9. O. Achouri, A. Panico, M. Bencheikh-Lehocine, et al.,"Effect of chemical coagulation pretreatment on anaerobic digestion of tannery wastewater." *J. Environ. Eng*., 143 (9): 04017039, 2017.
10. S.J. Kim, S.W. Hong, et al., "Performance evaluation of a newly developed flow diverted bed system for stream restoration", *Process Biochem.* Vol. 42, pp.199–209, 2007.
11. J. De Anda, A. López-López, E. Villegas-García, et al., "High-Strength Domestic Wastewater Treatment and Reuse with Onsite Passive Methods", *Water*, 10 (2), 99, 2018.
12. Qu F, et al., "Ultrafiltration membrane fouling caused by extracellular organic matter (EOM) from Microcystis aeruginosa: Effects of membrane pore size and surface hydrophobicity", *Journal of Membrane Science*,449, pp. 58-66, 2014.
13. I.K Kapdan, "Kinetic analysis of dyestuff and COD removal from synthetic wastewater in an anaerobic packed column reactor", *Process Biochemistry*, Vol. 40, No. 7, pp. 2545-2550, 2005.
14. L. Kopec, A. Kopec and J. Drewnowski, "The application of Monod equation to denitrification kinetics description in the moving bed biofilm reactor (MBBR)," *International Jounral of Enviromental Science and Technology*, vol. 16, pp 1479-1486, 2019.
15. N. N. Li, A. G. Fane, W. S. W. Ho, and T. Matsuura, "Advanced Membrane Technology and Applications. Hoboken," NJ, USA: John Wiley & Sons, Inc., 2008.
16. M.I Nelson, T. Nicholles and N. Hamzah, "A biological process subject to noncompetitive substrate inhibition in a generalized flow reactor," *The Anziam Journal*, Vol.54, No.4, pp. 273-290, 2013.
17. M.I Nelson, H. Bronwyn and H. Bradshaw, "An analysis of organic carbon removal in a two-reactor cascade with recycle and two-reactor step-feed cascade with recycle", *Asia-Pacific Journal of Chemical Engineering*, 2019.
18. H.S. Sidhu, M.I. Nelson and E. Balakrishnan, "An analysis of a standard reactor cascade and step-feed reactor cascade for biological processes described by Monod Kinetics", *Chemical Product and Process Modeling*, 2014.
19. K.H. Choo, et al., "Effect of coagulant types on textile wastewater reclamation in a combined coagulation/ultrafiltration system", Vol. 202, No.1-3, pp. 262-270, 2007.
20. WaterWorld, "Continuous Sand Filters Used in Major Saudi Irrigation Project," https://www.waterworld.com/international/wastewater/article/16200521/continuous-sand-filters-used-in-majorsaudi-irrigation-project, 2021.
21. L. Samineni, B.Xiong, et al., "7 Log Virus Removal in a Simple Functionalized Sand Filter," Environmental Science Technology, Vol. 53, No. 21, 2019.
22. W. Renata and K.K. Anna, "Treatment of waterborne pathogens by reverse osmosis," Waterborne Pathogens Detection and TreatmentI, pp 57-80, 2020.
23. Yang M, Zhao C, Zhang, et al., "Preparation of graphene oxide modified poly (m-phenylene isophthalamide) nanofiltration membrane with improved water flux and antifouling property," *Applied Surface Science*," No. 394, pp.149-159, 2017.
24. N. Philips, S. Heyvaerts, et al., "Mathematical modelling of small wastewater treatment plants: power and limitations", *Water Science and Technology*, Vol. 51, No.10, pp.47-54, 2005.
25. M. Torki, N. Nazari and T. Mohammadi, "Evaluation of biological fouling of RO/MF membrane and methods to prevent it," *European Journal of Advances in Engineering and Technology*, Vol.4, No.9, pp. 707-710, 2017.

Low Temperature Photoluminescence and Radioluminescence Properties of Nd^{3+} Doped $LiKYF_5$ Crystals Produced by Hydrothermal Method

G. O. Souadi

Physics Department, Jazan University, Jazan, Kingdom of Saudi Arabia

Abstract

In this paper, lithium potassium yttrium pentafluoride ($LiKYF_5$) crystals activated with various Nd^{3+} concentrations (1%, 1.5%, 3%, 5% and 10%) were synthesized via hydrothermal method and characterized by X-ray diffraction (XRD) and Energy Dispersive X-Ray Analysis (EDS). Neodymium (Nd) doped $LiKYF_5$ has the monoclinic structure with lattice parameters a=0.69925nm, b=1.1747nm, c=0.64669nm and $\beta = 113.7°$. Cathodoluminescence (CL) and Photoluminescence (PL) emission spectra of $LiKYF_5$ crystals prepared by hydrothermal method for different concentration of Nd^{3+} were carried out. According to Scherrer's equation, it is observed that the crystal size increases as the neodymium concentration increases. There are various several emission peaks of pure crystal based on different excitation mechanism at room temperature. The crystal excited efficiently by ultraviolet (UV) light and X-irradiation emit electronic transitions assigned to Nd^{3+} ion in the near-infrared (NIR) spectral region, mostly between 850nm and 950nm, in addition to some minor emission peaks in the visible region. The sharp 886nm peak in the NIR range of the released radiation was dominated by $^4F_{3/2} \rightarrow {}^4I_{9/2}$ transition of Nd^{3+} ions.

Keywords: $LiKYF_5$, rare earth, Photoluminescence, Radioluminescence.

1. Introduction

In the past, luminescence materials were developed by incorporating trivalent rare earth ions (RE) into complex alkali metal fluorites and yttrium fluorites such as K_2YF_5, KYF_4, CsY_2F_7, $CsGd_2F_7$ [1,2]. Due to the fact that the fluorides produce a series of various yttrium polyhedral with coordination numbers ranging from six to eleven, the rare earth ions can effectively replace Y^{3+} without substantially altering its crystallographic structure [3]. The solid-state lasers of the future will be made from single crystals of yttrium complex fluorides doped with trivalent rare earth ions (RE^{3+}). Rare earth (RE^{3+}) ions play a key role in many luminescence applications [4-6]. In particular, a trivalent form of neodymium (Nd) has been extensively studied for its use in optical applications, including laser emission and biomedical imaging [7-11]. Luminescence can be observed on the visible and near-infrared (NIR) spectrums when the Nd^{3+} ions are present. On the other hand, the Vis emission signals tend to have very low intensities, so little attention has been paid to them. Nd^{3+} ions are typically used in optical applications since their NIR emission signals are located around 860 nm and 1060 nm. In the near-

infrared range, the band appeared in around 1060 nm is especially appropriate for lasing design. Researches have focused on two directions for understanding the origin of this interest: (a) a study of the role host lattices in the development of efficient emitting materials, (b) examining Stokes and anti-Stokes energy transfer mechanisms resulting from relaxation channels in excited states. Fluoride compounds have high emission efficiencies because their phonon energies are generally low. Furthermore, in compared to oxide compounds, fluoride crystals offer several significant benefits such as wide band gap, the RE^{3+} ligand bond's strong ionic nature.

Fluoride compounds that are composed of KMF (M=rare earth) have been less studied than other fluorides due to preparation difficulties. More recently, the optical characteristics of Nd activated fluoride crystals such as K_2YF_5 [11,12], LuF_3 [13,14], KY_3F_{10} [15], LaF_3 [16] and $NaYF_4$ [17] have lately been examined due to benefits of fluoride crystals and particular spectroscopic features of Nd^{3+} ions. There are seven fluoride ions surrounding each Y^{3+} ion, forming a local point symmetry of C_{2v}. To the best knowledge, no reports have been published on the Photoluminescence (PL) at low temperature and Cathodoluminescence (CL) spectra of Nd doped $LiKYF_5$ phases crystallized in an orthorhombic system. Therefore, crystal structure via XRD, PL and CL properties of $LiKYF_5$ doped with Nd ions in the range of 1 to 10% have been studied. The current study was driven by a desire for knowledge on the effects of Nd doping.

2. Experiment

By using hydrothermal method, the concentration series of $LiKY_{1-x}Nd_xF_5$ single crystals (x= 1, 1.5, 3, 5, and 10%) were grown (under pressure, P≈150 MPa during 15 to 20 days) by Dr. N. Khaidukov in Kurnakov Institute in Russia [18].

A PANalytical EMPRYAN X-ray diffractometer with a voltage range of 20-50 kV was used to conduct the analysis (CuK-α radiation (1.5406 Å)). A total of 5-65° of diffraction angles were recorded in the XRD analysis (2θ) and compared with the XRD PDF2 card files of the Joint Committee on Powder Diffraction Standards using XPowder diffraction software. Comparison was also made with the $LiKYF_5$ reference XRD pattern data. PL experiments were carried out in a closed-cycle cryostat with a changeable temperature (10–300 K) using a diode laser with a 474 nm line. A Jobin Yvon monochromator with a 500 nm grating was used to analyse the luminescence, which was then detected using a dual color Si uncooled detector and a lock-in amplifier. Spectral adjustments are used to eliminate the impacts of the Jobin Yvon instruments from the PL data, and so all of the PL spectra described in this paper have been adjusted. By employing a steady white light source with a well-known spectral distribution, the conventional relative instrument response adjustments are used here. The RL spectra were stimulated in an X-ray unit using a Machlett OEG-50A tube that

delivered a dose rate of 30 Gy/min at a current of 15 mA and a voltage of 30 kV. With a 5-second integration time, a Jobin Yvon spectrometer and a liquid nitrogen cooled CCD detector were used to measure RL spectra in the range of 400-1000 nm at room temperature.

3. Results and Discussion

3.1. Crystal Structure and EDS Analysis

XRD patterns of $LiKYF_5$ crystals produced in the various Nd doping concentrations are depicted in Figure 1.

High crystalline quality is evident in the pattern, with well-defined peaks of high intensity. As seen in Figure 1, all of the diffraction peaks appear to be indexed in a monoclinic system with lattice parameters of a = 0.69925 (4) nm, b = 1.1747(1) nm and c = 0.64669 (5) nm, β≈ 113.7° and there are no unindexed reflexes, which match standard JCPDS data file No. 00-049-110, corresponding to pure orthorhombic $LiKYF_5$ fluoride. The ionic size of Nd^{3+} ions are close to Y^{3+} ions, and therefore, ions are likely to occupy the lattice site of Y^{3+} ions.

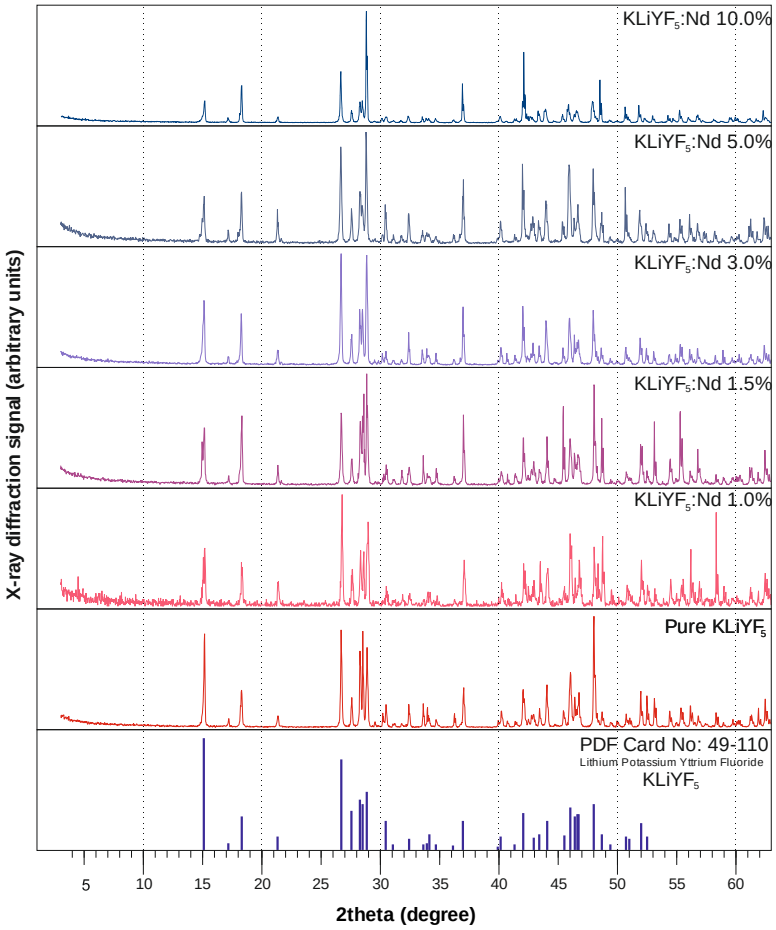

Figure 1. X-ray diffraction (XRD) patterns for $LiKY_{1-x}Nd_xF_5$ fluorides doped with of Nd^{3+} (0, 1, 1.5, 3, 5 and 10%), respectively.

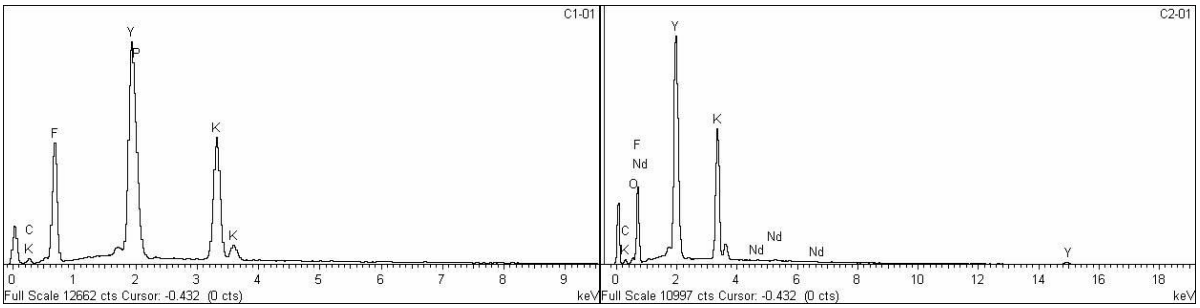

Figure 2. EDS spectra of pure and Nd activated $LiKYF_5$ (1%) crystals, respectively.

The crystallite size was assessed from three main single diffraction peaks using the well-known Scherrer's equation [19]:

$$L = \frac{0.89\,\lambda}{\beta cos\theta}$$

where, L is the normal crystallite dimensions (A°), λ is the X-ray wavelength (0.154 nm), θ is the diffraction angle and β is the full width at half maximum (FWHM) of this peak that is observed. Consequently, average crystallite sizes for each amount of Nd (1%, 1.5%, 3%, 5% and 10%) doped with $LiKYF_5$ crystal and undoped $LiKYF_5$ are estimated to be 65.28 nm, 65.70 nm, 66.7 nm, 67.09 nm, 69.9 nm and 57.02 nm, respectively. Note the Scherrer's equation only gives a rough average value regarding crystalline size.

EDS spectra obtained from 0 to 20 keV were used to determine sample composition uniformity. The EDS spectra of pure and a $LiKY_{1-x}Nd_xF_5$ samples were displayed in Figure 2. Based on the EDS results, atomic compositions of pure and Nd incorporated $LiKYF_5$ crystal are presented in Table 1. It is clear the presence of Nd atoms along with the very strong peaks for F, Y, and K suggesting the incorporation of Nd into the $LiKYF_5$ host crystal. Furthermore, no impurity peaks are observed from EDS analysis, as shown in Figure 2.

Element	Pure (%)	Nd doped (%)
C K	3.99	3.31
O K	0.0	3.45
F K	42.39	33.99
Nd L	0.0	0.63
K K	14.73	16.78
Y L	38.11	41.83
Totals	100.00	100.00

Table 1. Atomic composition of the pure and Nd doped $LiKYF_5$ crystal based on EDS results.

3.2. Luminescence of Pure and Nd doped $LiKYF_5$

As a function of temperature, the Photoluminescence (PL) of undoped $LiKYF_5$ and $LiKYF_5$ incorporated with Nd^{3+} ions were examined, as well as the radioluminescence (RL). Although often ignored in the literature, this and similar experimental studies will also be sensitive to impurities at low levels due to its sensitivity to ppm levels of impurities and processing. Despite the fact that materials are normally 99.99 percent pure, trace contaminants may still affect the results (and the results that other groups have reported on their samples). In the trivalent form, the rare earth substance employed here has a stable structure.

Rare earth ions have a significant effect on luminescence characteristics when employed either purposefully (in this case Nd) or as impurities introduced into a host crystal. As compared to the reference $LiKYF_5$, several (but not all) of the internal transitions inside the clearly and simply visible schematic energy level diagram greatly attenuate the RL signal observed for the trivalent lanthanide ion (e.g., Nd). Further radiative relaxation decay routes by suppressing the signals from host lattice emission may occur due to Nd ions. The fact that the emission lines are affected by the crystal fields at the host lattice sites should not be surprising, as variations in lattice constants, temperature, and stress would be expected, since it is dependent on the crystal field at each local site on the transition energies and intensities of luminescent lanthanide ions (i.e., Nd ions). In Figure 3, the RL spectrum for Nd^{3+} doped $LiKYF_5$ phosphor was measured at ambient temperature with a resolution of 1 nm. In the visible range and near infrared area, there is a distinct group of lines, as seen in Figure 3. In all doping concentrations, Nd^{3+} RL emission signals corresponding to $^4F_{3/2} \rightarrow {}^4I_{9/2}$ transition have been observed in the range of 830-930 nm. Closer inspection of the spectrum shows that there are two distinct emission peaks in the range of 850-950 nm as shown in Figure 4.

The photoluminescence (PL) spectra for Nd^{3+} doped $LiKYF_5$ are shown in Figure 5a and 5b as an isometric presentation of PL measurements, with the intensity (in arbitrary units) vs temperature versus wavelength, recorded between 300 nm and 1000 nm. As seen in Figure 5a, sharp peaks are observed at 488 nm and 573 nm in PL measurements taken from room temperature up to 40 K in undoped $LiKYF_5$ crystal, while there is a wide band between 624 nm and 788 nm peaked at 727 nm. As a general trend, as seen in Figure 4, the intensity of the peaks increases clearly as one moves towards lower temperatures. The intensity of PL is proportional to the number of radiation transitions (in this case excitonic) in the host crystal and therefore also proportional to the concentration of excitons in the sample. When the temperature is decreased, the thermal energy is also decreased, thereby, reducing the dissociation of the excitons and increasing the radiative decay of the excitons. That is the reason why the PL intensity at low temperatures increases.

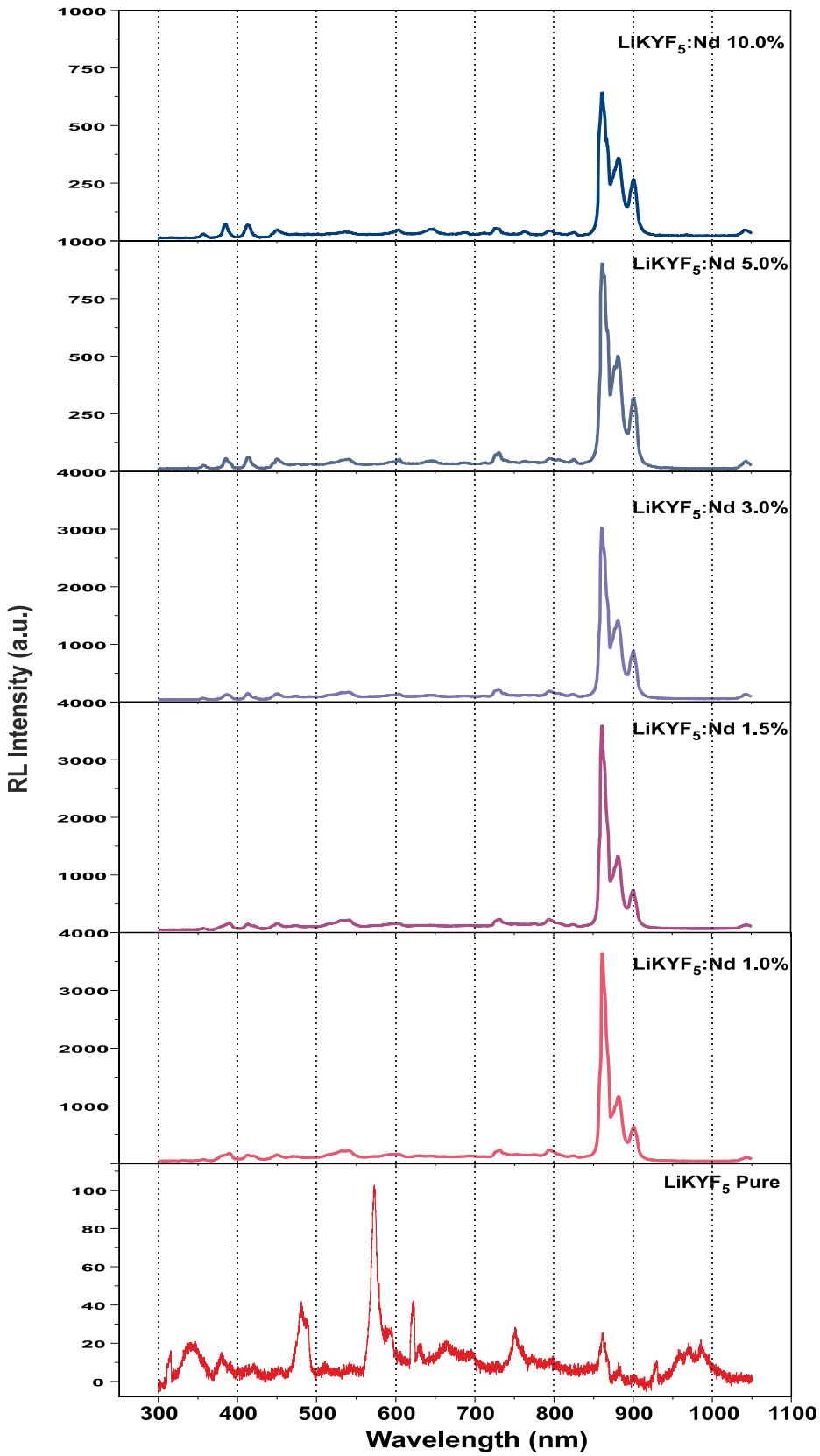

Figure 3. Radioluminescence (RL) emission spectrum of $LiKY_{1-x}Nd_xF_5$ crystals (x= 0, 1, 1.5, 3, 5, and 10%) doped with Nd^{3+} ions.

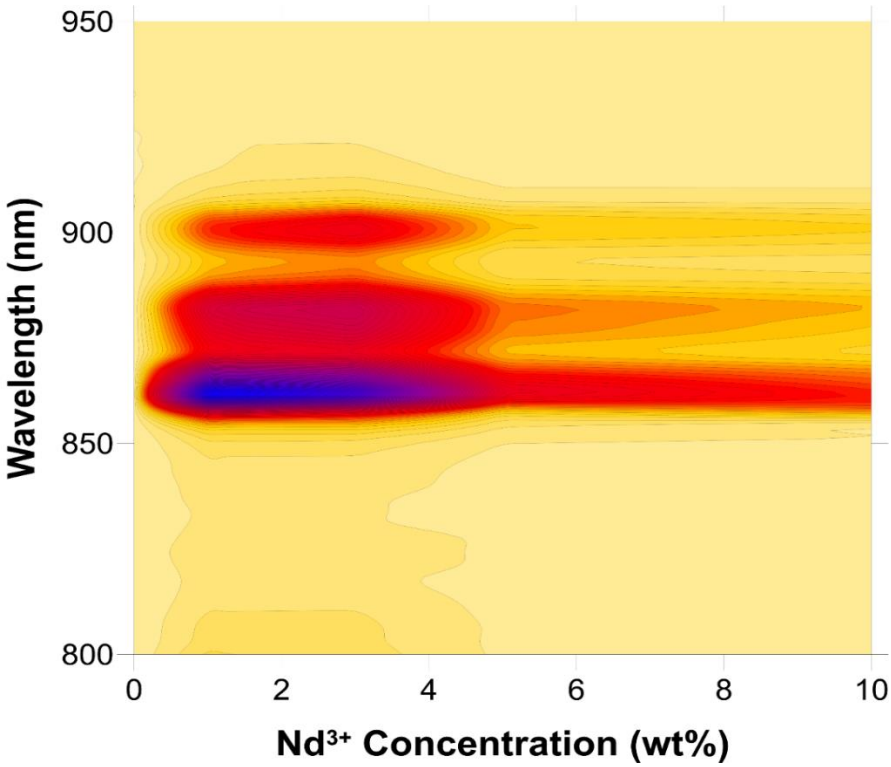

Figure 4. Contour view of $LiKY_{1-x}Nd_xF_5$ crystals x= (0, 1, 1.5, 3, 5, and 10%) doped with Nd^{3+} ions.

Clearly, the sample emits various luminescence signals attributed to different transitions occurred during the Nd^{3+} ion doping. It is also obvious that the strength of the variances between near room temperature and 40 K is different. However, Figure 5b exhibits a general pattern of narrow line rare earth emission characteristics in the luminescence signals. The $4f^3$ electronic configuration (i.e., $4I_{9/2}$ free ion ground state) is responsible for the Nd^{3+} ion's energy level. The $f-f$ internal orbital transitions of Nd^{3+} ions with Stark splitting have numerous highly defined photoluminescence peaks [20].

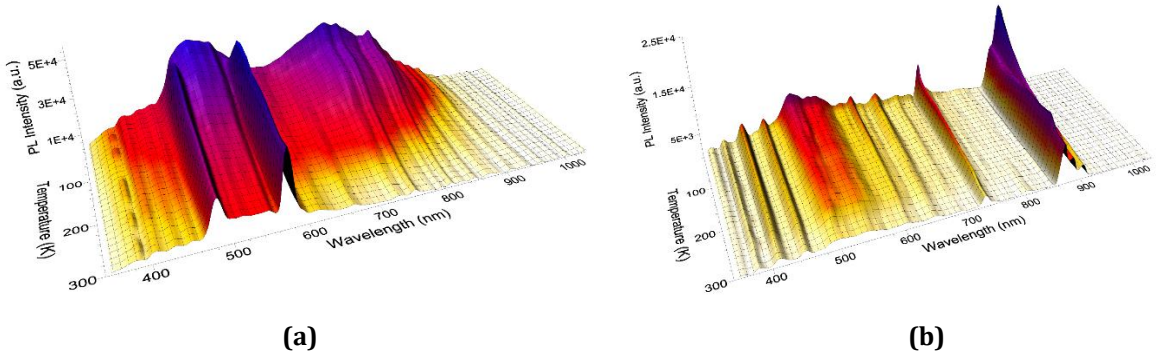

(a) **(b)**

Figure 5. Isometric views of low temperature photoluminescence from (a) pure and (b) $LiKYF_5$:1%Nd^{3+}.

4. Conclusions

Several conclusions may be drawn from the experiment findings. First, the synthesis of Nd^{3+} doped $LiKYF_5$ crystal was carried out using a hydrothermal reaction method. XRD and EDS analysis of $LiKYF_5$ phase with trivalent Nd doping confirmed the crystallinity and elemental composition of the samples. Nd doping effect has been observed on crystalline size. Second, PL data at room and low temperature and RL data at room temperature were collected to analyse the samples. The components of intrinsic defect complexes in $LiKYF_5$ would be altered by both PL and RL, but not by trivalent rare earth ions. As a result, it is suggested that the luminescence emission lines seen for Nd ions are distinctive of the 3+ state and are dependent on orbital rearrangements inside the host crystal. In the present study, the $^4I_{9/2} \rightarrow {}^4G_{5/2}$ transition peaked at 573 nm is identified as a hypersensitive transition following the selection rule $\Delta S=0$, $|\Delta L| \leq 2$, $|\Delta J| \leq 2$. Finally, due to their exceptional luminescent characteristics, PL and RL findings have indicated that these kinds of materials are fascinating systems with promising application potential. More research is being done to better understand the influence of the synthesis methods utilizing various approaches.

Acknowledgement

The author would like to thank Dr. N. Khaidukov in Kurnakov Institute in Russia who provided the $LiKYF_5$ samples.

References

[1] V.N. Makhov, N.M. Khaidukov, D. Lo, M. Kirm and G. Zimmerer, "Spectroscopic properties of Pr^{3+} luminescence in complex fluoride crystals", Journal of Luminescence, 102-103 (2003) 638-643.

[2] N.M. Khaidukov, S.K. Lam, D. Lo, V.N. Makhov and N.V. Suetin, "Luminescence spectroscopy from the vacuum ultra-violet to the visible for Er^{3+} and Tm^{3+} in complex fluoride crystals", Optical Materials, 19 (2002) 365-376.

[3] O. Greis, J.M. Haschke, in Handbook on the Physics and Chemistry of rare Earths, Ed. By Karl A. Gscheidner, Jr. and LeRoy Eyring (North-Holland, Amsterdam, 1982), vol.5, Chap.45, p. 387.

[4] P. V. Do, N. X. Ca, L. D. Thanh, N. V. Nghia and T.T. C. Thuy, "Optical properties and energy transfer in $KYF_4:Sm^{3+}$ and $KYF_4:Tb^{3+}$, Sm^{3+} polycrystalline materials", Phys. Chem. Chem. Phys., 22 (2020) 27590-27599.

[5] S. Ye, F. Xiao. Y.X. Pan, Y.Y. Ma and Q.Y. Zhang, "Phosphors in phosphor converted white light emitting diodes: recent advances in materials techniques and properties", Materials Science and Engineering R: Reports 71 (2010) 1-34.

[6] J. Xue, X. Wang, J.H. Jeong and X. Yan, "Spectral and energy transfer in Bi^{3+}-$Re^{:N+}$ (n=2,3,4) co-doped phosphors: Extended optical applications" , Phys. Chem. Chem. Phys., 20 (2018) 11516-11541.

[7] Y.V. Orlovskii, A.V. Popov, E.O. Orlovskaya, A.S. Vanetsev, E.A. Vagapova, M. Rahn, V. Sammelselg, I. Sildos, A.E. Baranchikov, P.V. Grachev, V.B. Loschenov and A.V. Ryabova, "Comparison of concentration dependence of relative fluorescence quantum yield and brightness in first biological window of wavelengths for aqueous colloidal solutions of $Nd^{3+}:LaF_3$ and $Nd^{3+}:KY_3F_{10}$ nanocrsytals synthesized by microwave-hydrothermal", Journal of

Alloys and Compounds, 756 (2018) 182-192.

[8] Z. Zhoua, W. Lia, J. Songb, B. Meia, G. Yia and Y. Yanga, "Application of Judd–Ofelt theory in analysing Nd^{3+} doped SrF_2 and CaF_2 transparent ceramics", Journal of European Ceramic Society, 399 (2019) 2446-2452.

[9] R. Tomala and W. Strek, "Emission properties of Nd^{3+}: $Y_2Si_2O_7$ nanocrystals under high excitation power density", Optical Materials, 96 (2019) 109257-109262.

[10] A.M.E. Santoa, A.F.H. Librantza, L. Gomesa, P.S. Pizanib, I.M. Ranieria, N.D. Vieira Jr.a and S.L. Baldochia, "Growth and characterization of $LiYF_4$:Nd single crystal fibres for optical applications", Journal of Crystal Growth, 292 (2006) 149-154.

[11] M. Yin, Y. Li, N. Dong, V.N. Makhov, N.M. Khaidukov and J.C. Krupa, "Spectroscopic studies, and crystal field calculation for Nd^{3+} in single crystal K_2YF_5", J. Alloys. Comp., 353 (2003) 95-101.

[12] D. Wang, Y. Min, S. Xia, V.M. Makhov, N. Khaidukov and J.C. Krupa, "Up conversion fluorescence of Nd^{3+} ions in K_2YF_5 single crystal", J. Alloys Compd., 361 (2003) 294-298.

[13] K. Fukuda, S. Ishizu, N. Kawaguchi, T. Suyama, T. Yanagida, Y. Yokota, M. Nikl and A. Yoshikawa, "Crystal growth and optical properties of the Nd^{3+} doped LuF_3 single crystals", Optical Materials, 33 (2011) 1143-1146.

[14] J. Pejchal, K. Fukuda, V. Babin, S. Kurosawa, Y. Yokota, A. Yoshikawa and M. Nikl, "Luminescence mechanism in doubly Gd, Nd-codoped fluoride crystals for VUV scintillators Journal of Luminescence, 169 (2016) 682-689.

[15] I.R. Martın, Y. Guyot, M.F. Joubert, R. Yu Abdulsabirov, S.L. Korableva and V.V. Semashko, "Stark level structure and oscillator strengths of Nd^{3+} ion in different fluoride single crystals", J. Alloys Compd., 323–324 (2001) 763-767.

[16] S.G. Fedorenko1, A.V. Popov, E.A. Vagapova, A.E. Baranchikov and YuV. Orlovskii, "Concentration self-quenching of luminescence in crystal matrices activated by Nd^{3+} ions: Theory and experiment", Journal of Luminescence, 198 (2018) 138-145.

[17] X. Xue, Z. Duan, T. Suzuki, R.N. Tiwari, M. Yoshimura and Y. Ohishi, "Luminescence properties of α-$NaYF_4$:Nd^{3+} nanocrystals dispersed in liquid: Local field effect investigation", J. Phys. Chem. C, 116 (2012) 22545-22551.

[18] A. A. Kaminskii, V.S. Mironov, S.N. Bagaev, N.M. Khaidukov, M.F. Joubert, B. Jacquier and G. Boulon, "Spectroscopy and laser action of anisotropic single centered $LiKYF_5$:Nd^{3+} crystals grown by the hydrothermal method", Phys. Stat. Sol. (a) 145 (1994) 177-195.

[19] M. Ayvacikli, Umit. H. Kaynar, Y. Karabulut, A. Canimoglu, M. Bakr, A. Akca and N. Can, "Synthesis and photoluminescence characteristics of Dy incorporated MoO_3 phosphor: suppression concentration quenching", Applied Radiation and Isotopes, 164 (2020) 109321-109331.

[20] V. Orsi Gordo, Y. Tuncer Arslanli, A. Canimoglu, M. Ayvacikli, Y. Galvao Gobato, M. Henini and N. Can, "Visible to infrared low temperature luminescence of Er^{3+}, Nd^{3+} and Sm^{3+} in $CaSnO_3$ phosphors", Applied Radiation and Isotopes, 99 (2015) 69-76.

خصائص التلالؤ الضوئي و الإشعاعي لبلورات الليثيوم البوتاسيوم الإيتريوم خماسي الفلوريد ($LiKYF_5$) المطعم بـــــــ Nd^{3+} الناتجة عن الطريقة الحرارية عند درجة حرارة منخفضة

غالب عمر سويدي
قسم الفيزياء، كلية العلوم، جامعة جازان، جازان، المملكة العربية السعودية

الملخص

في هذا البحث، تم تنفيذ أطياف انبعاث التلألؤ الضوئي و الإشعاعي لبلورات الليثيوم البوتاسيوم الإيتريوم خماسي الفلوريد ($LiKYF_5$) المحضرة بالطريقة الحرارية المائية لتركيزات مختلفة من أيون النيوديميوم Nd^{3+}. تم ملاحظة أن حجم البلورة يزداد مع زيادة تركيز النيوديميوم وفقاً لمعادلة شيرير .تُظهر هذه الطريقة العديد من قمم انبعاث الكريستال النقي بناءً على آلية الإثارة المختلفة في درجة حرارة الغرفة، حيث يتم تحفيز البلورة بكفاءة بواسطة الضوء فوق البنفسجي والإشعاع السيني الذي ينبعث من التحولات الإلكترونية المخصصة لأيون Nd^{3+} في المنطقة الطيفية للأشعة تحت الحمراء القريبة، و الذي غالباً ما يكون بين ٨٥٠ نانومتر و ٩٥٠ نانومتر ، بالإضافة إلى بعض قمم الانبعاث الطفيفة في منطقة الطيف المرئي. تَظهر الذروة الحادة لهذا التلألؤ عند ٨٨٦ نانومتر و الذي يكون في منطقة الأشعة تحت الحمراء القريبة و ذلك من خلال الانتقال $^4F_{3/2}\rightarrow{}^4I_{9/2}$ لأيونات Nd^{3+}.

Assessment of Osteoporosis using Dual-energy X-ray Absorptiometry (DEXA) Scan in Jazan City, Saudi Arabia

Sarra Ali[1]،Meaad Elbashir[1]، Sawsan Mohammed Elhassan[1], Nada Alomairy[1], Awatif Mohamed Ali Omer[2]

[1]Department of Diagnostic Radiologic Technology, Faculty of Applied Medical Sciences, Jazan University, Kingdom of Saudi Arabia

[2]Department of Diagnostic Radiology Technology, College of Applied Medical Sciences, Taibah University, Almadinah Almunawwarah, Kingdom of Saudi Arabia

Abstract:

DEXA is widely use for the measuring the bone composition, fat and fat-free soft tissue. The general aim of this study was to assess patients with osteoporosis in Jazan city hospitals using Bone Mineral Densitometry to identify the common risk factor and related measures. A prospective study consists of 78 patients clinically indicted for DEXA scan at King Fahd central hospital and Prince Mohammed bin Nasser hospital at Jazan city. Patient weight, height, age, and gender were taken to perform the scan. The area of the scan includes the lumbar spine, both hips, and forearm (in selected patient). The result showed that; the mean age, and weight at the time of diagnosis equal 66.9years and 61.4kg respectively. BMD quantified using T and Z scores which compared to WHO standardized values and guidelines, more than -2.5 SD indicates osteoporosis. This study reveals that the mean values for T and Z scores were (-3.01) and (-1.6) respectively. Correlation also intended to investigate the most common causative factor using Chi^2-test at a confidence interval of 95% and a *p*-value equal to 0.05, a strong relationship was noted between the T and Z score with patient age, gender, and weight, on other hand statistically significant difference noted between the Z score and male gender. Finally, osteoporosis is more predominant in females and strongly related to the age of post-menopausal women and patient weight.

Keywords: Osteoporosis, Post-menopausal Women, T-Score, Z-score.

1. Introduction:

Osteoporosis is a common abnormality characterized by a systemic bone mass impairment that results in decreasing bone mass and fractures. [1] World Health Organization (WHO), states the

standardized values of osteoporosis is a bone mineral density (BMD), more than 2.5 SD below the mean for a young white non-Hispanic female reference group. [2]

Osteopenia (low bone mass) is defined by a BMD value between (1.0 and 2.5) SD below the mean. The incidence of osteoporosis among patients undergoing spine surgery older than 50 years is 14.5% in males and 51.3% in females and the incidence of osteopenia is 46.1% in males and 41.4% in females. [3]

The risk factor for such disease as stated by much literature (e.g: Fawzy et al., [3]) are tobacco consumption, Family history of osteoporosis and fracture, and dietary habits also smoking is reported to be one of the important risk's factors.

Low weight and low body mass index also interrelated with osteoporosis. Also female is common gender affected by low bone density due to many variables (causes) especially the post-menopausal one in which about 40% of white postmenopausal women are affected by osteoporosis and, with an aging population, this number is expected to steadily increase shortly. [5-6]. in a study conducted by Iqbal et al. [4] For referral women less than 60yrs; low body mass index is good indicator to avoid the fracture risk in BMD measurements. The risk of fracture is 40% more common in osteoporotic patient, mostly occurred in the spine, hip, or wrist (figure 1), but other bones are also affected (e g., trochanter, humorous, or ribs). Major subsequent drops in patient quality of life due to osteoporosis were; fractures, autonomy and subsequent loss of mobility. Additionally, Fractures resulting from osteoporosis in hips and spine carry excess mortality of 12 months up to 20%, because they require hospitalization and they have subsequently enhanced risk of other complications, such as pneumonia or thromboembolic disease due to chronic immobilization (panel 1). [1-7]

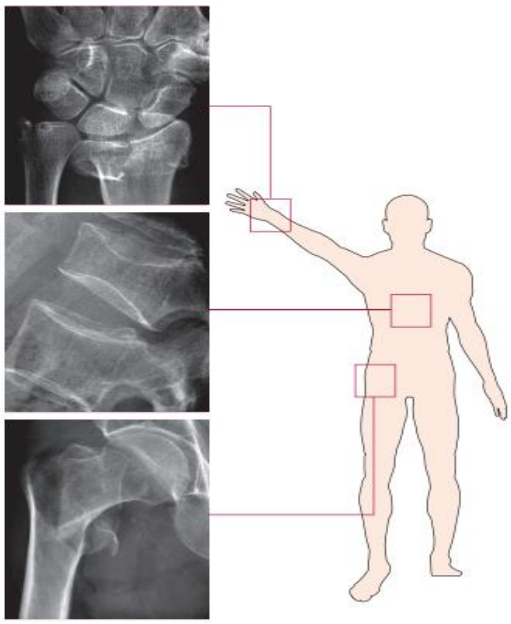

Figure (1) showed the most common area of fractures and Fragility fractures typically involve the wrist, vertebrae, and hip. Rachner et al., [1]

According to the previously mentioned information; it's important to diagnose such morbidity as early as possible to avoid the risk of fracture and bone loss, moreover, the screening program can significantly affect the management outcome.

2. Materials and Methods:

78 osteoporotic patients in the age range (48-85yrs) underwent BMD (bone mineral densitometry) using DEXA scan after a successful, detailed, full medical history and physical examination properly taken from the patient, also informed consent was written and taken according to established guidelines conducted by Jazan university. This was a prospective study presented at Jazan state hospital to identify the risk and to assess the osteoporosis in Jazan city. Patient with known conditions of osteoporosis were selected, on other hand patient with high bone density were excluded. Patient data were prepared for the scanning process including (ID, age, sex, height, weight, and pregnancy status (pregnant ladies are excluded)), all patients were prepared to clear all metallic objects and informed to wear light clothes and clear the shoes. DEXA scan is considered an accurate measure of bone density and the scan were including hips, Lumber spine [L1-L5], and the left arm in some patients for more accurate quantifications. Based on the WHO criteria the result is categorized into three subgroups (normal, osteopenia, osteoporotic) according to the T –score obtained. Also, the measures were correlated

with age, weight, height, and gender using a chi-square test at a confidence interval of 95% and a probability level equal to 0.05.

3. Results:

Table (1) statistics measure the data collected for the DEXA scan

Descriptive Statistics	Min	Max	Mean	Std. D
Z - score	-12.0	1.7	-1.6	1.6
T - score	-5.0	0.5	-3.01	1.1
Age of Menopause	42.0	60.0	47.3	3.2
Height	139.0	186.0	154.7	7.1
Weight	40.0	92.6	61.4	13.6
Age	48.0	85.0	66.9	9.3

Table (2) descriptive statistics for T and Z scores.

Descriptive S	Mean	Std. D
Z - score	-1.6	1.6
T - score	-3.01	1.1

Table (3) shows the relation between the patient height with T and Z-score

Patient height	N	Mean Z score	Mean T score
139-142.5	4	-1.725	-3.025
143-149.5	13	-1.469	-3.162
150-156.5	27	-1.930	-3.004
157-163.5	31	-1.368	-2.910
164-170.5	2	-1.400	-3.350
177 -186	1	-1.300	-3.400
Sig. (2-tailed) = 0.796			

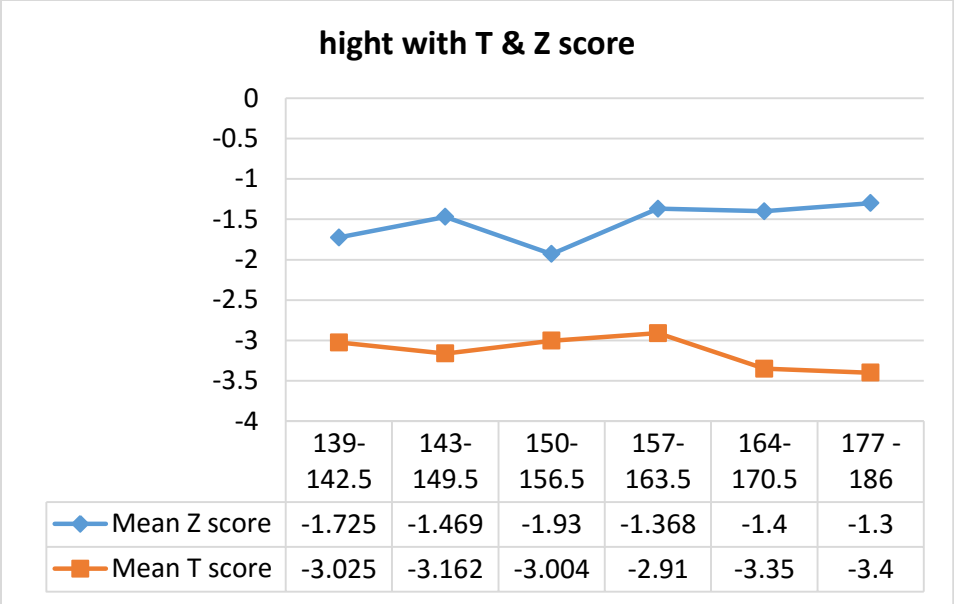

Figure (2) line graph demonstrates the difference in T and Z scores according to patient height.

Table (4) statistical measure for Weight at the time of diagnosis related to the mean values of T and Z scores of 78 osteoporotic patients.

Weight at the time of diagnosis	N	Mean Z score	Mean T score
40-47.35	14	-1.107	-2.900
47.4-54.79	10	-1.440	-3.020
54.8-62.15	16	-2.088	-3.081
62.2-69.55	18	-2.044	-2.889
69.6-76.9	12	-1.167	-3.058
77-84.35	4	-1.625	-3.375
84.4-93	4	-1.000	-3.075

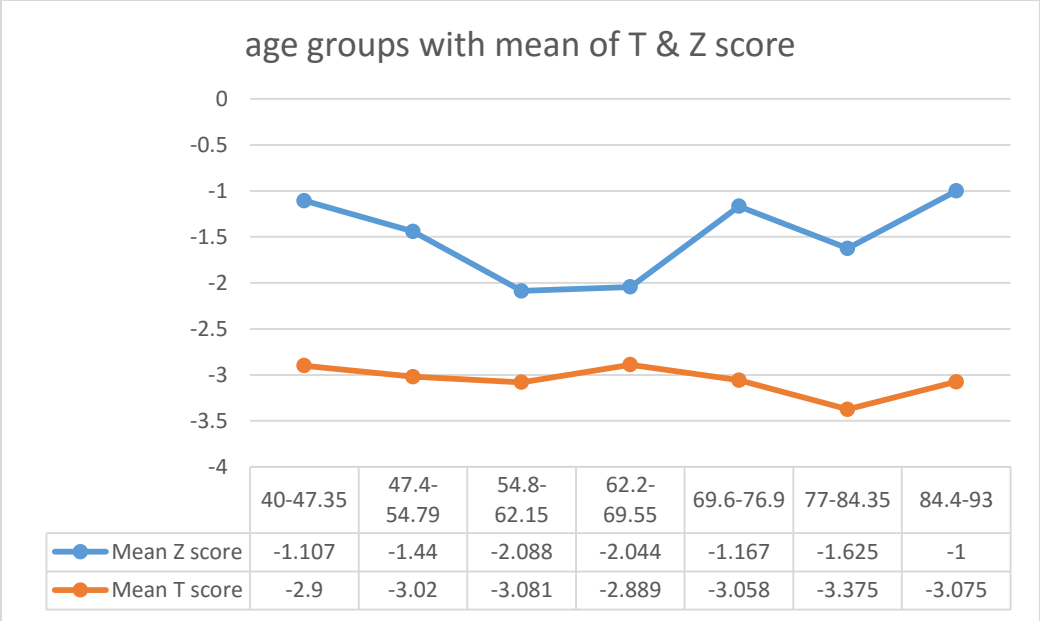

	40-47.35	47.4-54.79	54.8-62.15	62.2-69.55	69.6-76.9	77-84.35	84.4-93
Mean Z score	-1.107	-1.44	-2.088	-2.044	-1.167	-1.625	-1
Mean T score	-2.9	-3.02	-3.081	-2.889	-3.058	-3.375	-3.075

Figure (3) line graph demonstrates the difference in T and Z scores according to patient weight at the time of diagnosis.

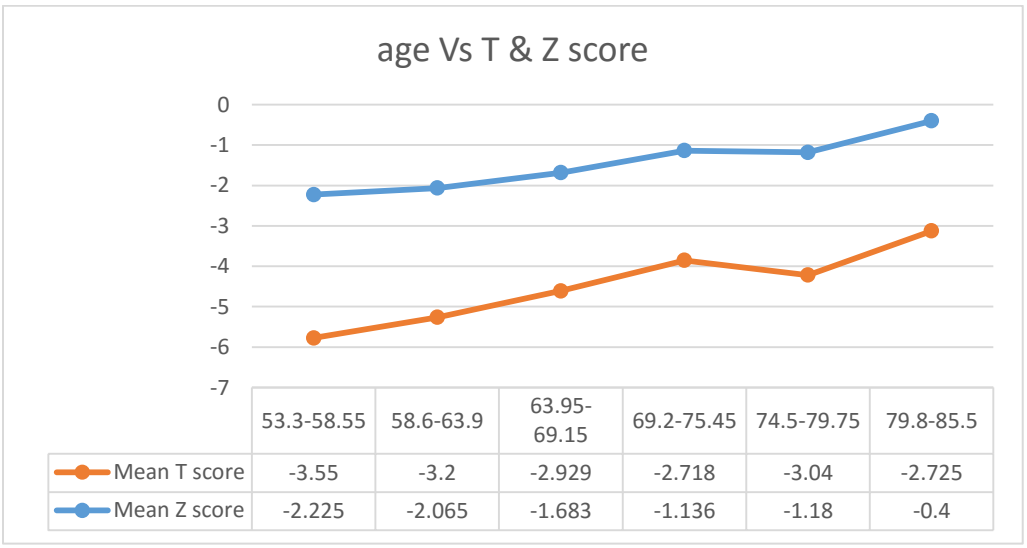

	53.3-58.55	58.6-63.9	63.95-69.15	69.2-75.45	74.5-79.75	79.8-85.5
Mean T score	-3.55	-3.2	-2.929	-2.718	-3.04	-2.725
Mean Z score	-2.225	-2.065	-1.683	-1.136	-1.18	-0.4

Figure (5) linear relationship between the age and T and Z score values of BMD

Table (5) statistical difference in T and Z scores according to the gender

Group Statistics	gender	N	Mean	Std. D	Sig. (2-tailed)
T-score	Female	73	-3.030	1.0679	0.640
	Male	5	-2.680	1.5156	
Z-score	Female	73	-1.407	1.0591	0.000
	Male	5	-4.380	4.3327	

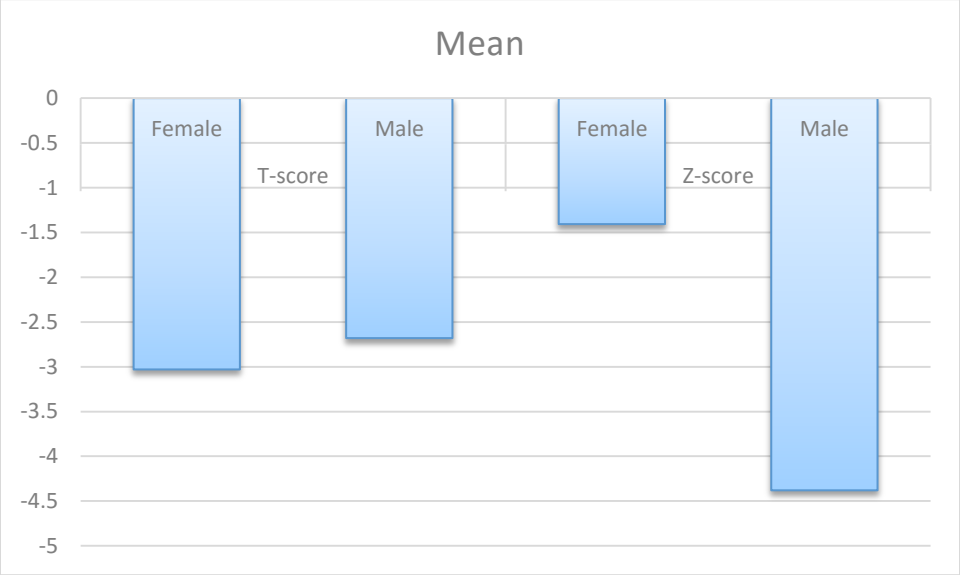

Figure (6) bar chart shows the difference in T and Z scores according to the gender

4. Discussion:

Osteoporosis is now considered as one of the major public health problem worldwide; however, the epidemiology of osteoporosis is not well known in most Middle East countries. [3] Bioelectrical impedance analysis (BIA) as stated by Marra et al., [12] is extensively used as epidemiological methods of measuring the body compositions, while BMI is used clinically. This study was conducted to assess the osteoporosis in Jazan city the mean age at the time of diagnosis was 66.9 yrs (range 48-85 years). Table (2) showed the T-score and Z –score values for all patients collectively, according to the standardized data obtained from the WHO criteria this value was considered as osteoporosis for all selected samples. Osteoporosis is identified according to the patient's bone density: (A T-score within 1 SD (+1 or -1) for young adult indicate normal results, A T-score of (1 to 2.5) SD lower than young adults, mean (-1 to -2.5 SD) indicates low bone density (mass). A T-

score of (2.5 SD) or more lower than young adult, mean (more than -2.5 SD) indicates osteoporosis). See tables (1 and 2) [8].

Alawi et al., [11] compared the density of bone in CT with DEXA results, stated that the mean density for both HU and T-score is decreased with increasing the age, 202.17 HU in the 5^{th} decade to 71 HU in the 9^{th} decade. T-score ranged from -4.4 to +2.4 (mean was -1.7±1.41), and their Bone Mineral Density ranged from 0.62 to 1.465 g/cm^2 (mean, 0.974±0.175 g/cm^2).

To investigate the effect of patient height on the risk of the osteoporosis, the study categorized the T and Z scores for 78 patients, the result showed a strong (statistically not significant) correlation between the T and Z score, patient height, recent studies showed a strong correlation between patient height and weight (BMI) with increasing the risk of fracture for low BMI post-menopausal women, also they stated that BMI was inversely associated with hip, clinical spine, and wrist fractures. See table (3) [9]. Other studies compare the body composition of Saudi children with other races and also at national level which results in; the average BMD & BMC in Saudi children is less than that of other races, with no significant difference at national level. [13]

The study sample consisted of 78 individuals gender distribution demonstrated that female was predominate (93.6%) while male considers 6.4% form the total population. The weight of osteoporotic patients at the time of diagnosis is subcategorized into 7 classes (over 77 are considered underweight). 18 out of 78 patients were at age of 62.2-76.9 which consider the most affected group while the highest T score was noted at age of (77 - 84.35yrs) which indicates that the T-score increased with weight (BMI) of the patient. According to [1-3] who stated that There was a statistically significant association between BMD and age. See figures (3 and 5).

Gender is one of the most important risk factors for osteoporosis in which the female was most affected than male, especially the postmenopausal women. Quantitatively this study consists of more than 93% female and 6.4 % male. There was a significant correlation between the male gender and the Z score. While a strong correlation was noted for both genders. Cawthon [10]. Stated that Postmenopausal females have a

higher prevalence of osteoporosis and a greater incidence of fracture than older men.

5. Conclusion

This study indicates that patients above 60yrs and females gender above that age have a higher incidence to have osteoporosis in Jazan city, in general, this study suggests that older people, postmenopausal women, and low-weight patients are important risk factors that should be considered for screening of normal people. Much more studies are suggested to investigate the effect of other factors related to osteoporosis; including smoking, sunlight, calcium intake, and other factors.

6. Reference:

[1] Rachner TD, Khosla S, Hofbauer LC. Osteoporosis: now and the future. The Lancet. 2011 Apr 9;377(9773):1276-87.

[2] World Health Organization. Guidelines for pre-clinical evaluation and clinical trials in osteoporosis. WHO; 1998

[3] Fawzy T, Muttappallymyalil J, Sreedharan J, Ahmed A, Alshamsi SO, Al Ali MS, Al Balsooshi KA. Association between body mass index and bone mineral density in patients referred for dual-energy X-ray absorptiometry scan in Ajman, UAE. Journal of osteoporosis. 2011 Jan 1;2011.

[4] S. I. Iqbal, L. S. Mørch, M. Rosenzweig, and F. Dela, "The outcome of bone mineral density measurements on patients referred from general practice," *Journal of Clinical Densitometry*, vol. 8, no. 2, pp. 178–182, 2005.

[5] Melton LJ 3rd, Chrischilles EA, Cooper C, Lane AW, Riggs BL. Perspective: how many women have osteoporosis? J Bone Miner Res 1992; 7: 1005–10.

[6] Ray NF, Chan JK, Thamer M, Melton LJ 3rd. Medical expenditures for the treatment of osteoporotic fractures in the United States in 1995: report from the National Osteoporosis Foundation. J Bone Miner Res 1997; 12: 24–35.

[7] Center JR, Nguyen TV, Schneider D, Sambrook PN, Eisman JA. Mortality after all major types of osteoporotic fracture in men and women: an observational study. Lancet 1999; 353: 878–82.

[8] Marcovitz PA, Tran HH, Franklin BA, O'Neill WW, Yerkey M, Boura J, Kleerekoper M, Dickinson CZ. The usefulness of bone mineral density to predict significant coronary artery disease. The American journal of cardiology. 2005 Oct 15;96(8):1059-63.

[9] Compston JE, Flahive J, Hosmer DW, Watts NB, Siris ES, Silverman S, Saag KG, Roux C, Rossini M, Pfeilschifter J, Nieves JW. Relationship of weight, height, and body mass index with fracture risk at different sites in postmenopausal women: the Global Longitudinal Study of Osteoporosis in Women (GLOW). Journal of Bone and Mineral Research. 2014 Feb;29(2):487-93.

[10] Cawthon PM. Gender differences in osteoporosis and fractures. Clinical Orthopaedics and Related Research®. 2011 Jul;469 (7):1900-5.

[11] Alawi M, Begum A, Harraz M, Alawi H, Bamagos S, Yaghmour A, Hafiz L. Dual-energy X-ray absorptiometry (DEXA) scan versus computed tomography for bone density assessment. Cureus. 2021 Feb 10; 13(2).

[12] Marra M, Sammarco R, De Lorenzo A, Iellamo F, Siervo M, Pietrobelli A, Donini LM, Santarpia L, Cataldi M, Pasanisi F, Contaldo F. Assessment of body composition in health and disease using bioelectrical impedance analysis (BIA) and dual energy X-ray absorptiometry (DXA): a critical overview. Contrast Media & Molecular Imaging. 2019 Oct; 2019.

[13] Ali GY, Abdelbary EE, Albuali WH, AboelFetoh NM, AlGohary EH. Bone mineral density & bone mineral content in Saudi children, risk factors and early detection of their affection using dual-emission X-ray absorptiometry (DEXA) scan. Egyptian Pediatric Association Gazette. 2017 Sep 1;65(3):65-71.

تقييم هشاشة العظام باستخدام الأشعة السينية مزدوجة الطاقة في مدينة جازان، المملكة العربية السعودية(DEXA)جهاز قياس الامتصاص

سارة علي[١]، ميعاد البشير[١]، سوسن محمد الحسن[١]، ندى العميري[١]

وعواطف محمد علي عمر[٢]

[١]قسم تكنولوجيا الأشعة التشخيصية- كلية العلوم الطبية التطبيقية- جامعه جازان

المملكة العربية السعودية

[٢]قسم تقنية الأشعة التشخيصية- كلية العلوم الطبية التطبيقية- جامعه طيبة

المملكة العربية السعودية

الملخص

يستخدم (مقياس امتصاص السينية مزدوجة الطاقة) على نطاق واسع لقياس تكوين العظام والأنسجة الرخوة الخالية من الدهون. كان الهدف العام من هذه الدراسة هو تقييم لمرضى هشاشة العظام في مستشفيات مدينة جازان باستخدام مقياس كثافة العظام المعدنية لتحديد عوامل الخطر والتدابير ذات الصلة. تتكون الدراسة التوقعيه من ٧٨ مريضا حسب الكشف السريري يحتاجون لإجراء مسح باستخدام مقياس كثافة العظام المعدنية في مستشفى الملك فهد المركزي ومستشفى الأمير محمد بن ناصر في مدينة جازان. تم أخذ وزن المريض وطوله وعمره وجنسه لإجراء الفحص. تشمل منطقة الفحص العمود الفقري القطني، وعظمتي الفخذين والساعد (في المريض المحدد).

أظهرت النتيجة أن متوسط العمر والوزن وقت التشخيص ٦٦,٩ سنة و٦١,٤ كجم على التوالي. تم قياس كثافة المعادن بالعظام باستخدام درجات T وZ التي تقارن بالقيم والمبادئ التوجيهية الموحدة لمنظمة الصحة العالمية، تشير أكثر من -٢,٥ SD إلى هشاشة العظام. تكشف هذه الدراسة أن القيم المتوسطة لدرجات T وZ كانت (-٣,٠١) و (-١,٦) على التوالي. يهدف الارتباط أيضًا إلى التحقيق في العامل المسبب الأكثر شيوعًا باستخدام اختبار Chi2 في فاصل ثقة بنسبة ٩٥ ٪ وقيمة p تساوي ٠,٠٥، ولوحظ وجود علاقة قوية بين درجة T وZ مع عمر المريض والجنس والوزن، من ناحية أخرى، لوحظ فرق ذو دلالة إحصائية بين درجة Z وجنس الذكور. أخيرًا، يعتبر مرض هشاشة العظام أكثر انتشارًا عند الإناث ويرتبط ارتباطًا وثيقًا بعمر النساء بعد انقطاع الطمث ووزن المريض.

الكلمات المفتاحية : هشاشة العظام ، النساء بعد سن اليأس ، النتيجة T النتيجة Z .

A Systematic Survey on Internet of Medical Things (IoMT) Frameworks during Covid-19 Pandemic

Fathe Jeribi[1 *]

[1]College of Computer Science and Information Technology, Jazan University, Jazan, Saudi Arabia

Abstract:

Since the emergence of the Internet of Things (IoT), many industrial revolutions have come to pass in diversified areas. The health industry is being impacted positively due to this overwhelming transformation. The Internet of Medical Things (IoMT) became popular during this COVID-19 pandemic by interconnecting medical equipment through information and communication technology (ICT) infrastructures for addressing focused issues. A wide variety of research frameworks have been brought up in the past one and a half years by addressing numerous medical problems in the pandemic with the use of IoMT. This work is aimed at pooling all the reliable IoMT research frameworks which are deployed for addressing health issues as part of dealing with the COVID-19 pandemic. It also provides the relevance of edge computing in the IoMT frameworks, which are referred to in this review. PRISMA-recommended review protocols are being followed for this systematic review.

Keywords: IoT; IoMT; Covid-19; Edge Computing

1 Introduction

The Internet of Things (IoT) generates a large volume of data that must be processed and analyzed before it can be used. With edge computing, computing services are moved closer to the user or the data source, including an IoT device. This allows IoT data to be obtained and processed at the edge, rather than having to send it back to a data center or cloud, allowing for faster pattern detection and action, such as anomaly detection for predictive maintenance. The potential of IoT devices to use computing power is now becoming increasingly relevant as a means of performing real-time data analysis. IoT is a term that refers to the process by which physical materials are connected to the internet. The Internet of Things is a broad term that encompasses any framework of physical IoT systems or devices that receive and transmit data over the network without human intervention. An IoT device can range from everyday household items such as light bulbs to healthcare assets such as medical devices, as well as wearable technologies, smart devices, and even traffic signals in cities. A typical IoT system operates in a feedback loop, constantly sending, receiving, and analyzing data. Machine Learning (ML) can conduct the analysis in near real-time or over a longer period of time [1].

In the World Health Organization's (WHO) view, health is a state of physical and mental well-being in which there are no diseases or illnesses [2]. People who work in healthcare do things like prevent, diagnose, and treat illnesses and injuries so that people can stay healthy or get better. There are a lot of problems with traditional healthcare because people make mistakes when they manage and keep track of things like a person's demographics, medical history, billing, and drug stock. It overcomes human errors and assists doctors in diagnosing diseases more quickly and accurately by connecting all monitoring devices via a network to a decision support system, which connects all monitoring equipment to each other and to the decision support system. This term refers to medical things that can send and receive information over a network without the help of humans or computers, which is called the Internet of Medical Things (IoMT). According to statista [3], it is projected that the worldwide end-user spending on IoT solutions will be 1567 billion US dollars in 2025. The topology of an IoMT environment is depicted in Fig.1.

Sensors and electronic circuits are used to collect biomedical signals from patients. A processing unit is used to process those signals, a network device is used to transmit biomedical data over a network, an internal or external storage unit is used, and a visualization platform with machine intelligence schemes is used to make clinically useful decisions [4].

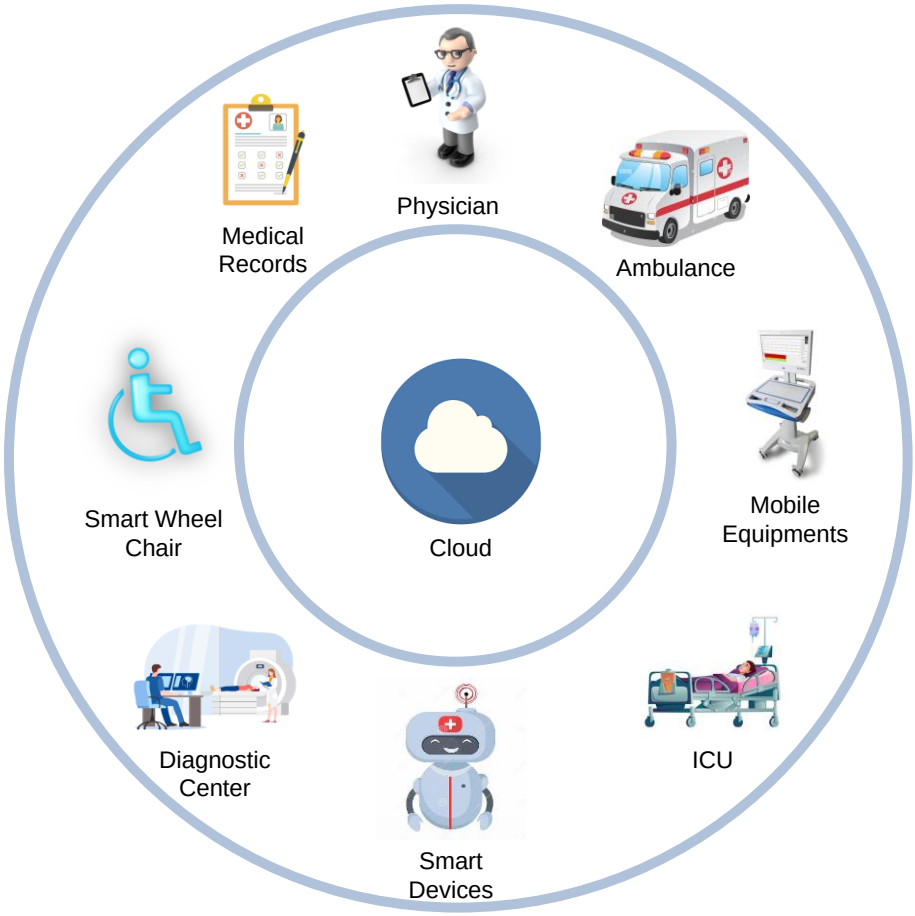

Figure 1: Internet of Medical Things (IoMT)

The Internet of Medical Things (IoMT) is important in the healthcare industry because it improves electronic device accuracy, reliability, and productivity. Researchers are always looking for ways to connect convenient healthcare devices and services and develop a digitized healthcare system. The COVID-19 infections (an animal-borne virus) originated in the Wuhan Region, China, in Dec 2019 and quickly spread around the world [5]. The virus spreads through physical contact with an infected person and airborne [6], and then enters the lungs, multiplies and causes pneumonia [7]. In March, 2020, the World Health Organization labeled the condition as a pandemic. Many deaths are being reported worldwide and some countries have high death tolls, such as the USA, India, Iran, and China. Fig. 2 depicts the most recent number of people infected as an effect of the pandemic.

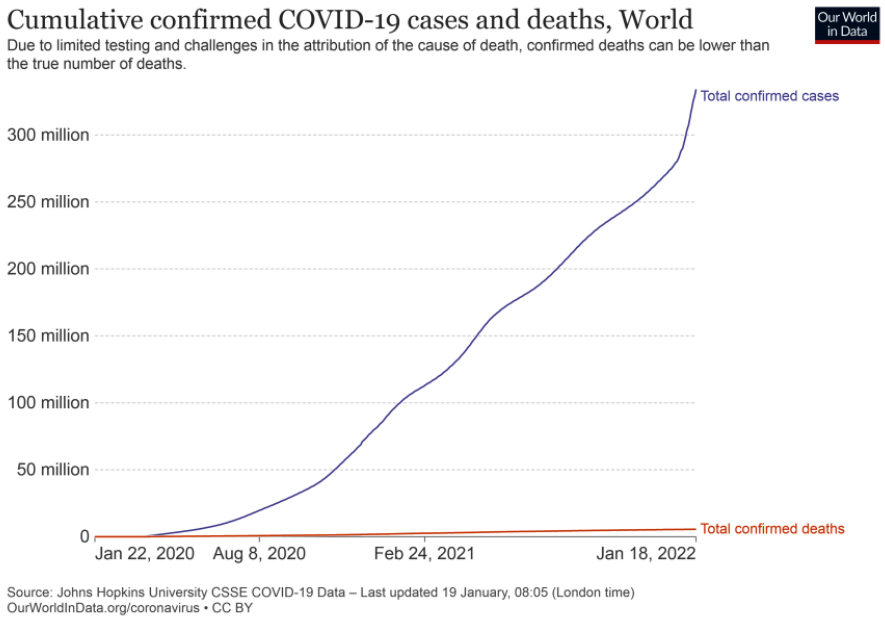

Figure 2: Confirmed COVID-19 cases and deaths as on 20-Jan-2022 [8]

Identifying the Covid-19 patients is crucial and significant in the early stages. The healthcare industry is on the lookout for modern techniques to track and restrict the rapid spread of the virus. The IoMT, in combination with machine intelligence, could help the healthcare system keep track of Covid-19 participants [9]. It improves patient satisfaction while also lowering hospital readmission rates. It may assist in quickly tracing the virus's spread, identifying high-risk patients, and helping in infection control. Similarly, by thoroughly investigating the patients' previous data, it can aid in the prediction of fatality risk [10]. This technology, as an evidence-based healthcare tool, can help with Covid-19 therapies, healthcare planning and management [11]. Several approaches were proposed to detect Covid-19, including medical imaging, reverse transcription polymerase chain reaction (RT-PCR) tests, and blood sample examinations [12]. This review article analyses the IoMT-based frameworks put forth by the researchers during the Covid-19 pandemic era and to assess how best they have been utilised for managing the pandemic.

The main objective of this survey is to explore the IoT and related technologies that were introduced into the healthcare frameworks during the COVID-19 pandemic. It is also aimed at bringing out the challenges in implementing IoMT in healthcare environments and identifying the prospective techniques to deal with those challenges.

The paper presents a comprehensive survey in the following manner: The Second Section examines various literatures, their methodologies, and the outcomes achieved in the context of dealing with the COVID-19 pandemic in detail. Section Three of this paper summarizes the technological aspects of the frameworks that were discussed in Section Two of this paper. Finally, in Section Four, the author elaborates on the significance of these Internet of Things-based frameworks as well as provides a critical analysis of those works. The evidence-based procedure for systematic review and reporting standards [13] called PRISMA (Preferred Reporting Items for Systematic Reviews and Meta-Analyses) was used for this systematic review.

2 Related Works

This section reviews recent IoT-based research aimed at managing the COVID-19 crisis. The IoMT frameworks for both clinical and Non-clinical management of Pandemic are being considered for this review.

An affective computing based IoMT application was introduced by M.A. Rahman et al. [14] during the COVID-19 pandemic. The framework was designed in such a way to run deep learning machines by using advanced processing units at the edge for alerting various COVID-19 related symptoms. This edge computing architecture was also aimed at protecting the environment from privacy and security issues. The authors claimed that their proposed IoMT-based healthcare application would be innovative and would be used when physicians are unavailable or during epidemic situations.

J. Liu et al. [15] proposed a IoMT system for cardiopulmonary observation system. The system was developed to obtain heart rates (HRs) and respiratory rates (RRs) from pressure signals received through a BCG sensor kept near the patient and use them to analyse heart rate variability (HRV), respiratory rate variability (RRV). A reliable HR/RR detection method was proposed. The proposed method's accuracy meets the requirements, according to 25 participants' results. These devices also monitored a COVID-19-treated discharged patient's HRV and RRV. In COVID-19 patients who have been discharged, the respiratory rhythm recovers faster than the heart rhythm. Despite the need for further research, verification and validation, the developed system offers a novel approach to monitoring COVID-19 discharged patients. It is noted that the system's noncontact remote observation facility can effectively lowering the risk of infection among doctors, according to the author's claim.

In order to ensure the security of the data communication over the IoMT system, M. Masud et al.[16] proposed a reliable model during the covid-19 pandemic. They introduced a security protocol between doctor and edge sensor node. The proposed MASK protocol's security was assessed formally and informally. The results of the evaluation have demonstrated the protocol's ability to protect the edge node from physical attacks. The protocol outperforms other conventional protocols in terms of attack prevention, computation and communication efficiency, etc. The proposed protocol provides authentication, confidentiality, integrity, and anonymity to protect IoMT networks. Because of this, it is immune to attacks such as imitation, duplication, and man in the middle, according to its security analysis. Additionally, the researchers say that the suggested protocol consumes fewer resources and is resistant to physical attacks, making it particularly well suited for Internet of Things-enabled medical networks.

Imran Ahmed et al. [17] introduced an IoT-based empirical analysis using deep learning for the early detection of coronavirus infection. This application is aimed at making the diagnostic process easy by examining chest X-rays for detecting the chest infection and limiting the pandemic spread. The model employed RPN to generate region proposals and detect anomalies. The experimental data sets for training and testing the proposed model are obtained from various publicly available data sources. The framework has achieved a detection accuracy of 98 percent. It is claimed that, based on the results of the experiments, the system can help the clinicians for the early assessment of Covid-19 among the infected patients.

A sleep data fusion network (SDFN) module with a star topology Bluetooth network was proposed by Fan Yang et al. [18]. The proposed IoT enabled data reprocessing mechanisms aim to reduce data jamming and save battery power. The experiments showed that the proposed subsystem and mechanisms save system energy and reduce data jamming. The authors believe that by developing a longer lifetime sleep healthcare IoMT system, they will be able to provide longer-term services to people in poor sleep conditions, particularly COVID-19 patients or survivors.

During the early stages of the covid-19 pandemic, Dilibal [19] proposed an edge computing architecture for online video consultation with IoMT based clinical monitoring and control system. The intended functional architecture includes an edge computing module which connects healthcare equipment to the clinical monitoring system. The established platform's accuracy was

validated through an initial demonstration using IoMT-based wearable eye testing equipment. The researcher discovered that the developed monitoring system works well within the proposed architecture framework.

Yuxuan Yang et al. [20] developed a distributed 3C (communication, computing, and cache) resource allocation framework by integrating edge computing technology with machine learning. They formulated gateway communications in IoMT as an endless game and allocated 3C resources cooperatively. To find the game's Nash equilibrium in a distributed setting, they proposed an edge learning algorithm called MSLA that learns from data, the strategy selection probabilities with varying medical criticality categories at the network's edges and converges to the game's Nash equilibrium. Performance evaluations demonstrate the proposed framework's effectiveness.

Ashok Kumar Das et al. [21] presented a blockchain-based, innovative security model for managing vaccine distribution in an IoMT-based cloud-enabled COVID-19 environment. Various operations relating to vaccine demands, orders, dispersion, and tracking are encapsulated in blocks on the blockchain. Due to the immutability, transparency, and decentralization inherent in blockchain technology, the proposed framework's security has been significantly enhanced. Additionally, the framework supports big data analytics powered by artificial intelligence (AI) on the information that is stored in the blockchain's blocks. Additionally, a blockchain simulation model was used to demonstrate the proposed framework in practice. The framework, it is claimed, not only maintains details pertaining to vaccine orders and dispersion, but also tracks medical personnel's vaccination status and any associated side effects, using the genuine and authentic data held in the blockchain's blocks.

Hong-Ning Dai et al. [22] proposed architecture of blockchain-enabled edge intelligence for IoMT. They provided COVID-19 solutions powered by blockchain-enabled edge intelligence, such as surveillance and tracing the source of the epidemic, a traceable pharmaceutical and vaccination supply chain, and online clinical consultations like telemedicine. Hong-Ning Dai et al. [23] also featured a blockchain-enabled IoMT with the goal of addressing IoMT security and privacy concerns. They proposed a multi-layer framework for blockchain-enabled IoMT for tracing pandemic origins, quarantining and social isolation, hospitals, medical data authenticity, and remote healthcare and telemedicine.

Kun Qian et al. [24] developed an innovative multitask speech corpus for COVID-19 research (MSC-COVID-19). They asserted that MSC-COVID-19 is the world's first extensive CA-based database suitable for COVID-19 research. The authors investigated the feasibility of determining the physical and/or mental status of patients based on their voices. Benchmarks using both classical machine learning and cutting-edge deep learning techniques revealed promising results for using CA to combat COVID-19. Upon further examination, it was shown that CA-based methodologies have great promise for the development of non-invasive, low-cost, and effective intelligent systems to aid in the fight against infectious disease crises.

In the aftermath of the COVID-19 pandemic, there are few concerns about post COVID care for young adults, older adults, and mentally depressed people. To address these issues, Tao Zhang et al. [25] proposed an IoMT system that is emotion-aware and intelligent and covers aspects such as data exchange, data management, patient tracking, gathering of data and analysis, healthcare, and others. In surveillance environments, smart IoMT systems are attached to collect multisensory data from patients. Furthermore, for the emotion analysis, the most recent clinical data from official sites and reports is tested. During the COVID-19 pandemic, the intended innovative IoMT system facilitates remote healthcare and emotion-aware decision-making in disease diagnosis, which will significantly contribute to persistent emotion-aware healthcare services. When compared to some mainstream models, experimental findings on some emotion data demonstrate that the designed framework achieves a superior impact. The authors' claim is that the presented

cognition-based evolving technology is a good way to accommodate a large number of devices and the COVID-19 pandemic applications.

Because of the pandemic's high contagiousness, technological breakthroughs are required. N. Naren et al. [26] proposed a prototype that combines IoMT, unmanned aerial vehicles (UAVs), and the DNN model to create a payload that can be deployed on a drone vehicle to aid in fast testing and related medical care. As part of the UAV payload, the proposed prototype includes safe and secured patient authorization, robotic sanitization, and sensors for medical equipment. It detects COVID-19 in real time using a DNN model. The authors claim that the proposed framework manages well with drone vehicle path planning, process management, charged up batteries, sanitizer refilling, and location mapping to deliver test kits and emergency health care to isolated locations with no need for direct human intervention.

A machine learning framework proposed by Qianlong Wang et al. [27] is a risk assessment system that relies on multikernel density estimation (MKDE) and deep neural networks (DNN) to help IoMT applications combat the COVID-19 pandemic. Reliable sources of data sets are acquired and used in the system. The MK-DNN uses two-level modelling to find risk metrics on a finer-grained map, which is useful in areas where disease-related data is lacking. Further to that, because of the inability of the model to train due to a lack of COVID-19 data, a trial based risk assessment method was proposed that evaluates the cumulative error in micro-level outputs using the intended validation value functions and then aids in the optimization of the hyperparameter in the MKDNN. The precision and strength pertaining to the MK-DNN risk assessment framework are demonstrated through simulation on real-world data.

P. Yanambaka et al. [28] introduced a privacy-aware identification module based on the physical unclonable function (PUF), an Internet-of-Medical-Things (IoMT) framework to track the virus-carrying host in a largely populated place. A person carrying the IoMT device or host's privacy and security are given top priority, as well as the data being sent does not include any information about the individual who is holding the device. The authors also propose a new multikey PUF architecture for generating unique identifying keys for the proposed protocol. The key is generated in an average of one second. The generated keys have a uniqueness and reliability of 49.49 percent and 48.20 percent, respectively. It should be noted that the proposed protocol is not dependent on communication, making it adaptable to a variety of platforms.

J. D. Trigo et al. [29] presented a tracking application for a hospital complex with multiple buildings connected by tunnels. The system makes use of IoMT-enabled communication technologies like Long Range Wide-Area Network (LoRaWAN) and the Near Field Communication (NFC) method. The LoRaWAN node locations were chosen based on several factors, including tunnel location, building services and medical equipment, and intra-hospital intensive care patient trips. For getting an accurate characterization, specific spots of the LoRaWAN were chosen using simulations. After the specific spots were determined, a LoRaWAN broadcast studio was set up. According to the authors, a single LoRaWAN hub is sufficient to cover all deployed over-the-ground LoRaWAN nodes. For underground coverage, a second would be required. Similarly, a remote cloud service infrastructure as well as a smart application was developed for handling the data generated. Field tests were conducted to determine the technological viability of the system. The smart application allows ICU patients to move around the complex on demand. The system might readily be adapted to various use cases while being built for ICU-admitted patients. Tab. 1 summarizes all the benchmarking IoMT frameworks proposed by prospective researchers during the pandemic of COVID-19.

SwatiSwayamsiddha et al. [30] explored various novel of cognitive Internet of Medical Things (CIoMT) applications for combating the existing COVID-19 health problem. The dynamic spectrum allocation technique based on cognitive radio (CR) is the solution for accommodating a large number of devices and applications. The CIoMT platform allows for

real-time tracking, remote health monitoring, rapid case diagnosis, contact tracking, clustering, screening, and surveillance, decreasing the workload on the medical industry for infection prevention and control. It has been discovered that CIoMT is a potential technique for rapid diagnosis, dynamic monitoring and tracking, better treatment and management, and preventing the virus from spreading to others.

Table 1: Summary of IoMT frameworks for clinical management of Covid-19

Ref.	Year	Nature of work	Technology Adopted	Outcome
[14]	2021	COVID-19-related symptoms tracker and Alarm	Affective Computing	Effective Next Generation Healthcare Support
[15]	2021	Cardiopulmonary function monitoring	Sensing Technology	A novel approach to monitoring COVID-19 discharged patients
[16]	2021	Ensure the Security of IoMT network	Security Protocol Design	Resistant to network attacks and ideal for IoT-enabled medical networks
[17]	2021	Automated Remote Diagnosis of Covid-19	Deep Learning	Early assessment of infection and Limit the pandemic spread and mortality
[18]	2021	Reduce data jamming and save battery power	Sleep data fusion network (SDFN), Machine Learning	provide longer-term services to COVID-19 patients or survivors
[19]	2020	IoMT based smart healthcare monitoring system for covid-19	Edge computing, Wearable technology	Highly accurate real-time video consultation using IoMT
[20]	2021	Distributed resource allocation framework for Covid-19	Edge Computing and Machine Learning	Formulated gateway interactions in IoMT
[21]	2021	Security framework for vaccine distribution and tracking	Big data analytics powered by artificial intelligence (AI)	Effective Vaccine distribution and Track Vaccination Status
[22] [23]	2020 2021	Contact Tracing, Track supply chain of medicines and vaccines, and healthcare facilities	Blockchain-enabled edge intelligence	Effective Management of Pandemic
[24]	2021	Identify the physical and/or mental status of patients using their voices	Multitask speech corpus for COVID-19	Noninvasive, low-cost, and efficient intelligent systems to assist in coping with the crisis caused by infectious diseases
[25]	2021	Emotional care for infants and children, the older adults, and mentally ill people.	Smart IoMT systems powered by Edge computing	Greatly contribute to convenient and persistent emotion-aware healthcare services.
[26]	2021	Combat the pandemic with less human intervention. Rapid testing and healthcare.	Unmanned aerial vehicles (UAVs) and the DNN	Manages the pandemic well with less human intervention

[27]	2021	Risk assessment framework to Combat COVID-19	Multikernel density estimation (MKDE) and deep neural network (DNN)	Worked well with real time data
[28]	2021	Track the virus-carrying host in a crowded area	Privacy-aware identification module based on the physical unclonable function (PUF)	Unique and reliable for pandemic management
[29]	2020	Patient tracking application in a hospital complex	Long Range Wide-Area Network (LoRaWAN) as well as Near Field Communication (NFC)	The framework working well with real time environment

3 Edge Computing and IoT

Edge computing, machine learning, deep learning, affective computing, block-chain, wearable, and sensing technology are among the technologies used in the IoMT-based works presented here. And edge computing is at the forefront. The terms IoT device and edge device are frequently used interchangeably to describe the same thing, which is misleading [31].

Edge computing is reshaping how millions of devices handle, analyze, and distribute data worldwide. The increasing number of network devices—the IoT—along with the development of innovative products that need real-time computational capability, maintains the momentum for the expansion of edge computing technology. Rapidly evolving internet technologies, such as 5G wireless, enable edge computing devices to develop real-time programs such as audio or signal processing, data analysis, artificial intelligence, and machine automation [32].

Edge computing, according to Gartner [33], is a component of a distributed computing topology in which information processing is positioned near to the edge—where devices and people produce or consume that information. Edge computing helps bring data processing and storage of data closer to the devices collecting data, rather than a centralized point located far away. This is done in order to eliminate latency concerns that could negatively impact the performance of an application. Firms could also save costs by minimizing the amount of data that must be managed centrally or in the cloud. The emergence of edge computing by the growth of IoT devices that connect to the network in order to either send or receive information to the cloud (also known as edge computing). And several IoT-enabled devices create huge volumes of data while operating. Figure 3 depicts the four factors that contribute to edge computing.

Consider devices that monitor factory equipment or a remote office's internet-connected video camera. Despite the fact that the data that is produced by an edge device can be simply transmitted across a network, problems arise when multiple units transmit simultaneously [34]. Make the number of devices that are transmitting live video a lot more than one. Latency not just degrades standards but also consumes a lot of bandwidth. As a result, many of these systems can benefit from edge computing hardware and services. An edge gateway can reduce bandwidth requirements by processing data at the edge and only sending relevant data back to the cloud. For real-time applications, it can also send information back to such an edge device. These edge devices can be an IoT sensor, a laptop, a smartphone, a security camera, or even any web-connected device. Edge gateways are devices that are located at the edge of a computing infrastructure [35].

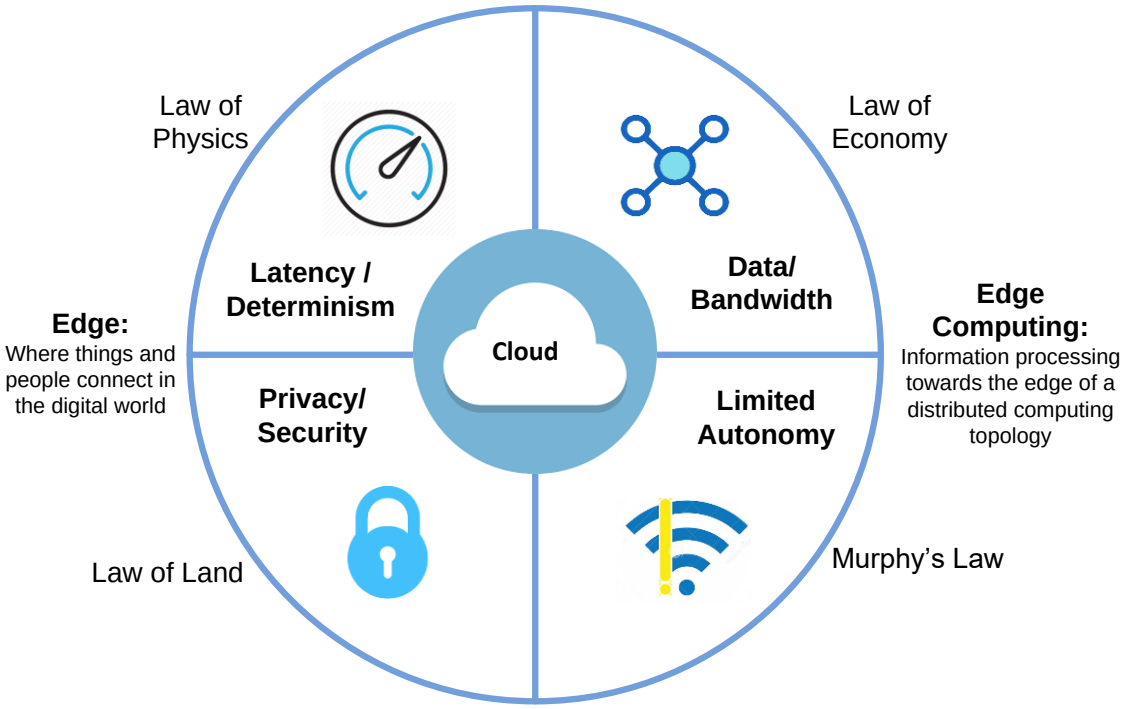

Figure 3: Four factors driving compute to the edge (Courtesy: Gartner Inc.)

Edge computing also helps with other problems such as how much data can be sent over slow cell or satellite connections, and how well systems can work even when there is no internet. Edge computing lets you take advantage of the huge amount of data that IoT devices send back and forth when they're connected. Analytical algorithms and machine learning models can be put on the edge so that they can be used to process data quickly and make quick decisions [36] . An important advantage of edge computing is that a lot of data can be combined together before it is sent to a central location for more processing or long-term storage. In order to improve the efficiency of the proposed works, majority of the benchmarked IoMT frameworks have used edge computing.

4 Discussion

The Internet of Medical Things, which is the health version of IoT, allows a doctor to monitor a patient's health from afar and quickly. During the current COVID-19 epidemic, the IoMT offers a variety of innovative cloud-based facilities and services to better manage pandemics by supporting patients. In such critical times of lockdown, the telemedicine system is extremely important. The efficient interconnected system of equipment, applications, the internet, databases, and so on enables consumers to use services more effectively. The Internet of Medical Things also contributes to the promotion of its solutions by developing cutting-edge smart healthcare applications. It has the potential to totally transform the working structure of healthcare facilities while providing orthopedic patients with a higher level of care and more happiness, which is especially important during the current COVID-19 pandemic [37]. Quality service makes this strategy more effective and worthwhile, even in difficult times. Monitoring and tracking elderly and otherwise disadvantaged patients in far-flung locations is made easier thanks to the Internet of Medical Things (IoMT).

The bench marked works reported in table-1 adopted diversified technologies in order to build intelligent healthcare using IoT. The IoMT frameworks reported here were implemented for different situations during the COVID-19 pandemic and are productive, according to the authors. The challenges faced during the development and implementation stages are highly significant and need to be addressed effectively. I believe the digital change will

allow patients and doctors in rural areas to have improved access to high-quality health care facilities in the near future.

5 Conclusion

The goal of this survey was to bring together the highly innovative IoMT frameworks used to manage the COVID-19 pandemic and examine the applicability, enhancements, and adoption of new technology. The benchmarking works were chosen because of their importance in the clinical and non-clinical management of pandemics. The notable innovative IoMT frameworks put forth during pandemic includes early detection of the decease, ICU care, covid-19 hospital bed allocation, contact tracing, supply chain management, risk assessment, vaccine distribution and patients' emotion detection. Along with IoT, wide range of technologies used in these frameworks including edge computing, affective computing, machine learning, wireless technologies and block chain techniques. It is expected that the massive increase in IoT and IoMT, particularly during the Covid-19 pandemic, will add feathers to the upcoming research in these domains.

References

[1] P. V. Dudhe, N. V. Kadam, R. M. Hushangabade and M. S. Deshmukh, "Internet of Things (IOT): An overview and its applications," 2017 International Conference on Energy, Communication, Data Analytics and Soft Computing (ICECDS), 2017, pp. 2650-2653, doi: 10.1109/ICECDS.2017.8389935.

[2] WHO's statement on Health in its Constitution. (1946). [Online]. Available: https://www.who.int/about/governance/constitution

[3] Worldwide IoT spending Projection as of 9 January 2022. (2022). [Online]. Available: https://www.statista.com/statistics/976313/global-iot-market-size/

[4] S. Ramson and D. J. Moni, "A case study on different wireless networking technologies for remote health care," *Intelligent Decision Technologies*, vol. 10, no. 4, pp. 353–364, 2016.

[5] J. F.-W. Chan et al., "A familial cluster of pneumonia associated with the 2019 novel coronavirus indicating person-to-person transmission: A study of a family cluster," *Lancet*, vol. 395, no. 10223, pp. 514–523, 2020.

[6] X. Peng, X. Xu, Y. Li, L. Cheng, X. Zhou, and B. Ren, "Transmission routes of 2019-nCoV and controls in dental practice," *Int. J. Oral Sci*., vol. 12, no. 1, pp. 1–6, 2020.

[7] S. Tian, W. Hu, L. Niu, H. Liu, H. Xu, and S.-Y. Xiao, "Pulmonary pathology of early phase 2019 novel coronavirus (COVID-19) pneumonia in two patients with lung cancer," *J. Thor. Oncol*., vol. 15, no. 5, pp. 700–704, 2020.

[8] COVID-19 Situation Update Worldwide, as of 4 November 2020. (2020). [Online]. Available: https://www.ecdc.europa.eu/en/geographicaldistribution-2019-ncov-cases

[9] Yang, Ting, Mattia Gentile, Ching-Fen Shen, and Chao-Min Cheng."Combining Point-of-Care Diagnostics and Internet of Medical Things (IoMT) to Combat the COVID-19 Pandemic," *Diagnostics* 10, no. 4: 224, 2020.

[10] R. Vaishya, M. Javaid, I. H. Khan, and A. Haleem, "Artificial intelligence (AI) applications for COVID-19 pandemic," *Diabetes Metab. Synd. Clin. Res. Rev*., vol. 14, no. 4, pp. 337–339, 2020.

[11] G. J. Joyia, R. M. Liaqat, A. Farooq, and S. Rehman, "Internet of Medical Things (IoMT): Applications, benefits and future challenges in healthcare domain," *J. Commun*., vol. 12, no. 4, pp. 240–247, 2017.

[12] A. Shoeibi et al., "Automated detection and forecasting of COVID-19 using deep

learning techniques: A review," 2020. [Online]. Available: arXiv:2007.10785.

[13] Preferred Reporting Items for Systematic Reviews and Meta-Analyses (PRISMA). (2022). [Online]. Available: http://www.prisma-statement.org/

[14] M. A. Rahman and M. S. Hossain, "An Internet-of-Medical-Things-Enabled Edge Computing Framework for Tackling COVID-19," *IEEE Internet of Things Journal*, vol. 8, no. 21, pp. 15847-15854, 1 Nov.1, 2021, https://10.1109/JIOT.2021.3051080

[15] J. Liu, F. Miao, L. Yin, Z. Pang and Y. Li, "A Noncontact Ballistocardiography-Based IoMT System for Cardiopulmonary Health Monitoring of Discharged COVID-19 Patients," *IEEE Internet of Things Journal*, vol. 8, no. 21, pp. 15807-15817, 1 Nov.1, 2021, doi: 10.1109/JIOT.2021.3063549.

[16] M. Masud et al., "A Lightweight and Robust Secure Key Establishment Protocol for Internet of Medical Things in COVID-19 Patients Care," *IEEE Internet of Things Journal*, vol. 8, no. 21, pp. 15694-15703, 1 Nov.1, 2021, https://10.1109/JIOT.2020.3047662

[17] I. Ahmed, A. Ahmad and G. Jeon, "An IoT-Based Deep Learning Framework for Early Assessment of Covid-19," *IEEE Internet of Things Journal*, vol. 8, no. 21, pp. 15855-15862, 1 Nov.1, 2021, doi: 10.1109/JIOT.2020.3034074.

[18] F. Yang et al., "Internet-of-Things-Enabled Data Fusion Method for Sleep Healthcare Applications," *IEEE Internet of Things Journal*, vol. 8, no. 21, pp. 15892-15905, 1 Nov.1, 2021, doi: 10.1109/JIOT.2021.3067905.

[19] Ç. Dilibal, "Development of Edge-IoMT Computing Architecture for Smart Healthcare Monitoring Platform," *in the proceedings of 4th International Symposium on Multidisciplinary Studies and Innovative Technologies (ISMSIT)*, 2020, pp. 1-4, doi: 10.1109/ISMSIT50672.2020.9254501.

[20] Y. Yang, X. Wang, Z. Ning, J. J. P. C. Rodrigues, X. Jiang and Y. Guo, "Edge Learning for Internet of Medical Things and Its COVID-19 Applications: A Distributed 3C Framework," *IEEE Internet of Things Magazine*, vol. 4, no. 3, pp. 18-23, September 2021, doi: 10.1109/IOTM.0100.2000154.

[21] A. K. Das, B. Bera and D. Giri, "AI and Blockchain-Based Cloud-Assisted Secure Vaccine Distribution and Tracking in IoMT-Enabled COVID-19 Environment," *IEEE Internet of Things Magazine*, vol. 4, no. 2, pp. 26-32, June 2021, doi: 10.1109/IOTM.0001.2100016.

[22] H. -N. Dai, Y. Wu, H. Wang, M. Imran and N. Haider, "Blockchain-Empowered Edge Intelligence for Internet of Medical Things Against COVID-19," *IEEE Internet of Things Magazine*, vol. 4, no. 2, pp. 34-39, June 2021, doi: 10.1109/IOTM.0011.2100030.

[23] H. -N. Dai, M. Imran and N. Haider, "Blockchain-Enabled Internet of Medical Things to Combat COVID-19," *IEEE Internet of Things Magazine*, vol. 3, no. 3, pp. 52-57, September 2020, doi: 10.1109/IOTM.0001.2000087.

[24] K. Qian *et al.*, "Computer Audition for Fighting the SARS-CoV-2 Corona Crisis—Introducing the Multitask Speech Corpus for COVID-19," *IEEE Internet of Things Journal*, vol. 8, no. 21, pp. 16035-16046, 1

Nov.1, 2021, doi: 10.1109/JIOT.2021.3067605

[25] T. Zhang, M. Liu, T. Yuan and N. Al-Nabhan, "Emotion-Aware and Intelligent Internet of Medical Things Toward Emotion Recognition During COVID-19 Pandemic," *IEEE Internet of Things Journal*, vol. 8, no. 21, pp. 16002-16013, 1 Nov.1, 2021, doi: 10.1109/JIOT.2020.3038631.

[26] N. Naren et al., "IoMT and DNN-Enabled Drone-Assisted Covid-19 Screening and Detection Framework for Rural Areas," *IEEE Internet of Things Magazine*, vol. 4, no. 2, pp. 4-9, June 2021, doi: 10.1109/IOTM.0011.2100053.

[27] Q. Wang, Y. Guo, T. Ji, X. Wang, B. Hu and P. Li, "Toward Combatting COVID-19: A Risk Assessment System," *IEEE Internet of Things Journal*, vol. 8, no. 21, pp. 15953-15964, 1 Nov.1, 2021, doi: 10.1109/JIOT.2021.3070042.

[28] V. P. Yanambaka, A. Abdelgawad and K. Yelamarthi, "PIM: A PUF-Based Host Tracking Protocol for Privacy Aware Contact Tracing in Crowded Areas," IEEE Consumer Electronics Magazine, vol. 10, no. 4, pp. 90-98, 1 July 2021, doi: 10.1109/MCE.2021.3065215.

[29] J. D. Trigo et al., "Patient Tracking in a Multi-Building, Tunnel-Connected Hospital Complex," *IEEE Sensors Journal*, vol. 20, no. 23, pp. 14453-14464, 1 Dec.1, 2020, doi: 10.1109/JSEN.2020.3007593.

[30] Swati Swayamsiddha, Chandana Mohanty, "Application of cognitive Internet of Medical Things for COVID-19 pandemic," Diabetes & Metabolic Syndrome: Clinical Research & Reviews, Vol 14, no 5, pp 911-915, 2020.

[31] Alam, Mehtab & Khan, Ihtiram. Edge Computing and its Impact on IoT. International Conference on Contemporary Issues in Engineering and Technology (CIET-2021), 2021. 10.6084/m9.figshare.14369642.

[32] Hassan etal., "Edge Computing in 5G: A Review," IEEE Access, pp.1-1, 2019, 10.1109/ACCESS.2019.2938534.

[33] Gartner. [Online]. (2022). Available: https://www.gartner.com/en/information-technology/glossary/edge-computing

[34] A. Galanopoulos, J. A. Ayala-Romero, D. J. Leith and G. Iosifidis, "AutoML for Video Analytics with Edge Computing," IEEE INFOCOM 2021 - IEEE Conference on Computer Communications, 2021, pp. 1-10, doi: 10.1109/INFOCOM42981.2021.9488704.

[35] Morabito, Roberto & Petrolo, Riccardo & Loscri, V. & Mitton, Nathalie, "LEGIoT: A Lightweight Edge Gateway for the Internet of Things," Future Generation Computer Systems. 2018, 92. 10.1016/j.future.2018.10.020.

[36] B. Varghese, N. Wang, S. Barbhuiya, P. Kilpatrick and D. S. Nikolopoulos, "Challenges and Opportunities in Edge Computing," 2016 IEEE International Conference on Smart Cloud (SmartCloud), 2016, pp. 20-26, doi: 10.1109/SmartCloud.2016.18.

[37] Pratap Singh R, Javaid M, Haleem A, Vaishya R, Ali S. "Internet of Medical Things (IoMT) for orthopaedic in COVID-19 pandemic: Roles, challenges, and applications," J Clin Orthop Trauma. 2020 Jul-Aug;11(4):713-717. doi: 10.1016/j.jcot.2020.05.011.

دراسة منهجية لأطر إنترنت الأشياء الطبية (IoMT) أثناء جائحة كورونا Covid-19

فتحي علي جريبي،
كلية علوم الحاسب وتقنية المعلومات، جامعة جازان، جازان، المملكة العربية السعودية

الملخص

منذ ظهور إنترنت الأشياء (IoT)، حدثت العديد من الثورات الصناعية في مناطق متنوعة. تتأثر الصناعة الصحية بشكل إيجابي بسبب هذا التحول الهائل. أصبح إنترنت الأشياء الطبية (IoMT) شائعاً خلال جائحة كورونا COVID-19 من خلال ربط المعدات الطبية من خلال البنى التحتية لتقنية المعلومات والاتصالات (ICT) لمعالجة القضايا. تم طرح مجموعة متنوعة من الأطر البحثية في العام ونصف العام الماضيين من خلال معالجة العديد من المشكلات الطبية في الوباء باستخدام إنترنت الأشياء الطبية (IoMT) . يهدف هذا البحث إلى تجميع أطر بحث (IoMT) الموثوقة والتي تم نشرها لمعالجة القضايا الصحية كجزء من التعامل مع جائحة كورونا COVID-19. كما يوفر أهمية الحوسبة المتطورة في أطر عمل إنترنت الأشياء ، المشار إليها في هذه المراجعة. تم اتباع البروتوكولات الموصى بها PRISMA لهذه الدراسة المنهجية.

الكلمات المفتاحية: إنترنت الأشياء، **إنترنت الأشياء الطبية، كورونا، حوسبة Edge**

PCR Detection and Identification of Virulent *Streptococcus thermophilus* Phages from the Fermented Milk "Laban" in KSA

[1,2] Yahya Ali & [1]Faisal Hadadi
[1]Biology Department, College of Science, Jazan University, KSA
[2]Animal Health Research Institute, Agricultural Research Center, Egypt

Abstract:

"Laban" is a popular fermented milk product in Middle East, especially in Saudi Arabia and in other Gulf countries. Twenty different samples of the fermented milk "Laban" representing 5 commercial dairy industries were collected from different local markets of Jazan City in Saudi Arabia and tested for the presence of lytic bacteriophages infecting the lactic starter bacterium *Streptococcus thermophilus (S. th.)*. A total of 45 isolates of *S. thermophilus* were selected after cultivation on M17 culture media, and used as sensitive strains for the detection and propagation of lytic bacteriophages. Moreover, filtrates (Whey) from "Laban" samples (L1 to L20) were tested for the existence of lytic bacteriophages using spot-test, plaque-test assays, transmission electron microscope (TEM) and multiplex PCR method. The results revealed that L4 and L9 were Spot-test positive against isolate *4.3ND*, with a phage titer 4×10^7 and 3.5×10^5 pfu/ml, respectively. The 2 phages were isolated, purified and named P4ND and P9ND. Transmission electron microscopy showed phage particles with isometric heads (59.5 nm Ø) and long non contractile tails (251 nm in length). Furthermore, A Multiplex PCR was developed and used for the detection and identification of the five *S. thermophilus* phage groups (*pac*, *cos*, 5093, 987 and P738) in the filtrates with expected PCR products of 432 bp, 514 bp, 638, 302 and 255 bp, respectively. Interestingly, the samples L4 and L9 showed PCR products of 514 bp, indicating that the phages P4ND and P9ND are members of *cos*-type *S. thermophilus* phages and confirming the results of spot test and electron microscopy.

Key words:

Streptococcus thermophilus, Laban, Bacteriophages, Multiplex PCR

1 Introduction:

Bacteriophage attack is the main reason of fermentation failures in dairy industry (Bruttin et al., 1997a; Marcó et al., 2012). *Streptococcus thermophilus* strains are used commonly in the production of yoghurt, Mozzarella and many other types of cheese and are considered the second most important starter bacteria after *Lactococcus lactis*. Morphologically, *S. thermophilus* are gram-positive nonmotile spherical to ovoid cells (0.7 – 0.9 μm Ø) appears in pairs or chains of microaerophilic, moderately thermophilic bacteria that possesses a relatively small genome size of approximately 1.8 Mb (Binetti et al., 2005; Duplessis et al., 2006; Fuquay et al., 2011)

The fermented "Laban" is a popular milk product in Middle East, especially in Saudi Arabia and in many other Gulf countries. Similar milk products are found in other countries, such as Lebanon, Egypt, Turkey, Tunisia and Morocco but under different names. Laban is manufactured mainly from cows' milk (may be full-fat, partially skimmed or free-fat milk) by industrial fermentation methods using lactic acid starter bacteria (especially *Lactobacillus delbrueckii subsp. Bulgaricus* and *Streptococcus thermophilus*), and on small scales traditionally by using artisanal starters (Béal and Chammas, 2016; Chammas et al., 2006).

Streptococcus thermophilus phages were firstly categorized into 2 groups, named *pac* and *cos* phages depending on the packaging mechanism of phage DNA during replication cycle (*pac*: head-full packaging, *cos*: from cohesive ends), and the major structural proteins pattern obtained after running samples in SDS-PAGE (Sodium dodecyl sulfate polyacrylamide gel electrophoresis) (Desiere et al., 1999; Le Marrec et al., 1997; Lucchini et al., 1999a; Lucchini et al., 1999b). Both *pac* and *cos* phages have the same morphology with long noncontractile tails (of more than 200 nm in length) and isometric heads (Capsids); thus, these phages are members of *Siphoviridae* family (Brussow et al., 1994; Guglielmotti et al., 2009; Mahony and Van Sinderen, 2014). Members of the *pac* phage group are virulent and temperate, while the most reported *cos* phages are virulent (Mahony and Van Sinderen, 2014). In 2011, the third group “5093 group” of *S. thermophilus* phages was discovered (Mills et al., 2011). The DNA sequence of this phage group shows notable similarity to

phages infecting nondairy streptococcal species. The morphology of *5093* phages differs from *pac* and *cos* phages, as the tail tips contain globular appendages. In 2016, the fourth group, which was named the "987 group", was identified (McDonnell et al., 2016). Members of this group share similarity with morphogenesis genes of some P335 phages infecting *Lactococcus lactis* and the replication genes of *S. thermophilus* phages. The morphology of 987 phages is different from morphology of the other 3 groups, as the 987 phages had greatly shorter tails than phages of the other groups and the tail tip possessed a broad appendage that resembled the baseplate of the P335 lactococcal phages. Recently, the fifth novel group of phages that infect a few strains *Streptococcus thermophilus*, named P738 group (P738 and D4446 phages), was identified (Philippe et al., 2020). Complete sequencing and analysis of P738 and D4446 phage genomes revealed genome sizes of 34,037 bp and 33,656 bp, as well as open reading frames (ORFs) of 48 and 46 ORFs, respectively. Furthermore, analysis of phage genomes showed that the 2 phages were highly similar to each other and shared similarities with streptococcal phages but showed very limited similarities to other *S. thermophilus* bacteriophages.

2 Materials and methods

2.1 Sample collection

Twenty different samples of the fermented milk "Laban" representing 5 commercial dairy companies were collected from different local markets of Jazan City in Saudi Arabia and tested for the presence of bacteriophages (lytic phages). The collected samples were cooled in icebox at 4 °C and transported immediately to the laboratory for examination.

2.2 Bacterial isolates and growth conditions:

All bacterial isolates were grown in M17 medium (HiMedia, India) for growth optimization of *S. thermophilus* strains at 42°C for 48 h.

2.2.1. Isolation of *S. thermophilus*

Three colonies with different sizes, shapes and colors were randomly picked from M17 agar plates for each "Laban" sample (total = 15 samples) and transferred to 10 ml of M17 broth and incubated at 42 °C for 48 h. The selected colonies were purified by streaking on fresh M17 agar plates and incubated at 42 °C for 48 h. Isolated strains were maintained by two methods, first for long-term

maintenance, by culturing in M17 broth at 42 °C overnight and storing at -20 °C after adding 25% glycerol (w/v) (Lavelle et al., 2018); second, by keeping grown strains on M17 agar slant at 4 °C and streaking every 4 weeks. Furthermore, prior to use, *S. thermophilus* strains were cultivated overnight in M17 broth at 42 °C.

2.2.2. Identification of bacterial isolates

2.2.2.1. 16S rRNA gene analysis

The 16S rRNA gene of the sensitive *S. thermophilus* strain isolated in this study was amplified using the universal primers 8F 5'-AGAGTTTGATCCTGGCTCAG-3' and 1525R 5'-AAGGAGGTGATCCAGCC-3' (Beumer and Robinson, 2005). The polymerase chain reaction (PCR) conditions used were one cycle of 95 °C for 5 min, followed by 35 cycles of 95 °C × 30 s, 51 °C × 30 s, 72 °C × 90 s, and a final extension of 72 °C × 7 min. The PCR product was mixed with 6x RUNESAFE staining buffer (Cleaver Scientific Ltd., United Kingdom), applied to a 1.5% agarose gel and visualized by UV illumination. The nucleotide sequence of the amplified fragment was determined at the Molecular Biology Research Center (Assiut University, Egypt) and was analyzed by National Centre for Biotechnology Information (NCBI)-Basic Local Alignment Search Tool (BLAST) at the NCBI website (https://blast.ncbi.nlm.nih.gov/Blast.cgi)

Phage assay

2.3.1. Preparation of filtrate (Whey) from "Laban" samples

From each "Laban" sample, 100 ml was filtered through sterile filter paper (VWR International LLC, PA, USA) using sterile glass funnels. Then, the filtrate was filtered again using a 0.45-µm Ø syringe filter (Sartorius, Göttingen, Germany). Finally, the filtrate was stored at 4 °C for further use in the spot test and plaque test for detection of phages and counting of the number of phages in each sample (pfu/ml).

2.3.2. Bacteriophages Isolation and Enumeration

Twenty filtrates (whey) of "Laban" samples were examined for the presence of phages with lytic activity against 45 *S. thermophilus* isolates. The spot and plaque tests were carried out by using the double layer (Bottom/solid and top/soft) agar technique according to Lillehaug (1997). In this technique, M17 broth was supplemented with 0.25% glycine, 10 mM $CaCl_2$, 1 mM $MgSO_4$ and 10 g/L (Bottom/solid) or 4

g/L (top/soft) agar-agar. Positive results were confirmed by the appearance of a clear zone of lysis in the bacterial lawn after incubation at 42°C for 24 h.

2.3.2.1. Spot test

Approximately 300 µl of host culture (OD_{620} nm = 0.3), 100 µl of 40 mM $CaCl_2$ and 100 µl of reconstituted skim milk (HiMedia, India) were added and mixed with 2.5 ml of molten soft agar (47°C). Subsequently, the agar suspension then poured immediately on bottom agar. After solidification, 10 - 50 µl of phage lysates were spotted on the surface and incubated at 42°C for 24 h.

2.3.2.2. Plaque test

Positive whey (filtrate) was diluted in serial dilutions from 10^{-1} to 10^{-8} in phage dilution buffer. From each dilution, 100 µl was mixed with 300 µl of log-phase host culture ($OD_{620\ nm}$ = 0.3). Then 100 µl of 40 mM $CaCl_2$ and 100 µl of reconstituted skim milk were added. The sample was incubated for 10 min at room temperature to allow adsorption of the phages to the cell surface. Subsequently, 2.5 ml of molten soft agar (47°C) was added, mixed and poured directly on M17 bottom agar plates. After incubation at 42℃ for 24 h, the phage titers indicated as plaque-forming units (pfu/ml) were determined.

Lytic *S. thermophilus* bacteriophages were obtained by propagation from single plaque isolates on sensitive strains in 10 ml M17 broth using different dilutions of the filtrate (whey) and tubes were incubated at 42℃ in water bath with continuous measuring of the OD_{620} every 15 min until complete lysis. Then the lysate was filtered with 0.45 µm Ø syringe filter (Sartorius, Göttingen, Germany) and stored at 4℃ for further use in electron microscopy, PCR and lytic propagation.

2.3.3. Electron microscopy

Phage lysate obtained from lytic propagation of the phage on sensitive strain in M17 broth, was adsorbed to freshly prepared carbon film, stained with 2% (w/v) uranyl acetate, the stained carbon film was carried onto a copper grid and analyzed under the transmission electron microscope JEOL 100CX-II at an accelerating voltage of 80 KV (Electron Microscope Unit, Assiut University, Egypt).

2.3 Multiplex PCR for detection of *S. thermophilus* phages

For detection and identification of all five groups of *S. thermophilus phages* (*Pac*, *cos*, 5093, 987 and P738) in collected "Laban" samples, a multiplex PCR assay was developed using 5 primer sets: 2 previously published

primer sets were used for the detection of *pac*- and *cos*-phages (Ali, 2009), and three newly designed primer sets (this study) were used for the detection of 5093, 987 and P738 phages.

All primers used in this work were manufactured by Eurofins, Genomics LLC, Kentucky, Louisville, KY, USA. All PCR primers are listed in Table 1.

To detect and identify *Streptococcus thermophilus* phage groups 5093, 987 and P738, three new primer sets were designed. For selection of the suitable primers, the complete genome sequences of published *Streptococcus thermophilus* phage groups 5093 in GenBank were aligned by using Basic Local Alignment Search Tool (BLAST), provided by the NCBI (https://blast.ncbi.nlm.nih.gov/Blast.cgi) with respect to the conserved minor capsid protein (mcp) gene and two primers (5093-F/5093R) were selected from the internal region of the mcp gene using Primer-BLAST developed by NCBI (https://www.ncbi.nlm.nih.gov/tools/primer-blast/). In silico analysis of the 2 primers gave a PCR product with 302 bp in length.

The same was done for selection of the specific primers for the detection and identification the *Streptococcus thermophilus* phage groups 987. The complete genome sequences of published *S. thermophilus* phage groups 987 in GenBank Data base were aligned with respect to the conserved anti-receptor gene, and 2 primers (987-F/987-R) were selected from the conserved nucleotide sequence of the anti-receptor gene using Primer-BLAST (https://www.ncbi.nlm.nih.gov/tools/primer-blast/). In silico analysis of the 2 primers gave a PCR product 638 bp in length.

Additionally, the same was done for the selection of specific primers for the detection and identification of *S. thermophilus* phage group P738 (P738 & D4446 phages). Thus, the published genome sequences of *S. thermophilus* phages P738 and D4446 in GenBank Data base were aligned with respect to the conserved *major head protein* gene (*orf302* & *orf300*) and 2 primers (738-F/738-R) were selected from the conserved nucleotide sequence using Primer-BLAST (https://www.ncbi.nlm.nih.gov/tools/primer-blast/). In silico analysis of the 2 primers gave a PCR product 255 bp in length.

Table 1: List of Primers used in this study

Primer Name	Primer sequence (5´→ 3´)	Target DNA	Amplicon, bp	Reference
YP-F	GCTCGTCTTGAAGCTATGC	Major head protein gene of *pac*-type *S. th.* phages	432 bp	(Ali, 2009)
YP-R	GATAAGAGTCAAGTGACCGTC			
YC-F	GCTATGCTTGACGATTCAGT	Major head protein gene of *cos*-type *S. th.* phages	514 bp	(Ali, 2009)
YC-R	AGCAGAATCAGCAAGCAA G			
5093-F	TTTAGGACAAGTGAAGAGGTTG	Phage 5093, minor capsid protein gene	302 bp	This study
5093-R	CTCAATTGTTCTTCAGCAATCC			
987-F	CTGGCGTTCATTTGCATTTC	Phage 987-Anti-receptor gene	638 bp	This study
987-R	TTATCAACTCGCTAAGAACCTG			
738-F	AATCATTTCCAGAAACAAATCTCAC	*S. th.* phage P738, major head protein gene	255 bp	This study
738-R	TTTTTGTTTCAGCTGGTTTTTGT			

S. th.: *Streptococcus thermophilus*

For detection and identification of all five groups of *S. thermophilus* phages (*Pac*, *cos*, 5093, 987 and P738/D4446) in collected "Laban" samples, a multiplex PCR assay was developed using 5 primer sets. The expected PCR fragments amplified by the 5 primer sets, *pac*-primers (YC-F/YC-R), *cos*-primers (YP-F/YP-R), 5093-primers (5093-F/5093-R) and 987-primers (987-F/987-R), and P738, had different lengths: 432 bp, 514 bp, 302 bp, 638 bp and 255 bp, respectively. The PCR program used was one cycle of 94 °C for 5 min, followed by 35 cycles of 94 °C × 30 s, 51.8 °C × 30 s, 72 °C × 50 s, and a final extension of 72 °C × 7 min. The resulting PCR products were mixed with 6x RUNESAFE staining buffer (Cleaver Scientific LTD, United Kingdom), applied to a 2% agarose gel and visualized by UV illumination.

3 Results

3.1 Isolation and Identification of *S. thermophilus* from "Laban"

A set of 45 strains were isolated from fifteen "Laban" samples representing the five commercial brands (MA, SA, NA, ND and AC). A preliminary identification of the isolates was performed by cultivation on M17 selective medium for *S. thermophilus*. Identification of all isolates was also confirmed by Gram staining and all isolates showed Gram positive (violet) cocci with spherical or ovoid morphology, present in pairs or chains, indicating that all isolates were *S. thermophilus*. The isolated phage sensitive strain *4.3ND* was genotypically identified by amplification of the entire fragment of the 16S rRNA gene (Beumer and Robinson, 2005), a PCR product of approximately 1.5-kb fragment was amplified. A partial fragment (1379 bp) of the 16S rRNA gene was sequenced at Molecular Biology Research Center (Assiut University, Egypt) and was

analyzed by NCBI-web site (NCBI-BLAST) for detection of similarity with other known sequences in the NCBI database. The nucleotide sequence was deposited in GenBank under the accession numbers OK533572.

Table 2. List of isolated *Streptococcus thermophilus* from "Laban" samples

Dairy Company	Commercial Product size (ml)	Bacterial isolates (*S. thermophilus*)	Source / Reference
A	180	*1.1AM, 1.2AM & 1.3AM*	This study
	360	*6.1AM, 6.2AM & 6.3AM*	This study
	1000	*11.1AM, 11.2AM & 11.3AM*	This study
B	180	*2.1AS, 2.2AS & 2.3AS*	This study
	360	*7.1AS, 7.2AS & 7.3AS*	This study
	850	*12.1AS, 12.2AS & 12.3AS*	This study
C	180	*3.1NA, 3.2NA & 3.3NA*	This study
	360	*8.1NA, 8.2NA & 8.3NA*	This study
	800	*13.1NA, 13.2NA, 13.3NA*	This study
D	180	*4.1ND, 4.2ND & 4.3ND*	This study
	360	*9.1ND, 9.2ND & 9.3ND*	This study
	800	*14.1ND, 14.2ND & 14.3ND*	This study
E	180	*5.1AC, 5.2AC & 5.3AC*	This study
	360	*10.1AC, 10.2AC & 10.3AC*	This study
	850	*15.1AC, 15.2AC & 15.3AC*	This study

3.2 Phage Screening using Spot-test

All filtrate (whey) samples were tested against the 45 *S. thermophilus* strains isolated from "Laban" samples. Spot tests showed that the *S. thermophilus* 4.3ND was sensitive to the filtrate (whey) of the "Laban" samples L4 and L9 (Fig. 1), and the detected phages were named P4ND and P9ND, respectively

Fig. 1: Spot test: *S. th. 4.3ND* screened against all filtrates (F1 to F20), positive results (lysis zone) obtained with F4 and F9

3.3 Plaque test:

The phage titers in phage-positive samples L4 and L9 were 4 x 10^7 and 3.5 x 10^5, respectively (Fig. 2). The new detected phages were purified by propagation of single plaque isolate on the host strain *S. th.4.3ND*, in 10 mL M17 broth supplemented with 10 mM $CaCl_2$ at 42°C, filtered through a 0.45 µm syringe filter, and stored at 4°C. The isolated phages were named P4ND and P9ND.

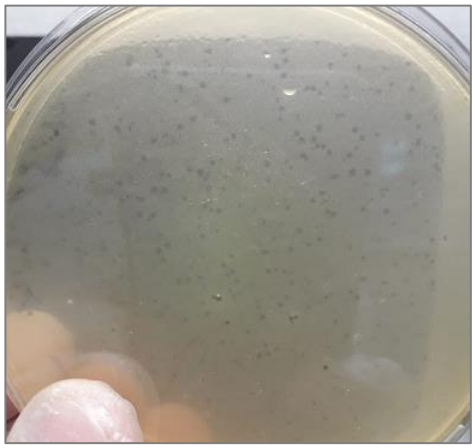

Fig. 2: Plaques of the phage P4ND in the bacterial lawn of the sensitive strain *4.3ND* incubated overnight at 42°C

3.4 Phage morphology

Transmission electron microscopy of the isolated phage P4ND showed that the phage particles (Fig.3) have isometric capsids (diameter: 59.5 nm Ø) and long, noncontractile tails (length: 251 nm).

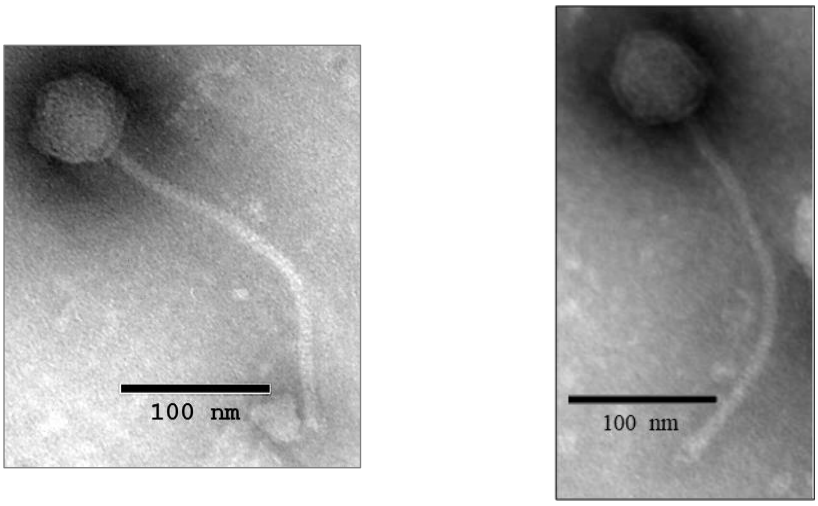

Fig. 3: Transmission electron micrograph of *S. thermophiles* phage P4ND & P9ND isolated from "Laban" samples.

3.5 Multiplex PCR for detection and differentiation of *S.th.* phages

The twenty filtrates (whey) of samples collected from 5 dairy commercial producers were screened for the prevalence and characterization of the five *S. th.* phage groups using the developed multiplex PCR. A PCR product of 514-bp (visualized on 2% agarose gel) was obtained from the 2 "Laban" samples L4 and L9 (Fig. 4).

Fig. 4: Agarose gel (2%) electrophoresis of PCR products obtained from 20 filtrates of "Laban" samples using Multiplex RCR for detection of *S. thermophilus* phage groups (lane: L1 to L20). Lane B: negative control (Blank). Lane M: 100 bp DNA Marker (Thermo Scientific, GeneRuler 100 bp DNA Ladder).

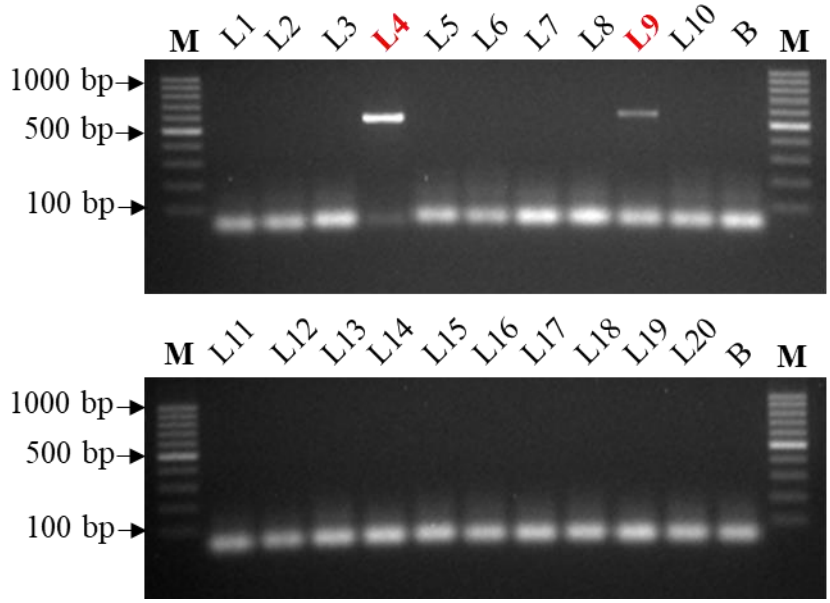

4 Discussion

Laban is a yogurt-like fermented milk product, and manufactured by fermentation of milk using mainly *Lactobacillus bulgaricus* and *S. thermophilus* (Tamime and Robinson, 1999). Usually, heat treatment of milk at 90°C during yoghurt production, kills most bacteriophages (Quiberoni et al., 2003), while in cheese production raw or pasteurized milk is used and many bacteriophages will resist pasteurization (Quiberoni et al., 2006).

In this study, 2 *Streptococcus thermophilus* phages were detected and isolated from twenty samples of the fermented milk product "Laban" in Jazan city, KSA. The two isolated

phages had the same morphology (isometric capsid: 59.5 nm Ø and long, noncontractile tail: 251 nm). This description correlates with the basic morphology of other *S. thermophilus phages* (DT1, Sfi19, Sfi21 and 2972) that have isometric heads with 45 to 65 nm Ø in diameter and long, noncontractile tails with 230 to 270 nm in length (Bruttin et al., 1997b; Le Marrec et al., 1997; Lévesque et al., 2005; Quiberoni et al., 2006; Tremblay and Moineau, 1999). Hence, it can be concluded that the phages P4ND and P9ND are members of the morphotype B1of the well-described *Siphoviridae* phage family (Bradley, 1967).

Interestingly, the two detected phages (P4ND & P9ND) were isolated from samples of the same dairy company (D), and those two phages infect the same bacterial isolate (*4.3ND*). Thus, there is a high probability that these are the same and not different phages. The sequence analysis showed that the isolate *4.3ND* had 100% identity to the 16S rRNA gene (partial sequence) of 57 *S. thermophilus* strains: *S. th.* strain 3352 (GenBank Accession No.: MT613636.1), *S. th.* strain 3285 (Accession No.: MT613594.1), *S. th.* strain 3281 (Accession No.: MT613590.1), *S. th.* strain 3271 (Accession No.: MT613584.1), *S. th.* strain 3202 (Accession No.: MT613548.1), *S. th.* strain 16t (Accession No.: MN994627.1), *S. th.* strain 159 (Accession No.: MN994626.1) and other 50 *S. thermophilus* strains. These nucleotide homology studies confirmed that the isolates belong to *S. thermophilus* strain. In addition, the phage titers were slightly high (4×10^7 and 3.5×10^5 pfu/mL). Contamination of dairy plants with bacteriophages originates from different sources. Raw milk is the most common source of lytic phages and they are naturally found in low titers, between 10^1- 10^3 pfu/ml. The other sources of phage contamination include milk powder & whey proteins, equipment, air as well as the starter bacteria containing temperate phages (Szczepankowska et al., 2013).

Screening of the filtrates (whey) collected from “Laban” samples using the developed multiplex PCR showed a 514 bp PCR product (Fig. 4) from L4 and L9 “Laban” samples, indicating that those two samples harbored *S. thermophilus* phages. This result correlates completely with the results obtained from phage screening using spot-test. Furthermore, the size of the obtained PCR fragment proved that the

2 phages (P4ND & P9ND) were members of *cos*-type phages (Ali, 2009). No PCR amplicons were obtained from the 3 new designed primer sets used for the detection of *S. th.* phage groups 5093, 987 and P738. Also, positive controls representing all the 5 groups of *S. th.* phages were not available to be used in the multiplex PCR.

The first multiplex PCR was designed for detection and identification of *pac* and *cos S. thermophilus* phages (Ali, 2009; Quiberoni et al., 2006). As the third and fourth *S. thermophilus* phage groups were identified (McDonnell et al., 2016; Mills et al., 2011), the second multiplex PCR was developed to detect and classify all the 4 groups of *S. thermophilus* phages (McDonnell et al., 2017). Unfortunately, in silico and in vivo analyses of the previously mentioned multiplex PCR showed that primer set, which was designed to detect 987-group phages, can bind to *L. lactis* phage ul36 and produce a PCR fragment of 1013 bp in length. Thus, it can give false positive results with phages from other dairy species (Szymczak et al., 2019). Consequently, an improved multiplex PCR was designed for detection and identification of all 4 phage groups infecting the starter bacterium *S. thermophilus* (Szymczak et al., 2019). Both multiplex PCR methods (McDonnell et al., 2017; Szymczak et al., 2019) showed low detection limit (10^6 - 10^7 pfu/ml) and were not able to detect phages directly from whey samples (Szymczak et al., 2019) in contrast to our proposed multiplex PCR. Moreover, our developed multiplex PCR was designed to detect and categorize all 5 phage groups (*pac*, *cos*, 5093, 987 and P738) infecting *S. thermophilus*.

5 Conclusion

Monitoring bacteriophages in dairy plants is essential to avoid economical losses due to phage attacks and requires rapid and reliable tools. In this study, Laban samples were screened for the presence of lytic *S. thermophilus* phages using conventional microbiological tools (spot and plaque test) and multiplex PCR methods, and the same result was obtained from both techniques. In contrast to microbiological tools that require a long time, the multiplex PCR method is rapid and sensitive, it can detect as well as identify all *S. thermophilus* phages in whey and phage lysates.

In the future, the P4ND phage genome will be isolated for more

characterization and the proposed multiplex PCR method will be examined for more validation to detect all five groups of *S. thermophilus* phages directly from whey samples.

Acknowledgments

We are grateful to the Medical Research Center (MRC), Deanship of Scientific research, Jazan University, especially the Head of MRC Dr. Nasser Bin Ali Shubayr, and Mr. Hussein A. Khadashi, for their continuous assistance and support during the practical experiments.

References

Ali, Y. 2009. Molecular Studies on Bacteriophages of the Food Starter Culture Streptococcus thermophilus. Vol. Ph.D. Christian Albrecht University, Kiel, Germany.

Béal, C., and G. Chammas. 2016. Production of Laban. *Handbook of Animal-Based Fermented Food and Beverage Technology*. 1:181.

Beumer, A., and J.B. Robinson. 2005. A broad-host-range, generalized transducing phage (SN-T) acquires 16S rRNA genes from different genera of bacteria. *Applied and Environmental Microbiology*. 71:8301-8304.

Binetti, A.G., B. Del Río, M.C. Martìn, and M.A. Alvarez. 2005. Detection and characterization of Streptococcus thermophilus bacteriophages by use of the antireceptor gene sequence. *Applied and Environmental Microbiology*. 71:6096-6103.

Bradley, D.E. 1967. Ultrastructure of bacteriophage and bacteriocins. *Bacteriological reviews*. 31:230.

Brussow, H., M. Fremont, A. Bruttin, J. Sidoti, A. Constable, and V. Fryder. 1994. Detection and classification of Streptococcus thermophilus bacteriophages isolated from industrial milk fermentation. *Applied and Environmental Microbiology*. 60:4537-4543.

Bruttin, A., F. Desiere, N. d'Amico, J.-P. Guérin, J. Sidoti, B. Huni, S. Lucchini, and H. Brüssow. 1997a. Molecular ecology of Streptococcus thermophilus bacteriophage infections in a cheese factory. *Applied and environmental microbiology*. 63:3144-3150.

Bruttin, A., F. Desiere, S. Lucchini, S. Foley, and H. Brüssow. 1997b. Characterization of the Lysogeny DNA Module from the TemperateStreptococcus thermophilusBacteriophage φSfi21. *Virology*. 233:136-148.

Chammas, G.I., R. Saliba, G. Corrieu, and C. Béal. 2006. Characterisation of lactic acid bacteria isolated from fermented milk “laban”. *International Journal of Food Microbiology*. 110:52-61.

Desiere, F., S. Lucchini, and H. Brüssow. 1999. Comparative sequence analysis of the DNA packaging, head, and tail morphogenesis modules in the temperate cos-site Streptococcus thermophilus bacteriophage Sfi21. *Virology*. 260:244-253.

Duplessis, M., C.M. Lévesque, and S. Moineau. 2006. Characterization of Streptococcus thermophilus host range phage mutants. *Applied and environmental microbiology*. 72:3036-3041.

Fuquay, J.W., P.L. McSweeney, and P.F. Fox. 2011. Encyclopedia of dairy sciences. Academic Press.

Guglielmotti, D.M., H. Deveau, A.G. Binetti, J.A. Reinheimer, S. Moineau, and A. Quiberoni. 2009. Genome analysis of two virulent Streptococcus thermophilus phages isolated in Argentina. *International journal of food microbiology*. 136:101-109.

Lavelle, K., I. Martinez, H. Neve, G.A. Lugli, C.M. Franz, M. Ventura, F.D. Bello, D.V. Sinderen, and J. Mahony. 2018. Biodiversity of Streptococcus thermophilus phages in global dairy fermentations. *Viruses*. 10:577.

Le Marrec, C., D. van Sinderen, L. Walsh, E. Stanley, E. Vlegels, S. Moineau, P. Heinze, G. Fitzgerald, and B. Fayard. 1997. Two groups of bacteriophages infecting Streptococcus thermophilus can be distinguished on the basis of mode of packaging and genetic determinants for major structural proteins. *Applied and Environmental Microbiology*. 63:3246-3253.

Lévesque, C., M. Duplessis, J. Labonté, S. Labrie, C. Fremaux, D. Tremblay, and S. Moineau. 2005. Genomic organization and molecular analysis of virulent bacteriophage 2972 infecting an exopolysaccharide-producing Streptococcus thermophilus strain. *Applied and environmental microbiology*. 71:4057-4068.

Lillehaug, D. 1997. An improved plaque assay for poor plaque-producing temperate lactococcal bacteriophages. *Journal of applied microbiology*. 83:85-90.

Lucchini, S., F. Desiere, and H. Brüssow. 1999a. Comparative genomics of Streptococcus thermophilus phage species supports a modular evolution theory. *Journal of Virology*. 73:8647-8656.

Lucchini, S., F. Desiere, and H. Brüssow. 1999b. The genetic relationship between virulent and temperate Streptococcus thermophilus bacteriophages: whole genome comparison of cos-site phages Sfi19 and Sfi21. *Virology*. 260:232-243.

Mahony, J., and D. Van Sinderen. 2014. Current taxonomy of phages infecting lactic acid bacteria. *Frontiers in microbiology*. 5:7.

Marcó, M.B., S. Moineau, and A. Quiberoni. 2012. Bacteriophages and dairy fermentations. *Bacteriophage*. 2:149-158.

McDonnell, B., J. Mahony, L. Hanemaaijer, H. Neve, J.-P. Noben, G.A. Lugli, M. Ventura, T.R. Kouwen, and D. van Sinderen. 2017. Global survey and genome exploration of bacteriophages infecting the lactic acid bacterium Streptococcus thermophilus. *Frontiers in microbiology*. 8:1754.

McDonnell, B., J. Mahony, H. Neve, L. Hanemaaijer, J.-P. Noben, T. Kouwen, and D. van Sinderen. 2016. Identification and analysis of a novel group of bacteriophages infecting the lactic acid bacterium Streptococcus thermophilus. *Appl. Environ. Microbiol.* 82:5153-5165.

Mills, S., C. Griffin, O. O'Sullivan, A. Coffey, O. McAuliffe, W. Meijer, L. Serrano, and R. Ross. 2011. A new phage on the 'Mozzarella'block: bacteriophage 5093 shares a low level of homology with other Streptococcus thermophilus

phages. *International dairy journal*. 21:963-969.

Philippe, C., S. Levesque, M.B. Dion, D.M. Tremblay, P. Horvath, N. Lüth, C. Cambillau, C. Franz, H. Neve, and C. Fremaux. 2020. Novel Genus of Phages Infecting Streptococcus thermophilus: Genomic and Morphological Characterization. *Applied and Environmental Microbiology*. 86.

Quiberoni, A., D.M. Guglielmotti, and J.A. Reinheimer. 2003. Inactivation of Lactobacillus delbrueckii bacteriophages by heat and biocides. *International journal of food microbiology*. 84:51-62.

Quiberoni, A., D. Tremblay, H.-W. Ackermann, S. Moineau, and J.A. Reinheimer. 2006. Diversity of Streptococcus thermophilus phages in a large-production cheese factory in Argentina. *Journal of Dairy Science*. 89:3791-3799.

Szczepankowska, A., R. Górecki, P. Kołakowski, and J. Bardowski. 2013. Lactic acid bacteria resistance to bacteriophage and prevention techniques to lower phage contamination in dairy fermentation. *Lactic acid bacteria-R & D for food, health and livestock purposes*:23-74.

Szymczak, P., F.K. Vogensen, and T. Janzen. 2019. Novel isolates of Streptococcus thermophilus bacteriophages from group 5093 identified with an improved multiplex PCR typing method. *International dairy journal*. 91:18-24.

Tamime, A.Y., and R.K. Robinson. 1999. Yoghurt: science and technology. Woodhead Publishing.

Tremblay, D.M., and S. Moineau. 1999. Complete Genomic Sequence of the Lytic Bacteriophage DT1 ofStreptococcus thermophilus. *Virology*. 255:63-76.

كشف وتوصيف البكتريوفاجات المحللة لبكتيريا استربتوكوكس ثيرموفيلس الموجودة فى الحليب المتخمر "لبن" بإستخدام تفاعل تسلسل البلمرة (بي سي أر)

[١،٢]يحيى علي & [١]فيصل على عبد الله حدادى

[١] قسم الأحياء - كلية العلوم – جامعة جازان

[٢] معهد بحوث صحة الحيوان – مركز البحوث الزراعية - مصر

الملخص

يعتبر الحليب المخمر "لبن" واحدا من منتجات الألبان المفضلة في الشرق الأوسط وفي العديد من دول الخليج. في هذه الدراسة ، تم تجميع عدد ٢٠ عينة مختلفة من الحليب المتخمر "لبن" والمصنعة من ٥ شركات ألبان تجارية مختلفة في مدينة جازان في المملكة العربية السعودية وتم اختبارها بحثًا عن البكتريوفاجات المحللة التي تصيب بكتيريا *Streptococcus thermophilus* . تم عزل عدد ٤٥ عزلة واستخدمت كسلالات حساسة للكشف عن الفاجات الموجودة. بعد ذلك ، تم تجميع الرشيح (مصل اللبن) من كل عينة (L1 إلى L20). أظهر اختبار البقعة (Spot-test) أن L4و L9 كانت موجبة ضد العزلة *4.3ND*. كذلك تم تقدير عدد الفاجات الموجودة باستخدام اختبار البلاك (Plague-test) وكان العدد هو ٤ x 10^7 و ٣,٥ x 10^5 فاج / ملليتر، على التوالي. تمت تنقية الفاجين المكتشفين تم تسميتهما P9ND & P4ND . أظهر فحص المجهر الإلكتروني (TEM) ان الفاجات تتكون من رأس متساوي (Isometric head) بقطر 59.5 نانومتر وذيل طويل غير قابل للأنقباض طوله ٢٥١ نانومتر. ويتطابق هذا الوصف تماما مع الشكل المورفولوجى للفاجات التى تصيب بكتيريا *Streptococcus thermophilus* . علاوة على ذلك، تم تطوير واستخدام تفاعل تسلسل البلمرة المتعدد (Multiplex PCR) لكشف وتوصيف الفاجات التى تصيب بكتيريا الأستربتوكوكس ثيرموفيلس (*S. thermophilus*) والتي تنتمي إلى المجموعات *pac*، *cos* ، ٩٨٧ و ٥٠٩٣ & P738 وكان طول المنتج المتوقع يبلغ ٤٣٢، ٥١٤، ٦٣٨، ٣٠٢ و ٢٥٥ زوج من القواعد النيتروجينية. ومن المثير للاهتمام أن العينات L4 و L9 أظهرت نواتج (PCR products) بطول ٥١٤ قاعدة نيتروجينية مما يشير إلى أن الفاجين P4NDو P9ND هما من مجموعة *cos* التى تصيب بكتريا الأستربتوكوكس ثيرموفيلس، مما يؤكد أن تفاعل تسلسل البلمرة المتعدد (Multiplex PCR) يعتبر طريقة فعالة وسريعة للكشف عن الفاجات فى العينات.

كلمات مفتاحية: إستربتوكوكس ثيرموفيلس – لبن – بكتريوفاج – فاج – بي سي أر متعدد

N_1,N_5-bis [azoaldehyde]-thiocarbohydrazone Pentadentate Schiff base Ligands and Their Cu(II) and Ni(II) Complexes: Characterization and Antimicrobial Activity

Sami A. Zabin*

Chemistry Department, Faculty of Science, Albaha University, Al-Baha, Saudi Arabia,

ABSTRACT

The main purpose of this research project was to synthesize copper and Nickel complexes using pentadentate (N_2O_2S) Schiff base ligands obtained from the condensation of thiocarbohydrazine (1,3-diaminothiourea) with azoaldehydes. These ligands were used to prepare metal complexes with Cu(II) and Ni(II) metal ions in 1:1 (M:L) molar ratio. Different spectroscopic and physicochemical analysis techniques were used for characterization and structure elucidation of the prepared ligands and their metal complexes. The results indicate that the ligand with five coordination sites produce penta-coordinate mononuclear complexes with square pyramidal geometry for both Cu(II) and Ni(II) metals. The organic ligands and their corresponding complexes were screened *in vitro* for their antimicrobial activity against both types of Gram-positive and Gram-negative bacteria and against the common fungus strain *Candida Albicans*. The observations showed that both organic Schiff base ligands and their Cu(II) and Ni(II) complexes found to have moderate activity against the Gram-positive *Staphylococcus aureus* bacteria and against the *C. Albicans* fungal strains which increased on coordination with metal ions. While the compounds were inactive against Gram-negative bacteria.

Key words: thiocarbohydrazone, metal complexes, Schiff bases, azo-aldehydes, biological activity**.**

1. INTRODUCTION

Thiocarbohydrazine is a very important and fascinating building block chemical used for synthesis of many organic compounds such as thiocarbohydrazones that have attracted the attention and interest of chemistry researchers due to their significance in biological and medicinal fields [Metwally *et. al.*, 2012]. Thiocarbohydrazones are synthesized easily through the direct reaction of thiocarbohydrazine as a primary amine with aldehydes or ketones. These compounds have synthetic flexibility and can act as multidentate ligands that usually coordinate with the metal ion through the nitrogen (of azomethine group) and sulfur (of thioamide group) as potential donor atoms forming coordination compounds with versatile architecture and enormous applications [Manoj *et. al.*, 2007; Potti *et. al.*, 2007, Chandra and Sharma, 2009; Tiwari *et. al.*, 2011]. The biological applications of thiocarbohydrazone derivatives have been investigated as potential antimicrobial, antiviral, and anticancer agents and reported to show sound biological activity that increased on coordination with metal ions [Shebl *et. al.*, 2010; Singh *et. al.*, 2010]. They are reported as fungicides for textile fabrics and have convulsant action [Metwally *et. al.*, 2012].

The presence of C=N and C=S as electron denoting groups along with adjacent other functional groups like –OH, SH, or COOH is considered as an excellent combination to form metal complexes of five or six membered coordination ring [Kabak *et. al.*, 1999; Lekha, 2014]. Many published research papers have shown that the presence of C=N and C=S groups is of considerable chemical and biological importance due to the presence of lone pair of electrons in a sp^2 hybridized orbital of the nitrogen atom [Ajlouni *et. al.*, 2012; Kumar *et. al.*, 2012].

With these properties introduced above, in this study we took the courage to

elemental analyzer Leco Model VTF-900 CHN-S-O 932 version 1.3x (ThermoFisher Scientific-USA) instrument was used for elemental analysis. Thermo Scientific Nicolet iS50 FT-IR spectrometer was used to record IR spectra in the range 400-4000 cm^{-1}. Attenuated Total Reflection (ATR) method was used for direct measurement of the IR spectrum for the powder solid samples. UV-visible spectra were recorded in DMSO solvent using Evolution 300 UV-visible double beam Spectrophotometer. A Varian Mercury-400BB (400 MHz) spectrometer operating at 400 MHz frequency for ^1H nuclei was used to obtain NMR spectra in CD_3OD solutions using TMS (^1H) as standard. The mass spectral data were recorded on Thermo Scientific-LCQ fleet ion trap mass spectrometer using electrospray ionization (ESI) method. Shimadzu thermo-analyzer 50H was utilized for thermogravimetric (TGA) studies at a heating rate 10°C min^{-1} in the temperature range 25-1000 °C in an atmosphere of dynamic nitrogen (20mL synthesize pentadentate Schiff base ligands of N_1,N_5-bis [azoaldehyde]-thiocarbohydrazone and their corresponding Ni(II) and Cu(II) complexes. The synthesized compounds were assessed for their potential antimicrobial behavior.

2. MATERIALS AND METHODS

2.1. Chemicals

Main chemicals, metal salts, aldehydes and primary amines used in this study were of AR grade and purchased from Sigma-Aldrich and BDH Analytical Chemicals Company. Thiocarbohydrazide (1,3-diaminothiourea) was synthesized in our laboratory by the condensation reaction between hydrazine (H_2N-NH_2) and carbon disulfide (CS_2) according to the reported procedure [Metwally *et..al.*, 2012].

2.2. Physical measurements and Analytical Methods

Electrothermal (Cat NO. TA9100) melting point apparatus was used to determine melting points. CHN/S/O

Pascal's constants values [Bain and Berry, 2008].

2.3. Preparation Experiments

2.3.1. Preparation of thiocarbohydrazide(1,3diaminothioure)

Thiocarbohydrazide was prepared according to the reported method [Metwally *et. al.*, 2012]. Carbon disulfide 15 mL (0.2 mol) was added dropwise to a solution of 50 mL (1 mol) Hydrazine hydrate (N_2H_4) (85%) in 30 mL distilled water. The mixture was stirred vigorously and heated up to 60 °C to remove H_2S gas evolved. The reaction is depicted in the following chemical equation (1).

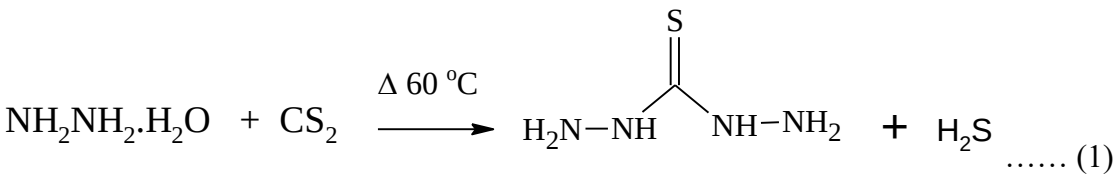

…… (1)

hydroxyl aldehydes (salicylaldehyde or o-vaniline) as shown in scheme 1 following well-known methods [Mentai *et. al.*, 2013; Sarigul *et. al.*, 2015].

2.3.2. Synthesis of azo-aldehydes

The two azo-aldehyde compounds as starting materials were synthesized by diazotization of aniline with substituted

min^{-1}) and the sample masses were 5 mg. Hanna instrument HI8633N Multi-range conductivity meter was utilized to measure the molar conductivities of freshly prepared 1.0×10^{-3} M solutions of the metal complexes in DMSO.

Gouy's method apparatus balance (Holmarc's Magnetic Susceptibility - Gouy's Method Apparatus (Model No: HO-ED-EM-08)) was used for magnetic susceptibility measurements at room temperature with $Hg[Co(SCN)_4]$ as calibrant. The measured magnetic susceptibilities were calculated and corrected for their diamagnetism using

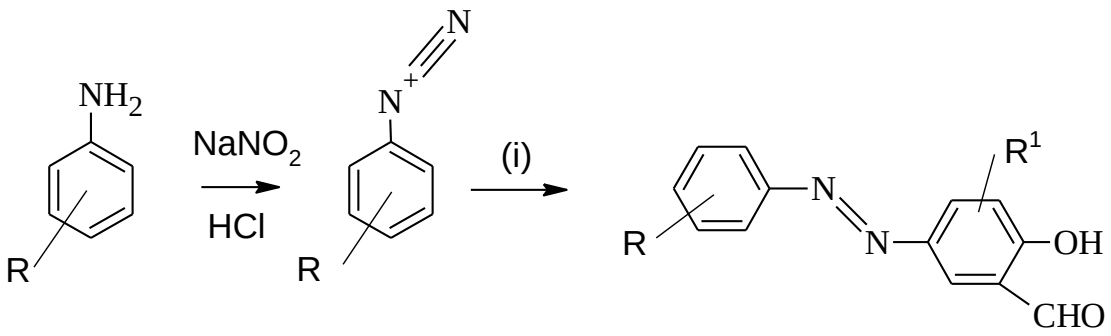

(i) Salicylaldehyde or o-vaniline ; R = H; R^1 = H or m-OCH_3

Scheme 1

The melting points and physical properties are as follow:

5-phenylazosalicylaldehyde: solid orange powder, yield (85%) and m.p = 122 (reported 120) [Mentai *et. al.*, 2013]. 5-phenylazo-2-hydroxy-3-methoxybenzaldehyde: Dark Yellow solid, yield (80%) and m.p =146.

were mixed in molar ratio of (1:2). The mixture was refluxed at 90 °C and stirred magnetically for 3 hours. After cooling to room temperature, the colored solids of the Schiff bases obtained were filtered and washed several times with methanol, ethanol and finally with diethyl ether. The Schiff base ligands were recrystallized and air-dried. The melting points and yields of the synthesized azo-Schiff bases are given in Table 1.

2.3.3. Preparation of Azo-containing Schiff bases

Scheme 2 shows preparation of the azo-containing Schiff base ligands according to the well-known reported condensation general procedure [Zou *et. al.*, 2004; Mentai *et. al.*, 2013; Hashemi *et. al.*, 2015]. The ethanolic solution of the diamine compound (thiocarbohydrazide) and the ethanolic solution of azo-aldehyde

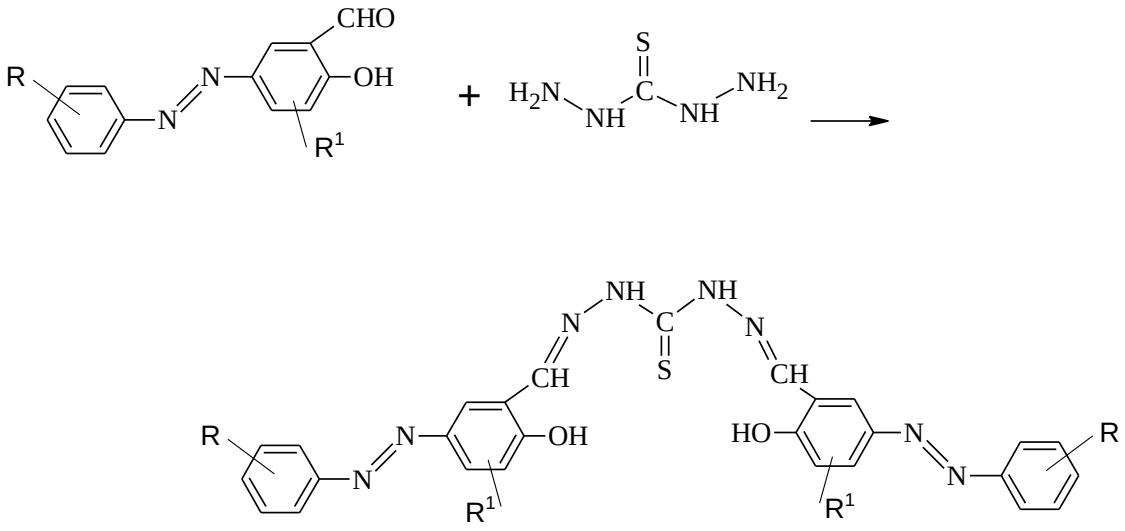

Scheme 2

Table 1: Elemental analysis and physical properties of the synthesized ligands and their complexes

Compound	Empirical Formula	Formula wt.	Color	Yield %	m.p./d.p. °C	Elemental Analysis Calcd. (Found)				
						C	H	N	O	S
LD_1	$C_{27}H_{22}N_8O_2S$	522	yellow	75%	273	62.07 (62.22)	4.21 (4.22)	21.45 (21.20)	6.13	6.13
LD_2	$C_{29}H_{26}N_8O_4S$	582	yellow	71%	286	59.79 (60.02)	4.48 (4.44)	19.24 (19.40)	10.99	5.50
$NiLD_1$	$NiC_{27}H_{20}N_8O_2S$	578.7	Reddish orange	62%	>300 °C (dec).	55.99 (56.12)	3.46 (3.39)	19.35 (19.42)	5.53	5.53
$NiLD_2$	$NiC_{29}H_{24}N_8O_4S$	637.7	Reddish orange	60%	>300 °C (dec).	54.57 (54.60)	3.76 (3.72)	17.56 (17.67)	10.03	5.01
$CuLD_1$	$CuC_{27}H_{20}N_8O_2S$	583.5	Yellowish brown	67%	>300 °C (dec).	55.53 (55.32)	3.43 (3.36)	19.19 (19.42)	5.48	5.48
$CuLD_2$	$CuC_{29}H_{24}N_8O_4S$	643.5	brown	64%	>300 °C (dec).	50.08 (49.96)	3.73 (3.60)	17.40 (17.36)	9.95	4.97

LD_1 = 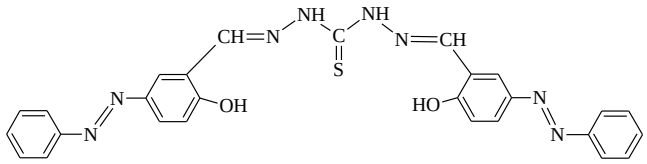 ; LD_2 = 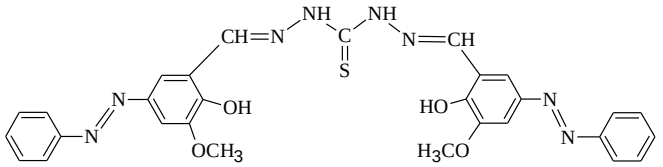

(1:1). The colored powder solid complexes formed were filtered, washed with C_2H_5OH, $CHCl_3$ and finally with $(C_2H_5)_2O$, then dried in open air. Colors, yields and melting points are shown in tables 1. Elemental analysis, spectroscopic, magnetic moment measurements and thermogravimetric analyses were performed to confirm the proposed structure and geometry of the obtained metal complexes (structures 1).

2.3.4. Template Synthesis of Metal Complexes

Cu(II) and Ni(II) complexes were synthesized as reported procedure in the literature [Mentai *et. al.*, 2013; Ozkan *et. al.*, 2015] by adding the appropriate metal salts (1.0 mmol, in 20 ml ethanol) to a hot solution of the ligand (1.0 mmol, in 20 ml chloroform). The mixture was stirred and refluxed at 90 °C for about 4 hours. The ligand: metal stoichiometric ratio was

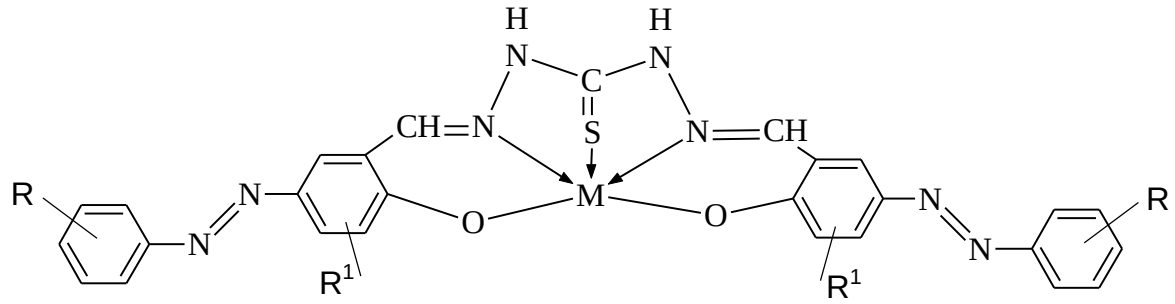

Structure 1: M = Cu or Ni (square pyramidal geometry)

al., 2016]. The prepared ligands and complexes were tested against *Proteus Mirabilis* and *Klebsiella pneumonia* as Gram-negative bacteria strains, and *Staphylococcus aureus* and *Enterococcus faecalis* as two Gram-positive pathogenic bacteria types. *Candida Albicans* was used

2.4. Biological Assessment

The antimicrobial assessment experiments were carried out *in vitro* at the microbiological laboratories of the Blood Bank Centre at Albaha city-KSA. The Clinical and Laboratory Standards Institute (CLSI) susceptibility testing technique was utilized for bacteria and yeasts [Balouiri *et.*

3. RESULTS AND DISCUSSION

3.1. Characterization of the Compounds

The Cu(II) and Ni(II) complexes were successfully synthesized using the synthesized symmetrical pentadentate azo-Schiff base ligands (scheme 2) following the standard reported procedures as mentioned in the materials and methods section above (section 2.3.4). The symmetrical azo-schiff base ligands were obtained by the reaction between the prepared substituted azo-aldehydes and the diamine compound thiocarbohydrazide containing thioamide (-C=S) group (section 2.3.3). These chelating ligands containing N=N and CH=N linkages along with thioamide (-C=S) group. Both ligands and complexes were obtained in the solid form and were stable at room temperature. The prepared azo-azomethine ligands were soluble in hot ethanol, acetone, DMF and chloroform, while the corresponding metal chelates were generally soluble in hot DMF and DMSO. Table 1 present the yield percentages, melting points and other

as common fungi for the antifungal activity assessment.

Agar disc-diffusion standard technique using Mueller Hinton Agar (MHA) as growth medium was utilized for the *in vitro* growth inhibitory activity experiment against the bacterial and fungal strains [Balouiri *et. al.*, 2016]. The stock solutions were prepared by dissolving 0.01gm of each compound in 5 mL DMSO solvent DMSO solvent was used as negative control. Saturated filter paper discs (6 mm in diameter) containing the tested compounds were placed on the agar surface in petri dishes. The petri dishes were put in an incubator at 35˚C for 24 hours in case of bacteria and at 35 ˚C for 48 hours for fungus. Zones of complete inhibition were measured (in mm) around the holes after the incubation period to monitor the fungal and bacterial susceptibilities. Each test was repeated in triplicate, and statistical analysis were performed using SPSS 16.0 for windows.

equivalent to the calculated M. Wt. (582). These mass spectra observations confirm the formula proposed for these ligands.

The synthesized azo-azomethine ligands and their corresponding Cu(II) and Ni(II) complexes are depicted in scheme 2 and structure 2. The organic ligands and their corresponding complexes were characterized using micro-elemental analysis, mass spectra, UV-visible, IR, NMR, Magnetic susceptibility and TGA analysis techniques to prove the proposed structures and geometries.

physical measurements of the organic ligands and their corresponding metal complexes. The results indicated that all the complexes decomposed at temperatures higher than 300 °C.

The molecular weights of the synthesized Schiff base ligands were confirmed using mass spectrum measurements. A molecular peak for the Schiff base ligand LD_1 ($C_{27}H_{22}N_8O_2S$) was observed at 522.58 which is equivalent to its calculated M. Wt. (522) (figure 1). For the ligand LD_2 ($C_{29}H_{26}N_8O_4S$) the observed peak was at 582.36 that is

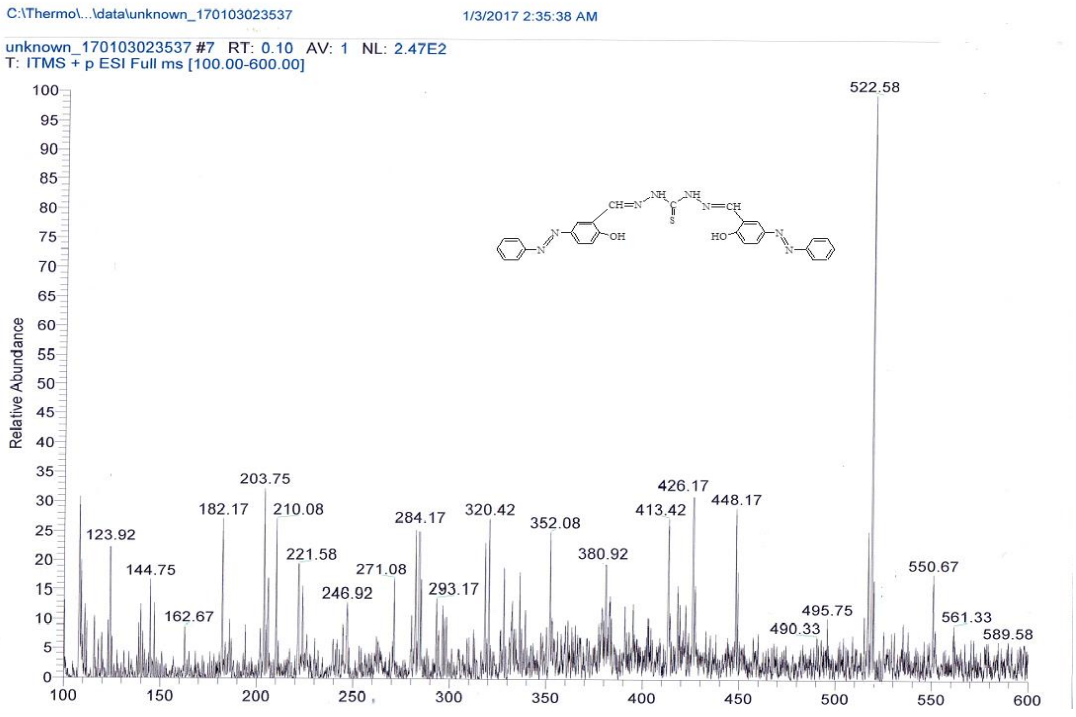

Figure 1: *Mass spectra for LD_1 ($C_{27}H_{22}N_8O_2S$) (calculated M. Wt. = 522)*

groups, two oxygen atoms of the phenolic groups and the sulfur atom of the thioamide group (i.e. N_2O_2S). Metal complexes obtained from pentadentate azo-azomethine ligands showed square-pyramidal coordination geometry (figure 2) around the metal ions.

Azo-azomethine ligands interact with copper and nickel atoms to form mononuclear complexes of pentadentate ligands. The azo-azomethine ligands behave as pentadentate towards Cu(II) and Ni(II) and binding through the usual two nitrogen donor atoms of the azomethine

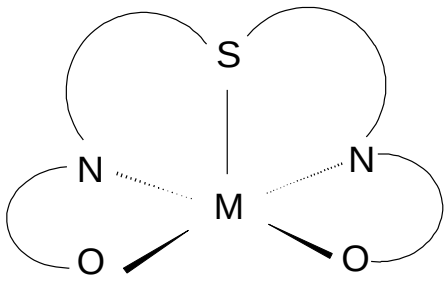

Figure 2: *Square-pyramidal geometry*

Ni(II) complexes are shown in figures 3-4. The observed mass spectra peak for $CuLD_1$ ($CuC_{27}H_{20}N_8O_2S$) is 583.52 (calculated M. Wt. = 583.5) and for $NiLD_2$ ($NiC_{29}H_{24}N_8O_4S$) the observed mass spectra was 639.00 (calculated M. Wt. = 637.7). These mass spectrum observations confirm and support the proposed structure for these complexes.

3.2. UV-visible Spectra and Magnetic Susceptibility Measurements

The UV-vis absorption spectra (figure 5) were recorded in DMSO for the azo-

The elemental analysis data (Table 1) indicate that azo-azomethine ligands of thiocarbonyldihydrazide react with metal ions in the ratio of 1:1 (M:L) forming pentadentate monomeric metal complexes of the general formula [M(LD)]. The elemental analysis are in agreement with the proposed structures of the complexes. In addition, the mass spectra of the synthesized complexes were carried out to determine and confirm the molecular weights. Some typical representative mass spectra of some synthesized Cu(II) and

absorption in the region 332-345 nm may be assigned to $\pi \rightarrow \pi^*$ transitions in C=H and N=N groups [Pal et al., 2015]. The second band appeared at 465-440 nm attributed to $n \rightarrow \pi^*$ transitions [Ozkan *et. al.*, 2015]. The third band observed in the range 440-480 nm can be assigned to an n-π^* electronic transition of azo-aromatic chromophore [Alghool *et. al.*, 2010; Khamohammadi *et. al.*, 2014]. In some ligands, a band appears at 380-395 nm which may be due to the absorption wave length for yellow color characteristics. Two bands around 350, 352 and 358, 360 nm were observed in the UV-vis spectra of the Ligands LD_1 (figure 5) and LD_2 which can be assigned to $n \rightarrow \pi^*$ transitions of the azomethine and thioamide groups respectively [Lessa *et. al.*, 2012].

linked Schiff base ligands and their Cu(II) and Ni(II) complexes in the range of 200-800 nm at room temperature. The important spectra data of the ligands and their complexes results are summarized in table 2. The electronic spectra of the symmetrical ligands obtained by the condensation of the azo-aldehydes with thiocarbohydrazide are similar. The UV-visible absorption spectra of the**se** ligands show three important bands: the first broad band appeared at 345-332 nm that can be attributed to $\pi \rightarrow \pi^*$ transitions within the ligand molecule involving the π electrons of the azomethine and azo groups [Khamohammadi *et. al.*, 2014]. Since the $\pi \rightarrow \pi^*$ transitions of imine and azo linkages appear in close proximity, the two bands may overlap in each other, thus the broad

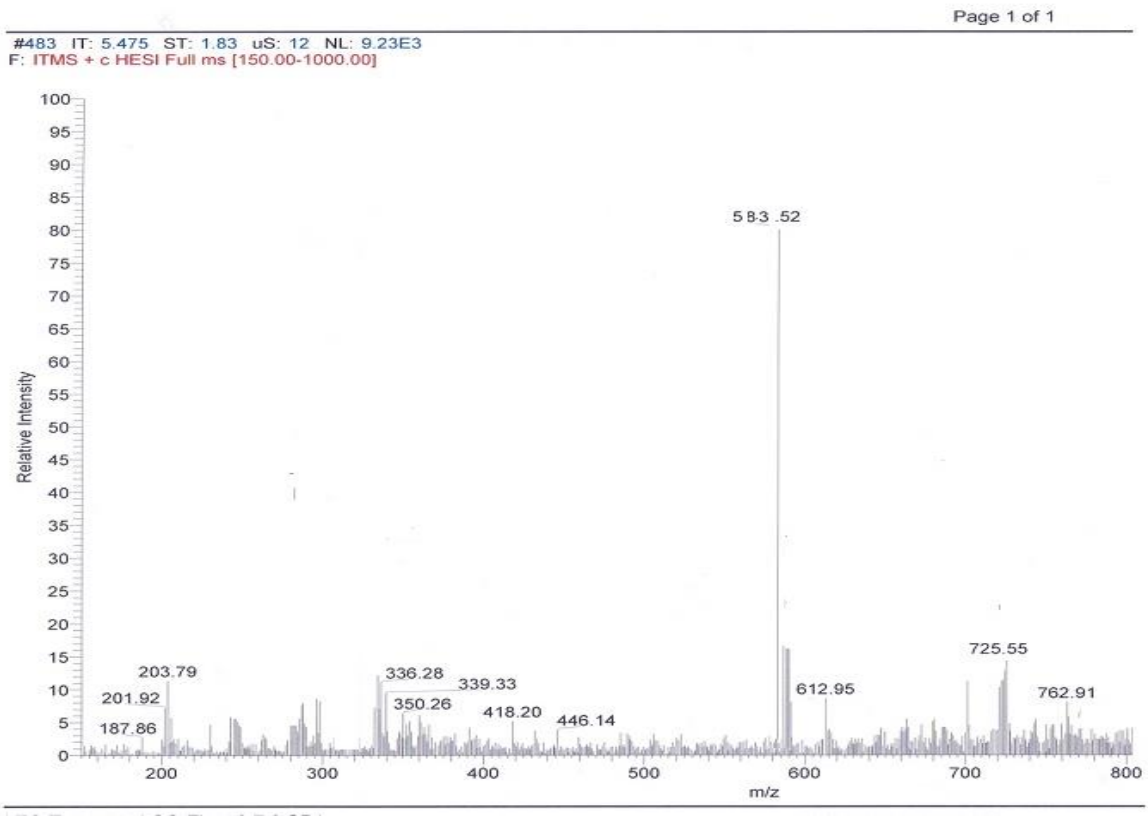

Figure 3: *Mass spectra of CuLD$_1$ ($CuC_{27}H_{20}N_8O_2S$) (calculated M. Wt. = 583.5)*

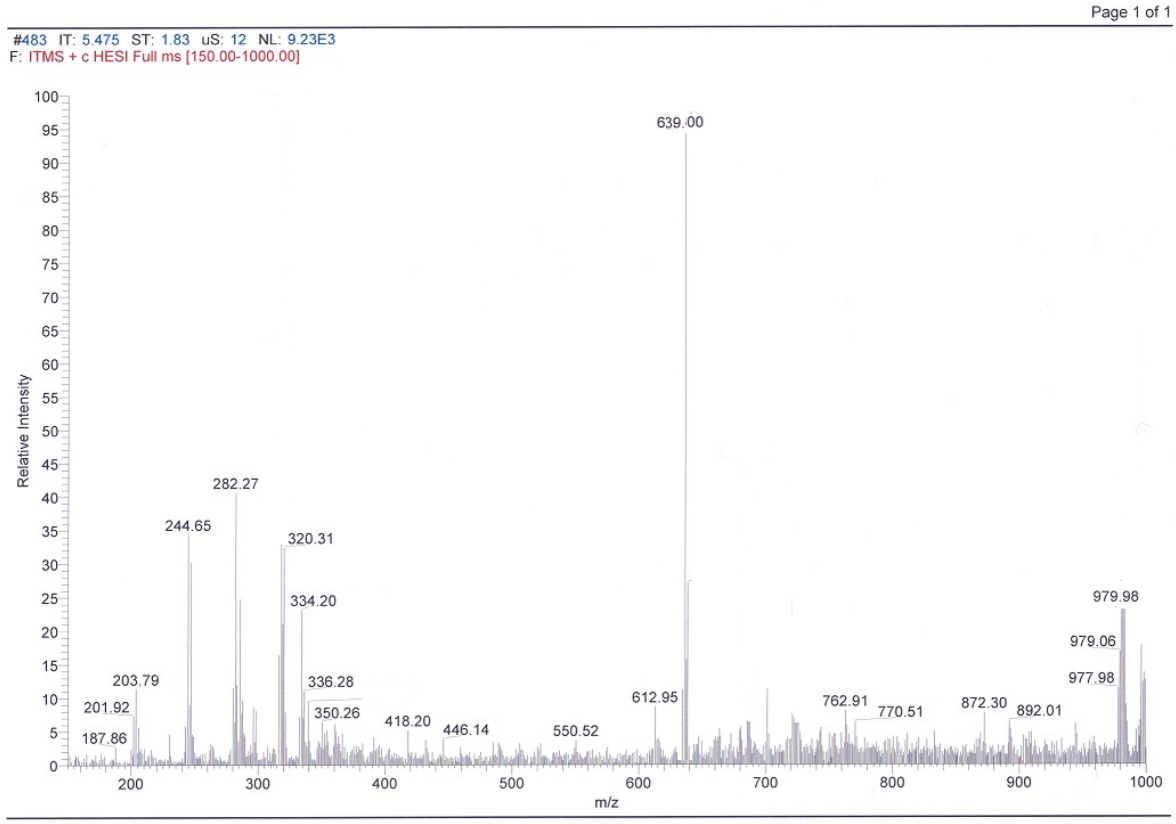

Figure 4: *Mass spectra of NiLD$_2$ ($NiC_{29}H_{24}N_8O_4S$) (calculated M. Wt. = 637.7)*

by the magnetic susceptibility values obtained (table 3). The magnetic moment measurements for the Cu(II) complexes (i.e. [Cu(LD_1)] and [Cu(LD_2)]) were in the range of 1.76 -1.82 which are closed to the spin only magnetic moment value for the d^9 Cu(II) supporting the mononuclear nature of these complexes (Keypour *et. al.*, 2015). These values support the presence of square pyramidal geometry around copper metal [Bheemanna *et. al.*, 2014]. The room temperature μ_{eff} values (table 3) obtained for Nickel (II) complexes ([Ni(LD_1)] and [Ni(LD_2)]) were 3.2 and 3.4 B.M. respectively, which are in the expected range for Square pyramidal geometry [Bheemanna *et. al.*, 2014].

The spectra of Cu(II) and Ni(II) complexes did not show these bands and appear at lower intensities and shifted to longer wavelength (batho-chromic effect). This observation confirms the coordination of ligands with copper and nickel ions (Ozkan *et. al.*, 2015). The band shoulder appeared in the range of 440-465 nm in the spectra of complexes may be assigned to ligand-metal charge transfer (LMCT) (Pal *et. al.*, 2015). When compared with that of ligands we notice the n-π* absorption bands of the organic ligands shifted to lower frequencies on coordination with copper or nickel atoms.

The monomeric nature of the Ni(II) and Cu(II) complexes with azo-azomethine ligands and their geometry were supported

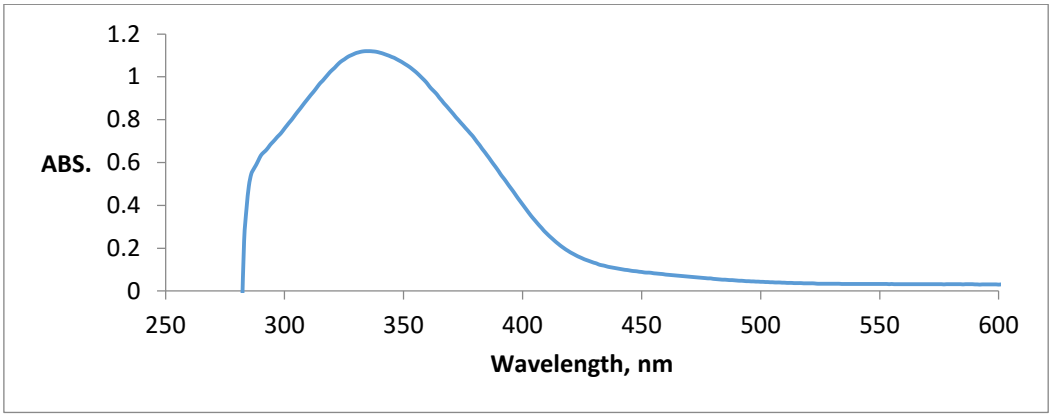

Figure 5: *UV-visible spectra for LD_1*

Table 2: Important UV-vis spectral data for the ligands and their complexes (nm)

Compound	Absorption bands (λ in nm)
LD_1	345, 350, 358, 395
LD_2	343, 352, 360, 380
$NiLD_1$	318, 347, 355, 450
$NiLD_2$	320, 345, 354, 446
$CuLD_1$	325, 348, 354, 388, 458
$CuLD_2$	324, 346, 356, 455

Table 3: Molar conductivity values and magnetic susceptibility of the complexes.

Compound	**Molar Conductance Λ_m ($\Omega^{-1}.cm^2.mol^{-1}$)**	**μ_{eff} (B.M.)**
$NiLD_1$	5.6	3.2
$NiLD_2$	6.2	3.4
$CuLD_1$	11.4	1.76
$CuLD_2$	10.2	1.82

atom of the C=N group to the metal atom during the process of coordination. This proves the coordination of the azomethine group through nitrogen atom to the metal ion [Alghool *et. al.*, 2010; Kurtoglu *et. al.*, 2014]. Another band was observed in the FT-IR spectrum of the organic ligands at 1450 and1460 cm^{-1} that may be have assigned to the stretching vibration of the azo chromophore ν(N=N) group [Kurtoglu *et. al.*,2014]. This band does not show any shift in the spectra of the metal complexes indicates that azo group does not

3.3. FT-IR Spectra

Important infrared spectral data for the ligands and their complexes are summarized in table 4. Figure 6 shows representative IR spectra for the ligand LD_1. In the FT-IR spectrum of organic Schiff bases a strong band appeared around 1620 and1625 cm^{-1} is assigned to the stretching vibrations of the azomethine (C=N) band [Alghool *et. al.*, 2010]. In the spectra of the metal complexes this band was shifted downward by nearly 25-30 cm^{-1} due to donation of the electrons from N

shifted downward in the IR spectrum of the metal complexes indicating the involvement of the C=S group in the coordination sphere to the metal ion through the sulfur atom [*de* Sousa *et. al.*, 2001; Al-Obaidi, 2012]. This was supported by the appearance of ν(M-S) stretching vibrations at 380 - 410 cm^{-1} in the spectrum of the metal complexes [Al-Obaidi, 2012].

The high frequency broad bands shown in the IR spectra of the ligands LD_1 and LD_2 (table 4) centered in the range 3280-3320 cm^{-1} may attributed to the ν(N-H) stretching vibrations. These bands remains unchanged in the spectra of the complexes suggesting that NH group is not taking part in coordination to metal ions [*de* Sousa *et. al.*, 2001; Alaghaz *et. al.*, 2014]. Therefore, the IR spectra reveal that the ligands of azo-Schiff bases with thiocarbonyldihydrazide act as pentadentate molecules and coordinated to the metal ions via two phenolic oxygen, participate in coordination [Erdem *et. al.*, 2009]. The spectra of the azo-azomethine ligands shows a stretching broad band of the phenolic OH group at 3430-3440 cm^{-1}. This band disappeared in the metal complexes spectra indicating the formation of M-O bond and losing the proton of the phenolic group on complexation [Ahmed *et. al.*, 2011; Alghaz *et. al.*, 2014].

In the FT-IR spectra of the metal complexes two new bands appeared, the first in the range 530 – 540 cm^{-1} which may assigned to (νM-O) band vibrations and the second at 420-435 cm^{-1} may be assigned to (νM-N) band vibrations [Alghool *et. al.*, 2010; Alghaz *et. al.*, 2014]. These bands were not observed in the spectra of the ligands, which proves the coordination of the metal ions with phenolic oxygen (OH) and azomethine nitrogen of CH=N group.

The strong band observed at the frequency 1200 cm^{-1} of the Schiff base ligand can be assigned to ν(C=S) group. This frequency become broadened and

3.5. Molar Conductivity of Metal Complexes

The synthesized metal complexes were tested for their conductivity nature using 10^{-3} M solutions in DMSO at room temperature to establish the charge of the metal complexes. The molar conductivity values observed (table 3) for the complexes are of lower values in the range of (5.6-11.4 $\Omega^{-1}.cm^2.mol^{-1}$) within the non-electrolytic nature of conductivity [Alghool *et. al.*, 2010]. This shows that no any charged anions are present outside the coordination sphere of the complexes and the complexes are neutral (non-ionic). These results were strongly supported by the elemental analysis data.

two azomethine nitrogen and one thioamide sulfur atoms.

These IR spectral data are in accord to the proposed structures of the ligands and their corresponding complexes as shown in structures 1 and 2.

3.4. ^{1}H NMR Spectroscopy

The ^{1}H NMR spectra of the prepared ligands carried out for some compounds and chemical shifts for signals were observed. In the ^{1}H NMR spectrum of the azo-azomethine ligand, a signal at δ 10.71 ppm assigned to the phenolic -OH protons [Ahmad *et. al.*, 2011]. All ligands exhibit a characteristic singlet signal at range of δ 8.65 -8.90 ppm is assignable to azomethine protons (CH=N) [Ahmad *et. al.*, 2011; Ahmadi and Amani, 2012; Ozkan *et. al.*, 2015].

Table 4: Important infrared spectral data for the ligands and their complexes (cm^{-1})

Compound	ν(CH=N)	ν(N=N)	ν(-NH)	ν(OH)	ν(COOH)	ν(C=S)	ν(M-N)	ν(M-O)	ν(M-S)
LD_1	1620	1450	3280	3430	--	1200	--	--	--
LD_2	1625	1460	3320	3440	--	1200	--	--	--
$NiLD_1$	1590	1450	3280	--	--	1185	425	535	395
$NiLD_2$	1590	1460	3280	--	--	1190	425	540	380
$CuLD_1$	1595	1450	3320	--	--	1188	435	540	410
$CuLD_2$	1590	1460	3320	--	--	1190	430	530	400

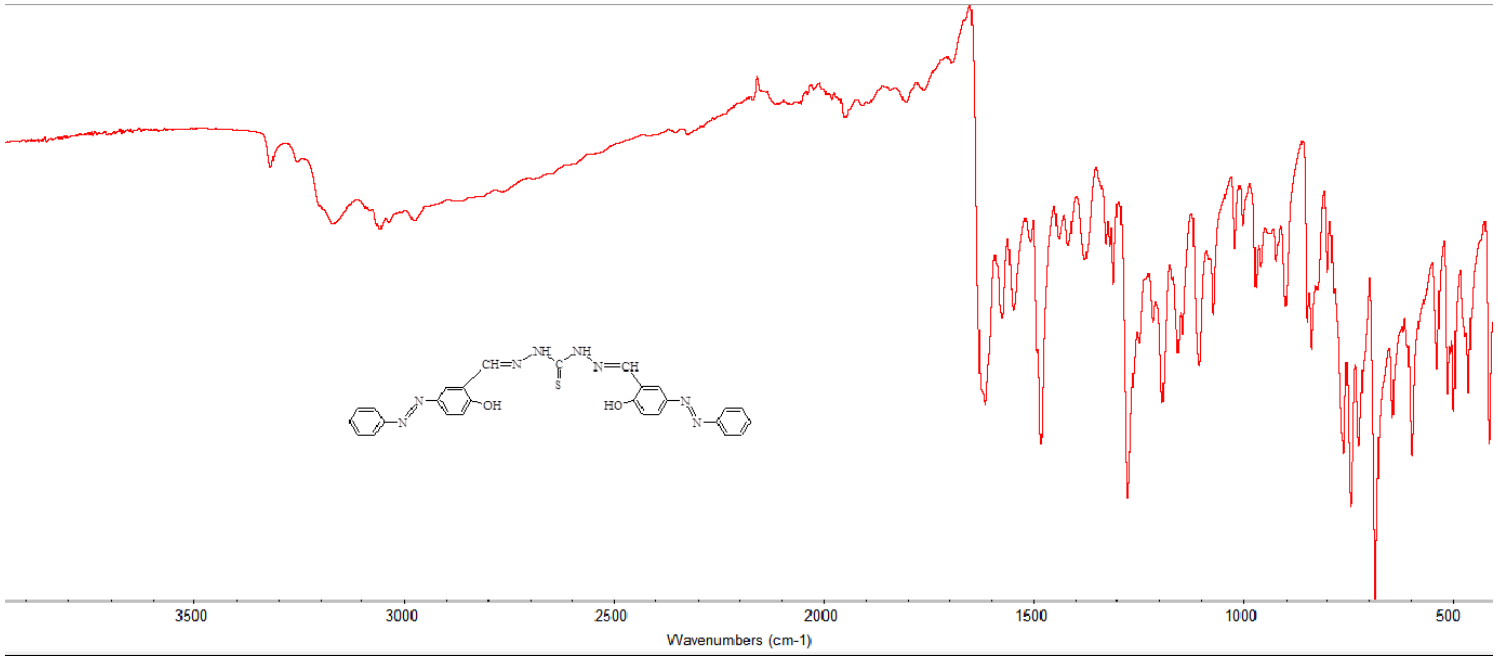

Figure 6: *FT-IR Spectra of LD_1*

3.6 Thermogravimetric (TGA) Analysis

We used TGA as a useful chemical analysis technique corroborating the proposed compounds' structures through monitoring the mass loss due to decomposition, which is measured as a function of temperature with constant heating rate. TGA investigation was carried out by pyrolysis the compounds under nitrogen atmosphere and heating up to 650 ^{0}C at constant heating rate 10 ^{0}C/min. The TGA curves obtained for complexes with LD_1 and LD_2 are very similar. The TGA curves show descending order that indicates a weight loss have occurred during pyrolysis process.

Figure 7 exhibit the TGA thermogram for Cu(LD1) complex which indicates no mass loss up to 350 ^{0}C indicating no water molecules are associated with metal complex. The curve shows mass loss in the range 350-570 ^{0}C with a mass loss of 89.4%, which can be attributed to the decomposition of the organic ligand $C_{27}H_{20}N_8O_2S$ (calculated 89.117%). This shows that the organic moiety part was decomposed in one-step. The decomposition ended with the formation of stable CuO residue with a percentage found (12.70%) and calculated (13.53 %).

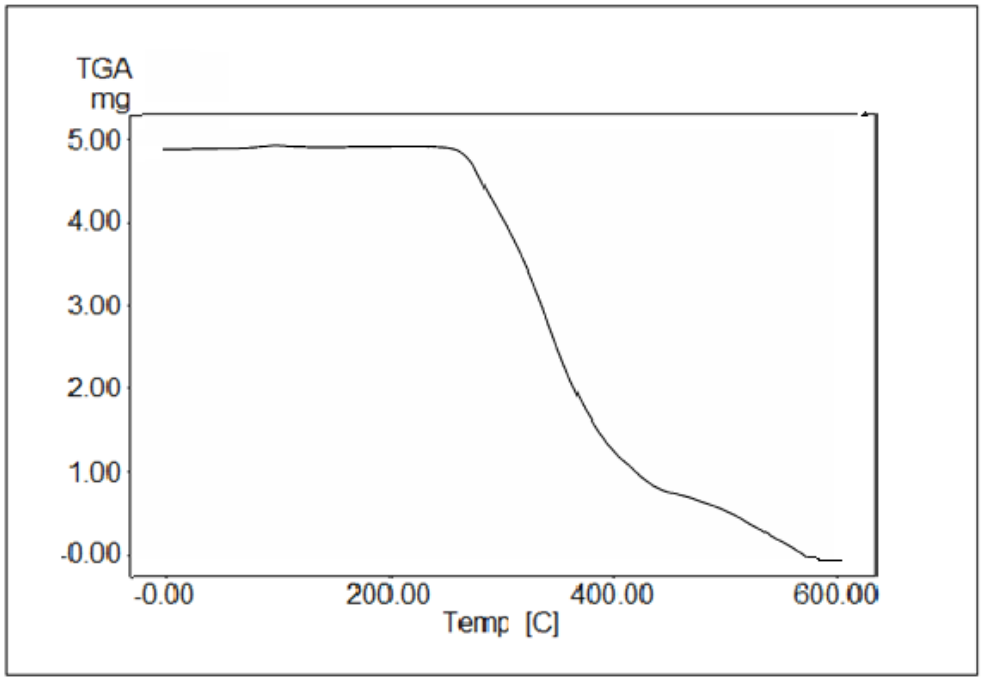

Figure 7: *Thermogravimetric (TGA) curve of Cu(LD$_1$) complex.*

common fungal strains named *Candida Albicans*.

Table 5 presents the observed results (zone of inhibitions in mm) of the antimicrobial experiments, which indicate that the examined compounds exhibit moderate and variable antibacterial potential against the Gram-positive bacteria types while, both Gram-negative bacteria showed resistance and the compounds did not cause any effect against it. Comparing the activity of the organic Schiff base ligands and their corresponding complexes, the ligands were comparatively had week effect against the

3.7 Antimicrobial Assessment Study

Antibacterial and antifungal susceptibility assessment were investigated *in vitro* using Agar disc-diffusion technique [Zabin and Abdelbaset, 2016]. DMSO was used as solvent and as a control in these experiments. The prepared compounds were examined against the pathogenic bacteria strains *Staphylococcus aureus* and *Enterococcus faecalis* as Gram-positive and *Proteus Mirabilis* and *Klebsiella pneumoniae* as Gram-negative bacteria. In addition, the compounds were assessed for their potential antifungal activity against the

formation of a hydrogen bond through the azomethine nitrogen atom (CH=N) with the cell micromolecules causing adverse effects in the normal cell process [El-sherif *et. al.*, 2012; Alaghaz *et. al.*, 2014].

Observations also showed that metal complexes were more active against ***Enterococcus faecalis*** (inhibition zone of 13.0-17.2 mm) the Gram-positive bacteria compared to other types of bacteria. This result was in agreement with other similar reported research [Metwally *et. al.*, 2012]. This may be attributed to the difference in cell wall structure of the different bacteria strains [Alaghaz *et. al.*, 2014].

The experimental results also indicated that the metal complexes were more active with and inhibition zones range of (16.3-20.6 mm) against the fungus *C. Albicans* while, the organic ligands were weakly influenced the growth of the yeast *C. Albicans* with inhibition zones range of (12.6-14.2). Compared to the antibacterial activity, the antifungal susceptibility was more. This difference in the effectiveness Gram-positive bacteria with and inhibition zones range of 10.4 -11.8 mm. The complexes were more toxic with an inhibition zones range 12.0-17.2 mm. That is, the metal ion on complexation with the ligands had positive influence and increased the antibacterial activity. This enhancement can be explained on the ground of chelation theory and the adverse effect of the metal ion on the normal cell processes [Alaghaz *et. al.*, 2014; Mahal *et. al.*, 2015; Zabin and Abdelbaset, 2016]. Coordination may reduce the polarity of the metal ion due to the partial sharing of the positive charge with the donor atoms of the ligands that result in delocalization of π-electrons within the entire chelate ring system formed during coordination that enhances solubility of the metal complexes [El-sherif *et. al.*, 2012; Mahal *et. al.*, 2015]. The increase of the liposolubility of the metal chelates enhances the penetration through the lipid layers of the microbial cell membranes and hence causing death of the cell. Moreover, there may be

Therefore, the results of this investigation may indicate that the nature of the central metal ion of the coordination sphere and the presence of different donating atoms of the ligand may be effective factors that affect the antimicrobial activity of the compounds. The prepared compounds in this study showed moderate toxicity against the yeast strains and low bacterial activity compared to standard drugs used as fungicides and bactericides.

of different complexes against different organisms (i.e. fungus and bacteria) depends either on the impearmeability of the cells of the microbes or the difference in riboisomes of the microbial cells [El-sherif *et. al.*, 2012; Alaghaz *et. al.*, 2014].

The observed results also indicate that the Cu(II) metal complexes were more active with inhibition zones of 20.2 and 20.6 mm against the yeast *C. Albicans* compared with other analogous Ni(II) complexes (inhibition zones range 16.3-16.4). The higher stability constant of Cu(II) complexes may be the factor that affect this difference [El-sherif *et. al.*, 2012].

Table 5: Antibacterial and antifungal activity of the ligands and their Cu(II) and Ni(II) complexes

(*inhibition zone in mm*)

Compound	Zone of inhibition (mm) ± SD				
	Gram-positive bacteria		Gram-negative bacteria		Fungus
	Enterococcus faecalis	***Staphylococcus aureus***	***Proteus Mirabilis***	***Klebsiella pneumonia***	***C. Albicans***
LD_1	10.4 ± 0.022	11.6 ± 0.030	R	R	12.6 ± 0.003
LD_2	11.2 ± 0.025	11.8 ± 0.042	R	R	14.2 ± 0.032
$NiLD_1$	13.0 ± 0.050	12.0 ± 0.020	R	R	16.3 ± 0.050
$NiLD_2$	13.8 ± 0.035	13.2 ± 0.040	R	R	16.4 ± 0.034
$CuLD_1$	15.0 ± 0.051	15.4 ± 0.02	R	R	20.6.0 ± 002
$CuLD_2$	17.2 ± 0.042	15.6 ± 0.035	R	R	20.20 ± 0.032

Key to interpretation: R = Resistant, less than 10 mm = inactive, 10–15 mm = weakly active, 15–20 mm = moderately active; more than 20 mm = highly active.

activity tests showed moderate activity that increased on coordination with metal ions. The compounds were active against the Gram-positive bacteria type and fungus, while inactive against Gram-negative bacteria.

ACKNOWLEDGEMENT

The author is gratefully acknowledged that this work was supported financially by Albaha University (Project No: 73/1436) and I am grateful to the Scientific Research Deanship at AlBaha University. I am very thankful to the Dean, Faculty of Science Dr. Saad Howladar for the facilities and support.

REFERENCES

Ahmadi, R. A. and Amani, S. (2012). "Synthesis, Spectroscopy, Thermal Analysis, Magnetic Properties and Biological Activity Studies of Cu(II) and Co(II) Complexes with Schiff Base Dye Ligands". Molecules, 17: 6434-6448.

Ahmed, I. S., Moustafa, M. M., Abd El Aziz, M. M. (2011). "Mono and

CONCLUSION

In the present project work we prepared some Schiff base ligands containing azo (N=N), azomethine (CH=N) linkages and thioamide (C=S) group. The pentadentate ligands were derived from the condensation of azo-aldehydes with 1,3-diaminothiourea. These ligands were used to synthesize Cu(II) and Ni(II) complexes. The ligands and their complexes were characterized using different spectroscopic, physical and physicochemical techniques. The results showed that ligands behave as pentadentate ligands forming square pyramidal complexes with 1:1 (M:L) reaction ratio, and were coordinated through two phenolic oxygen, two nitrogen of the azomethine groups, and one sulfur atom of the thioamide group. The proposed monomeric structures of the prepared copper and nickel complexes shown in structure 2 are consistent with the chemical, physical, spectroscopic data and thermal analysis. The biological

on azo-containing Schiff base dye and its Cobalt(II), Chromium(III) and Strontium(II) complexes". Journal of Molecular Structure, 983: 32–38.

Al-Obaidi, O. H. (2012). "Synthesis, Characterization and Antimicrobial Screening Mixed-Ligand Cu(II) and Zn(II) Complexes: DNA Binding Studies on Cu(II) Complex". Open Journal of Inorganic Non-metallic Materials, 2: 59-64.

Bain, G. A. and Berry, J. (2008). "Diamagnetic Corrections and Pascal's Constants". *J.* Chem. Educ., 85 (4): p 532.

Balouiri, M., Sadiki, M., Ibnsouda, S. K. (2016). "Methods for in vitro evaluating antimicrobial activity: A review". Journal of Pharmaceutical Analysis 6: 71–79.

Bheemanna, H. G., Gayathri, V., Gowda, N. M. N. (2014). "Synthesis and spectral studies on Co (II), Ni(II) and Cu(II) complexes with 1,2- bis(N-methylbenzimidazolyl)benzene". IOSR

binuclear Ag(I), Cu(II), Zn(II) and Hg(II) complexes of a new azo-azomethine as ligand: Synthesis, potentiometric, spectral and thermal studies". Spectrochimica Acta Part A 78: 1429–1436.

Ajlouni, A. M., Taha, Z. A, Al Momani, W., Hijazi, A. K, Mohammad Ebqa'ai. (2012). 'Synthesis, characterization, biological activities, and luminescent properties of lanthanide complexes with N,N0-bis(2-hydroxy-1-naphthylidene)-1,6-hexadiimine". Inorg. Chim. Acta, 388: 120-126.

Alaghaz, A. M. A, Ammar, Y. A., Bayoumi, H. A., Aldhlmani, S. A. (2014). "Synthesis, spectral characterization, thermal analysis, molecular modeling and antimicrobial activity of new potentially N_2O_2 azo-dye Schiff base complexes". Journal of Molecular Structure, 1074: 359–375.

Alghool, S.,Abd El-Halim, H. F., Dahshan, A. (2010). "Synthesis, spectroscopic thermal and biological activity studies

Spectrochimica Acta Part A: Molecular and Biomolecular Spectroscopy, 98: 307–321.

Erdem, E., Sari, E.Y., Kilincarslan, R., Kabay, N. (2009). "Synthesis and characterization of azo-linked Schiff bases and their nickel(II), copper(II), and zinc(II) complexes". Transition Met Chem, 34: 167–174.

Hashemi, M., Solat,i Z., Ghods,i A., Ahmadian, S. (2015). "Azo-substituted Schiff base complex of Pt(II): Synthesis, characterization, DFT and TD-DFT study". Synthetic Metals 210: 398–403.

Kabak M., Elmali, A., Elerman Y. (1999). "Keto–enoltautomerism, conformations and structure of N-(2-hydroxy-5-methylphenyl), 2-hydroxybenzaldehydeimine". J. Mol. Struct., 477: 151-153.

Keypour, H., Shayesteh, M., Salehzadeh, S., Dhers S., Maleki, F., Onver, H., Dilek, N. (2015). "Probing the effect of arm lenth and inter-andintramolecular

Journal of Applied Chemistry, 7(4) Ver. II. : 17-22.

Chandra, S. and Sharma, A. K. (2009). "Biological and spectral studies of transition metal complexes with a quinquedentate Schiff base, 2,6-diacetylpyridine bis(thiocarbohydrazone)". Journal of Coordination Chemistry, 62(22): 3688-3700.

de Sousa, G. F., Deflon, V. M., Niquet, E., Abras, A. (2001). "Synthesis and Characterization of Heptacoordinated Tin(IV) Complexes. X-ray Crystal Structure of [nBu2Sn(dappt)]·(Me2CO)0.5 [H2dappt = 2,6-diacetylpyridine bis(4-phenylthiosemicarbazone)]". J. Braz. Chem. Soc., Vol. 12, No. 4: 493-498.

El-Sherif, A. A., Shoukry, M. M., Abd-Elgawad, M. M. A. (2012). "Synthesis, characterization, biological activity and equilibrium studies of metal(II) ion complexes with tridentate hydrazone ligand derived from hydralazine".

Lekha L. (2014). "Studies on the synthesis, characterisation and antimicrobial applications of rare earth metal Schiff base complexes". PhD thesis, submitted to B.S. Abdur Rahman University (June 2014): p5.

Lessa, J. A., Ferraz, K. S. O., Guerra, J. C., de Miranda, L .F., Romeiro, C. F. D, Souza-Fagundes, L. M., Barbeira, P. J. S., Beraldo, H. (2012). "Spectroscopic and electrochemical characterization of gold(I) and gold(III) complexes with glyoxaldehyde bis(thiosemicarbazones): cytotoxicity against human tumor cell lines and inhibition of thioredoxin reductase activity". Biometals, 25:587–598.

Mahal, A., Abu-El-Halawa, R., Zabin, S. A., Ibrahim, M., Al-Refai, M., Kaimari, T. (2015). "Synthesis, Characterization and Antifungal Activity of Some Metal Complexes Derived From Quinoxaloylhydrazone". World Journal of Organic Chemistry, vol. 3, no. 1: 1-8.

interactions in the formation of Cu(II) complexes of Schiff base ligands derived from some unsymmetrical tripodal amines". New J. Chem., 39: 7429-7441.

Khanmohammadi, H., Pass, M., Rezaeian, K., Talei, G. (2014). "Solvatochromism, spectral properties and antimicrobial activities of new azo–azomethine dyes with $N_2S_2O_2$ donor set of atoms". Journal of Molecular Structure 1072: 232–237.

Kumar, S. L. A., Kumar, M. S., Jenniefer, J., Muthiah, T., Sreekanth, A. (2012). 'Synthesis, Spectral, and Structural Characterization of Bisthiocarbohydrazone Derivatives. Phosphorus Sulfur and Silicon and the Related Elements". 188(8): 1110 -1118.

Kurtoglu G., Avar B., Zengin H., Kose M., Sayin K., Kurtoglu M. (2014). "A novel azo-azomethine based fluorescent dye and its Co(II) and Cu(II) metal chelates". Journal of Molecular Liquids, 200:105–114.

Manoj, E., Kurup, M. R. P. and Fun, H. K. (2007). "Macrocyclic molecular square complex of zinc(II) self-assembled with a carbohydrazone ligand". Inorg. Chem. Commun., 10(3): 324–328.

Menati, S., Azadbakht, A., Azadbakht, R., Taeb, A., Kakanejadifard, A. (2013). "Synthesis, characterization, and electrochemical study of some novel, azo-containing Schiff bases and their Ni(II) complexes". Dyes and Pigments, 98: 499-506.

Metwally, M. A., Khalifa, M. E., Koketsu, M. (2012). "Thiocarbohydrazides: Synthesis and Reactions". American Journal of Chemistry, 2(2): 38-51.

Ozkan, G., Kose, M., Zengin, H., McKee, V., Kurtoglu, M. (2015). "A new Salen-type azo–azomethine ligand and its Ni(II), Cu(II) and Zn(II) complexes: Synthesis, spectral characterization, crystal structure and photoluminescence studies". Spectrochimica Acta Part A: Molecular and Biomolecular Spectroscopy 150: 966–973.

Pal, M. K., Kushwah, N., Wadawale, A. P., Manna, D., Sudarsan, V., Ghanty, T.K., Jain, V.K. (2015). "Synthesis, characterization, photoluminescence and computational studies of mono- and diorgano-gallium complexes containing azo linked salicylaldimine Schiff bases". Journal of Organometallic Chemistry 776: 98-106.

Potti, M. E., Kurup, M. R. P., Fun, H. "2007". "Macrocyclic molecular square complex of zinc(II) self-assembled with a carbohydrazone ligand". Inorg.Chem. Commun., 10(3): 324-328.

Sarigul, M., Deveci, P., Kose, M., Arslan, U., Dagi, H.T., Kurtoglu, M. (2015). "New tridentate azo–azomethines and their copper(II) complexes: Synthesis, solvent effect on tautomerism, electrochemical and biological studies". Journal of Molecular Structure 1096: 64–73.

N^1,N^5-bis[pyridine-2-methylene]-thiocarbohydrazone Schiff-base ligand". Spectrochimica Acta Part A: Molecular and Biomolecular Spectroscopy, 79(5): 1050-1056.

Zabin, S. A. and Abdelbaset, M. (2016). "Oxo/dioxo-vanadium (V) complexes with Schiff base ligands derived from 4-amino-5-mercapto-3-phenyl-1,2,4-triazole". European Journal of Chemistry**,** *7(3): 322-328*.

Zou, Y., Liu, W. Lu, C., Wen, L., Meng, Q. (2004). "Synthesis and Characterization of a novel copper(II)-Silver(I) mixed-metal coordination polymer Ag[CuL] (L = Schiff base derived from glycylglycine and o-vanillin)". Inorganic Communications, 7: 985-987.

Shebl, M., Saied, M. E. K. and Faizah, S. A. G. (2010). "Preparation, spectral characterization and antimicrobial activity of binary and ternary Fe(III), Co(II), Ni(II), Cu(II), Zn(II), Ce(III) and UO2(VI) complexes of a thiocarbohydrazone ligand". Journal of Molecular Structure, 980(1–3): 78–87.

Singh, D. P., Kumar, K. and Sharma C. (2010). "New 14-membered octaazamacrocyclic complexes: Synthesis, spectral, antibacterial and antifungal studies". European Journal of Medicinal Chemistry, 45(3): 1230–1236.

Tiwari, A. D., Mishra, A. K., Mishra, S. B., Mamba, B. B., Maji, B., Bhattacharya S. (2011). "Synthesis and DNA binding studies of Ni(II), Co(II), Cu(II) and Zn(II) metal complexes of

لجاندات قواعد ستشف (Schiff bases) المشتقة من N_5,N_1 - ثنائي [أزوالدهيد]- ثيوكربوهيدرازون ومعقداتها المعدنية مع النحاس الثنائي والنيكل الثنائي : توصيفها ونشاطها ضد الميكروبات

سامي عبد اللطيف زبن

قسم الكيمياء - كلية العلوم – جامعة الباحة – المملكة العربية السعودية

الملخص

الهدف الرئيس من هذا المشروع البحثي هو تحضير مركبات معقدة من النيكل والنحاس باستخدام لجاندات قواعد ستشف خماسية الربط المشتقة من تكاثف الثيوكربوهيدرازايد (thiocarbohydrazide) مع الأزولدهيدات (azoaldehyde). وتم استخدام هذه الليجاندات لتحضير معقدات معدنية مع ايونات النحاس والنيكل الثنائية بنسبة مولية ١:١ (معدن: ليجاند). استخدمت تحليلات طرق طيفية وكيموفيزيائية (physicochemical) لتوصيف وتحديد بنية الليجاندات والمعقدات التي تم تحضيرها. تشير النتائج الى أن الليجاندات المحتوية على خمسة مواقع ربط تعطي معقدات أحادية النواة بخمسة روابط تساهمية تناسقية وذات شكل هندسي رباعي هرمي لكل من معدني النحاس والنيكل. تم فحص الليجاندات العضوية ومعقداتها المقابلة لها كمضادات للميكروبات في المختبر ضد كل من سلالات البكتيريا الموجبة والسالبة ونوع من الفطريات الشائعة المعروف باسم (*C. Albicans*). تشير النتائج الى أن كلا الليجاندات العضوية ومعقداتها مع النحاس والنيكل لها نشاط متوسط ضد سلالة البكتيريا الموجبة المسماة (*S. aureus*) وضد الفطر (*C. Albicans*)، وتزيد الفعالية عند الارتباط بالأيونات المعدنية. ووجد أن جميع المركبات المحضرة أنه ليس لها نشط ضد سلالة البكتيريا السالبة.

الكلمات المفتاحية: ثيوكربوهيدرازون، المعقدات المعدنية، قواعد ستشيف، أزرالدهيدات، النشاط البيولوجي

مجلة جامعة جازان

للعلوم التطبيقية

دورية علمية محكمة

المجلد ١٠ العدد ٢ ربيع الثاني ١٤٤٤ هـ (نوفمبر ٢٠٢٢م)

المراسلات

توجه جميع المراسلات إلى:

رئيس هيئة التحرير مجلة جامعة جازان للعلوم التطبيقية جازان -المدينة الجامعية -البرج الإداري - ص ب ١١٤. -الرمز البريدي ٤٥١٤

المملكة العربية السعودية أو على البريد الإلكتروني jas@jazanu.edu.sa

المملكة العربية السعودية
وزارة التعليم
جامعة جازان

مجلة جامعة جازان

للعلوم التطبيقية

دورية علمية محكمة

المجلد ١٠ العدد ٢ ربيع الثاني ١٤٤٤هـ - نوفمبر ٢٠٢٢م)

ردمد: ١٦٥٨-٩٦١٣

قواعد النشر في المجلة

مجلة جامعة جازان للعلوم التطبيقية دورية علمية محكمة تنشرها الجامعة، وهي تهدف إلى إتاحة الفرصة للباحثين لنشر إنتاجهم العلمي وتقوم المجلة بنشر المواد الآتية :

١ـ البحث : ويندرج تحت تخصص الباحث ويجب أن يحتوي على إضافة للمعرفة في مجاله .

٢ـ المقالة الاستعراضية التي تتضمن عرضًا نقدياً لبحوث سبق إجراؤها في مجال معين أو أجريت في خلال فترة زمنية محددة.

٣ـ البحث المختصر.

٤ـ نقد الكتب .

٥ـ الخطابات الموجهة إلى المحرر ، والملاحظات والردود ، والنتائج الأولية .

تقوم هيئة التحرير، بالنظر في نشر المواد المعرفية ذات الصلة بذلك الفرع، وتقدم البحوث الأصلية، التي لم يسبق نشرها، وفي حال قبول البحث للنشر تؤول كل حقوق النشر للمجلة و لا يجوز نشره في أي منفذ نشر آخر ورقيا أو إلكترونياً، دون إذن كتابي من رئيس هيئة التحرير .

تعليمات النشر في المجلة

١ـ تقديم المواد : يقدم أصل البحث مخرجا في صورته النهائية متضمنا الإشارة إلى أماكن الجداول والأشكال داخل المتن و مطبوع على هيئة صفحات مرقمة ترقيما متسلسلا، مع ضرورة إرفاق قرص ممغنط مطبوع عليه البحث على برنامج Ms Word باستخدام النظام المتوافق مع IBM ، وسيعتذر عن قبول أي بحث لا يلتزم مؤلفه بهذه التعليمات.

٢ـ الملخصات: يرفق ملخصان بالعربية والإنجليزية للبحوث و المقالات الاستعراضية والبحوث المختصرة على ألا يزيد عدد كلمات كل منهما على ٢٠٠ كلمة، وعلى عمود واحد بعرض كتابة ١٣ سم.

٣ـ لا بد من احتواء كل بحث على كلمات مفتاحية (Key Words) توضع أسفل الملخصين العربي والانجليزي على ألا تزيد عن عشر كلمات.

٤ـ الجداول والمواد التوضيحية: يجب أن تكون الجداول والرسومات واللوحات مناسبة لمساحة الصف في صفحة المجلة ١٦ ٢٤ سم بالحواشي، ويتم إعداد الأشكال الخطية على برامج الحاسب الآلي، ولا تقبل إلا أصول الأشكال. كما يجب أن تكون الخطوط واضحة ومحددة ومنتظمة من حيث كثافة الحبر وتناسب سمكها مع حجم الرسم، ويراعى أن تكون الصور الفوتوغرافية (الضوئية) الملونة وغير الملونة مطبوعة على ورق لماع، أو محملة على برنامج (Adobe Photoshop) مع كتابة عنوان لكل جدول، وتعليق لكل شكل وصورة، والإشارة إلى مصدر المادة إن كانت مقتبسة.

٥ـ الاختصارات: يجب استخدام الاختصارات المقننة دولية مثل : سم، مم، م، كم، سم، مل، مجم، كجم...إلخ.

٦ـ المراجع :يشار إلى المراجع داخل المتن بنظام الاسم والتاريخ، وتوضع المراجع جميعها في قائمة المراجع بنهاية المادة مرقمة ومتبعة نظام ترتيب البيانات الببليوجرافية التالي :

أـ يشار إلى الدوريات في المتن بنظام الاسم والتاريخ بين قوسين على مستوى السطر، أما في قائمة المراجع فيبدأ المرجع بذكر الاسم الأخير للمؤلف، ثم الاسم الأول، ثم الأسماء الأخرى أو اختصاراتها بالخط الأسود، ثم سنة النشر بين قوسين، فعنوان البحث كاملا بين علامتي تنصيص" " ، فاسم الدورية، فرقم المجلد، ثم رقم العدد : ثم أرقام الصفحات تفصل بشرطة .

مثال : هادي، أحمد بن جابر. (٢٠١١م)،" استخدام تقنية النانو لتعريف الشفرات الوراثية "مجلة جامعة جازان، ١، ١ : ٢٠٠ـ٢٢٠.

بـ يشار إلى الكتب في المتن داخل قوسين بالاسم والتاريخ . أما في قائمة المراجع، فيكتب الاسم الأخير للمؤلف، ثم الاسم الأول، ثم الأسماء الأخرى أو اختصارا تها، ثم سنة النشر بين قوسين، فعنوان الكتاب بين علامتي تنصيص، ثم بيان الطبعة، فالناشر، فمدينة النشر :ثم صفحات الكتاب إن وجدت.

مثال :

عبدالهادي، محمد علي، (١٤٣٣هـ)،" مقدمة في التقنية الحيوية"، جامعة جازان، جازان.

ويجب عدم استخدام الاختصارات المرجعية مثل :المرجع نفسه . المرجع السابق...إلخ.

٧ـ أـ الحواشي: تستخدم لتزويد القارئ بمعلومات توضيحية، ويشار إليها في المتن بأرقام مرتفعة عن السطر .وترقيم التعليقات متسلسلة داخل المتن. وفي حال الضرورة؛ يمكن الإشارة إلى مرجع داخل الحاشية عن طريق استخدام كتابة الاسم والتاريخ بين قوسين وبنفس طريقة استخدامها في المتن، وتوضع الحواشي أسفل الصفحة التي تخصها والتي ذكرت بها و تفصل بخط عن المتن وبخط أصغر.

بـ يستخدم في تخريج الأحاديث والآثار الطريقة المنهجية المعتمدة في هذا الفن وهي كالآتي : اسم المؤلف ـ اسم الكتاب ـ رقم الجزء والصفحة والحديث.

٨ـ المواد المنشورة في المجلة تعبر عن وجهة نظر صاحبها، ولا تعبر بالضرورة، عن رأي مجلة جامعة جازان.

٩ـ يتأكد الباحث من صحة اللفظ وسلامة لغة البحث، وخلوه من الأخطاء اللغوية والنحوية.

١٠ـللمجلة الحق في تحديد أولويات نشر البحوث.

١١ـالمجلة غير ملزمة بإعادة البحوث التي تصل إليها سواء أجيزت للنشر أم لم تجز.

١٢ـيتم إخضاع جميع البحوث المستلمة لفحص مبدئي، من قبل هيئة التحرير، لتقرير أهليتها للتحكيم، ويحق لها أن تعتذر عن قبول البحث دون إبداء الأسباب.

١٣ـتصدر المجلة مرتين في العام.

المملكة العربية السعودية
وزارة التعليم
جامعة جازان

مجلة جامعة جازان

للعلوم التطبيقية

دورية علمية محكمة

المجلد ١٠ العدد ٢ (ربيع الثاني ١٤٤٤هـ - نوفمبر ٢٠٢٢م)

ردمد: ١٦٥٨-٦٩١٣